

---

# Collection of experimental data on the behavior of TCM/PCM-materials to benchmark numerical codes

---

Report A3.2 of the Working Group on Numerical Modelling

December 2012

Paul Gantenbein  
Camilo Rindt

A report of the IEA Solar Heating and Cooling / Energy Conservation through Energy Storage programme – Task 42/Annex 24:

## Compact Thermal Energy Storage: Material Development for System Integration



# Collection of experimental data on the behavior of TCM/PCM-materials to bench- mark numerical codes

by

Paul Gantenbein, Camilo Rindt

## Short description Working Group A3 Numerical Modelling

### INTRODUCTION

The activities in this working group are aimed at developing and testing numerical models that help to understand and optimise the material behaviour and the dynamic behaviour of compact thermal energy storage systems and components based on Phase Change Materials (PCM's) and Thermo Chemical Materials (TCM's). Ultimately, these numerical models could help to find ways to optimise the materials in combination with the system components. The activities in this working group help to lay the foundation for such models.

The Working Group includes the following activities:

- Micro-scale modelling
- Meso-scale modelling
- Macro-scale modelling
- Multi-scale approach
- Thermo-mechanical modelling
- Reactor models

Not all activities receive the same amount of attention in the Working Group and the distinction between the various scales is not always clear. The figure below presents an attempt to quantify the micro-, meso- and macro-scales in a time-length framework but it has to be realised that the definition of the scales is highly dependent on the problem at hand.

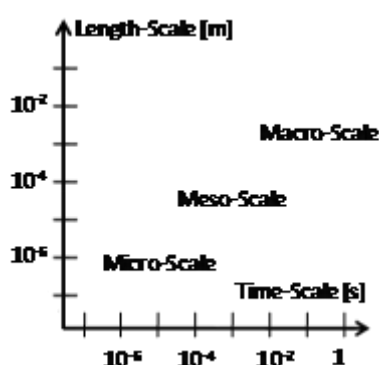


Figure 1: Definition of micro-, meso- and macro-scales in a time-length framework.

### DELIVERABLES

The following deliverables are set.

#	Deliverable	Month
A3.1	Report on state-of-the-art modeling techniques of TCM/PCM-materials on micro-, meso- and macro scales	12
A3.2	Collection of experimental data on the behavior of TCM/PCM-materials which can be used to bench-mark numerical codes	30
A3.3	Overview of material properties required for increased storage performance compared to conventional storage techniques	48
A3.4	Final report on the (validated) numerical models developed for the micro-, meso-, macro and multi-scale	48

## **Deliverable A3.2: collection of experimental data on the behavior of TCM/PCM-materials to validate numerical models**

### **MOTIVATION**

In the developing process of a heat storage device experiments play a dominant role because in the prototype stadium a physical system has to be built to acquire measurement data for fine tuning of the pilot and market product. In this development process numerical modelling plays the role of reducing the number of time consuming and cost intensive experiments. And modelling should help to understand how the limiting parameters can or should be adapted for the assigned task.

In the former deliverable A3.1 it is shown that numerical models are being developed for all kind of length scales (and time scales), ranging from the molecular level, f.e. Molecular Dynamics simulations to gain insight into the hydration/dehydration kinetics, up to the reactor level, f.e. CFD-calculations to simulate the time-dependent heat and vapour flows in a fixed-bed reactor. For validation purposes all these models need to be confronted with results of detailed experiments and it is needless to say that this should be done on as many length scales as possible. Therefore, the contribution of experimental results from one group and the use of these results to validate numerical models developed in another group is appreciated.

This report contains a collection of various experiments. The focus is not only on the measuring results but the report also presents detailed descriptions of the experimental set-ups, the materials tested and their physical properties and the measuring procedures.

### **OUTLINE**

The document is structured in two main parts focussing on PCM and TCM experiments. Each section describes a typical experiment and has a fixed outline:

1. introduction;
2. lay-out of the experimental set-up including dimensions and material properties;
3. detailed description of the measuring procedure;
4. results presented in graphical or table form;
5. closure containing contact details.

## Table of contents

<b>SHORT DESCRIPTION WORKING GROUP A3 NUMERICAL MODELLING .....</b>	<b>3</b>
introduction.....	3
Deliverables .....	3
<b>DELIVERABLE A3.2: COLLECTION OF EXPERIMENTAL DATA ON THE BEHAVIOR OF TCM/PCM-MATERIALS TO VALIDATE NUMERICAL MODELS .....</b>	<b>4</b>
Motivation .....	4
Outline .....	4
<b>TABLE OF CONTENTS .....</b>	<b>5</b>
<b>PHASE CHANGE MATERIAL MODELS.....</b>	<b>7</b>
Introduction.....	7
Detailed experimental results for PCM Melting and solidification in circular tubes and spherical shells.....	8
Detailed Experimental Results for Submerged Finned Heat Exchanger in PCM Based Thermal Energy Storage .....	12
Experimental results for PCM-Air heat exchangers: Melting and solidification in flat plates (CSM panels from rubitherm).....	15
Heat storage system coupled with a photovoltaic panel.....	21
<b>THERMO-CHEMICAL MATERIAL MODELS .....</b>	<b>27</b>
Introduction.....	27
<b>HYDRATION AND DEsHYDRATION OF SORPTION MATERIALS: EXPERIMENTS IN A SMALL-SCALE REACTOr .....</b>	<b>28</b>
Adsorption heat storage: Dynamic properties.....	34
Fixed bed reactor for Hydration / dehydration or adsorption / desorption experiments .....	39
Adsorption heat storage: EQUILIBRIUM properties DETERMINATION WITH COMPARISON TO MOLECULAR SIMULATIONS .....	45
Characterization OF the dehydration reaction OF SEVERal crystalline salt hydrates uNDER the condtions of the seasonal heat storage .....	51
Short Description of Task 42/ annex 24.....	55

<b>Objective.....</b>	<b>55</b>
<b>Scope.....</b>	<b>55</b>
<b>Structure.....</b>	<b>55</b>
<b>IEA SOLAR HEATING AND COOLING PROGRAMME .....</b>	<b>57</b>
<b>Appendix "Detailed Experimental Results for Submerged Finned Heat Exchanger in PCM Based Thermal Energy Storage" by NM. J. CHIU and V. MARTIN.....</b>	<b>61</b>

## Phase Change Material Models

### INTRODUCTION

Nowadays, thermal energy storage systems are essential for reducing dependency on fossil fuels and then contributing to a more efficient environmentally benign energy use.

Thermal energy storage can be accomplished either by using sensible heat storage or latent heat storage. Sensible heat storage has been used for centuries by builders to store/release passively thermal energy, but a much larger volume of material is required to store the same amount of energy in comparison to latent heat storage. The principle of the phase change material (PCM) use is simple. As the temperature increases, the material changes phase from solid to liquid. The reaction being endothermic, the PCM absorbs heat. Similarly, when the temperature decreases, the material changes phase from liquid to solid. The reaction being exothermic, the PCM desorbs heat.

The phase change materials used in applications can be either organic materials or inorganic materials. The organic PCM are paraffins, fatty acids and the polyethylene glycol (PEG). They present a congruent phase change, they are not dangerous, and they have a good nucleation rate.

The advantages of organic PCM are:

- availability in a large temperature range,
- freeze without much super cooling,
- ability to melt congruently,
- self nucleating properties,
- compatibility with conventional material of construction,
- no segregation,
- chemically stable,
- high heat of fusion,
- safe and non-reactive,
- recyclable.

The disadvantages of organic PCM are:

- low thermal conductivity,
- low volumetric latent heat storage capacity,
- flammable (depending on containment).

The inorganic PCM are salt hydrates.

The advantages of inorganic PCM are:

- high volumetric latent heat storage capacity,
- low cost and easy availability,
- sharp phase change,
- high thermal conductivity,
- non-flammable.

The disadvantages of inorganic PCM are:

- high volume change,
- super cooling,
- segregation.

PCM are used in systems for passive or active applications. The objective of numerical modeling is to predict the behavior of systems depending on the heat and/or mass transfers involved.

## DETAILED EXPERIMENTAL RESULTS FOR PCM MELTING AND SOLIDIFICATION IN CIRCULAR TUBES AND SPHERICAL SHELLS

G. ZISKIND, Heat Transfer Laboratory, Department of Mechanical Engineering, Ben-Gurion University of the Negev, Beer-Sheva 84105, Israel

### INTRODUCTION

Extensive experimental investigations are performed for circular vertical tubes and spherical shells containing paraffin-type PCMs. Visualization makes it possible to obtain melt fractions and patterns for various instants. Thus, a significant database is created for validation of the numerical codes, not only in terms of overall parameters but also concerning the details.

### LAY-OUT OF THE EXPERIMENTAL SET-UP

The experimental set-up for melting is shown schematically in Figure 1. Experiments are performed in a transparent tank, filled with water. In order to keep a constant water temperature, an electric heater is used, and its power is adjusted using a variable voltage controller. In order to ensure uniform temperature of water inside the tank, a mechanical turbine-type stirrer is used. In a typical experiment, a transparent vertical tube/spherical shell filled with the solid PCM is placed into the water. The experiment continues until the PCM has melted completely.

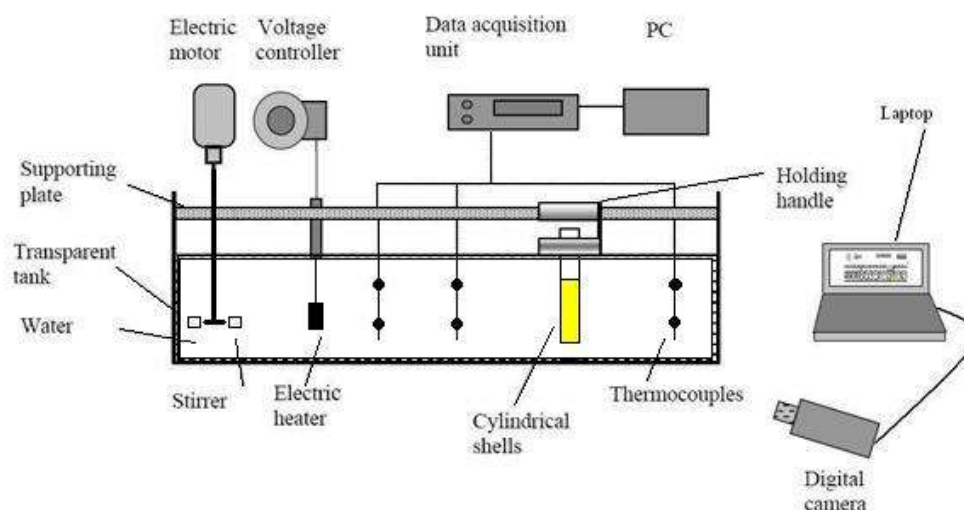


Figure 1: Schematic view of the experimental set-up.

Circular tubes of four different diameters are used, with the inner diameters of 0.9, 1.93, 3.14, and 3.92 cm. These tubes are referred to using their nominal diameters of 1, 2, 3, and 4 cm, respectively. The water level is set at 23.5 cm above the tank bottom. The height of the solid PCM inside the tube is 6, 12 or 17 cm. At its top, the tube is open to atmosphere, in order to allow free expansion of the melt liquid. From below, the tube is sealed by a cork made of an insulating material. In each tube the experiments are performed at the water bath temperatures 10, 20 and 30°C above the melting point of the PCM. Thus, the four different diameters, three heights and three temperature differences bring the total number of cases explored in the present study to thirty-six. Similar experiments are performed for spherical shells and could be expanded to various diameters and temperature differences. Details of the shells are given in the references.

Solidification is studied using a Neslab RTE 7 circulating thermostatic bath, which maintains a desired temperature within 0.1°C. The bath is kept typically at 10 or 20 °C below the mean solidification temperature. The shell is inserted in the bath when the PCM temperature is typically few degrees above its mean melting temperature.

### Material properties

The material used in the experimental study is the RT27 paraffin wax (Rubitherm GmbH), claimed to be suitable for heat-storage applications. Its properties, given in the references, are close to *n*-octadecane. Melting occurs at a temperature about 28°C.

### **DETAILED DESCRIPTION OF THE MEASURING PROCEDURE**

For melting, the initial shape of the solid PCM is cylindrical/spherical, with a flat top. In order to achieve a desired shape, the tube/shell is filled gradually with a liquid PCM allowing the latter to solidify at each stage. As a result, no void is formed close to the centerline/centerpoint of the tube/shell. Sample preparation is performed at a reduced ambient pressure, in order to prevent air entrapment in the PCM. Visualization has been chosen as the major method of investigation. Melting images are recorded by a digital camera at various stages of the process. Then, these images are analyzed and the experimental values of the melt fraction are calculated at various instants.

For solidification, thin plastic shells are used, which can be sawed with the PCM after the latter has solidified completely or on the intermediate stages of the process. Two series of the experiments are performed. The first series is conducted in shells of 30 mm and 70 mm in diameter up to complete solidification. The shells are then cut in halves, and the solid shape recorded. The second series is conducted in shells of 40mm in diameter, where each shell is withdrawn from the bath at a prescribed time. The shell is cut in halves, the remaining liquid is removed and the solid shape is recorded.

### **RESULTS**

The results for melting in circular tubes are summarized in Figure 2, in terms of the melt fraction versus time. The melt fraction is defined as the melted mass divided by the total mass of the sample.

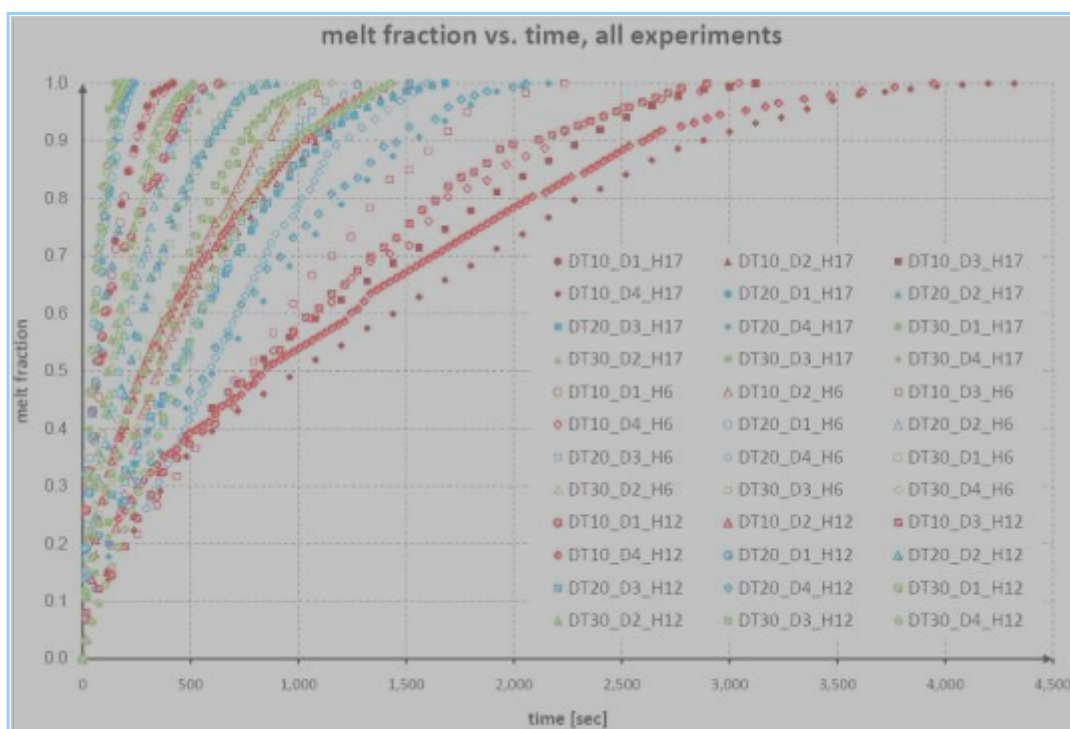


Figure 2: Experimental results for melting in circular tubes.

An example of the visualization results for solidification in a spherical shell is presented in Figure 3, along with its numerical simulation.

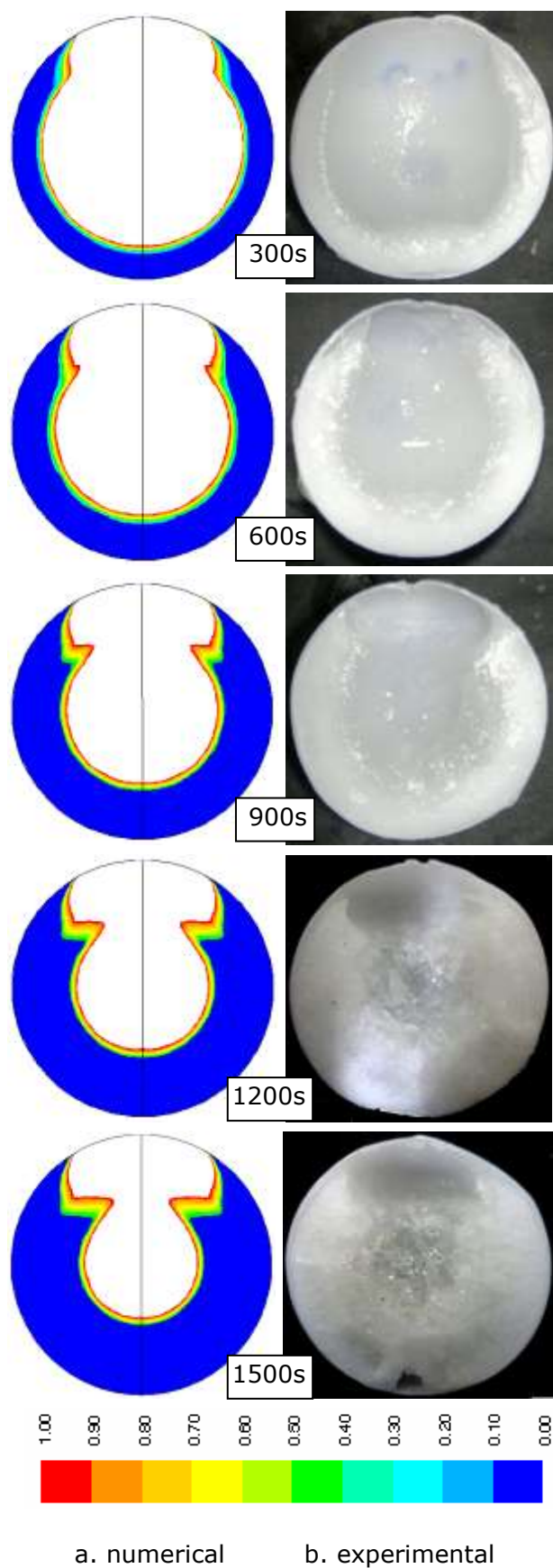


Figure 3: Example of the results for solidification in spherical shells ( $D=40$  mm,  $\Delta T=20$  °C).

## CLOSURE

An extensive database has been created for melting and solidification of PCM in circular vertical tubes and spherical shell. The accumulated data includes also detailed melting/solidification patterns based on visualization. Thus, these data can be used for benchmarking. Further information is available (see the Bibliography or contact gziskind@bgu.ac.il).

#### **BIBLIOGRAPHY**

- [1] E. Assis, L. Katsman, G. Ziskind, R. Letan (2007) Numerical and experimental study of melting in a spherical shell. *Int. J. Heat Mass Transfer* 50, 1790-1804.
- [2] L. Fraiman, E. Benisti, G. Ziskind, R. Letan, Experimental investigation of melting in vertical circular tubes, *Proceedings of the ASME Biennial ESDA Conference, Haifa, Israel, 7-9 July 2008.*
- [3] E. Assis, G. Ziskind, R. Letan (2009) Numerical and experimental study of solidification in a spherical shell. *ASME Journal of Heat Transfer* 131, 024502.
- [4] H. Shmueli, G. Ziskind, R. Letan (2010) Melting in a vertical cylindrical tube: Numerical investigation and comparison with experiments. *Int. J. Heat Mass Transfer* 53, 4082-4091.

## DETAILED EXPERIMENTAL RESULTS FOR SUBMERGED FINNED HEAT EXCHANGER IN PCM BASED THERMAL ENERGY STORAGE

NW. J. CHIU\* and V. MARTIN, Department of Energy Technology, Royal Institute of Technology, 10044 Stockholm, Sweden (\*[Justin.chiu@energy.kth.se](mailto:Justin.chiu@energy.kth.se))

### INTRODUCTION

Various means have been investigated for the goal of overcoming the low thermal storage/extraction rate with use of phase change materials (PCMs) in active thermal energy storage systems (TESs). The most common means employed are surface extension techniques, such as encapsulation, heat-exchange-surface extension, and material thermal property enhancement, for instance with highly conductive additives/matrices. Numerous simulations predicting the effect of the enhancement are available [1,2,3], however, only limited number of experiments are made available to serve as basis for model validation. This article, as part of the IEA Task 42/Annex 24 official report, aims at providing experimental data for use in validating and verifying gelled PCM-based TESs with submerged finned pipe heat exchanger. This work was carried out at Royal Institute of Technology, Sweden.

### DETAILED DESCRIPTION OF THE EXPERIMENTAL SET-UP

The submerged finned pipe heat exchanger based latent heat TES is characterized by specifications listed in Table 1. The water temperature is practically uniform, and the material is gelled. This means that at different fins the process is practically the same. However, to avoid any disturbance of temperature due to edge effect on the first and the last fin, 4 fins were mounted, and the temperature was taken from the center 2 fins. The insulation is attached to the shell of the unit. Water was utilized as the heat transfer fluid (HTF). The mass flow rate of the HTF was maintained at a sufficient level to assure uniform heat flux between the storage and the HTF in this experimental study. The HTF temperature variation from inlet to outlet was maintained below 0.1 °C. Temperature sensors are thermocouples type T, calibrated to 0.1 °C accuracy.

*Table 1 Characteristics of the Thermal Energy Storage Unit and Experimental Parameters*

Parameter		Parameter	
Fin spacing	30 mm	Heat transfer fluid	Water
Fin thickness	1 mm	PCM	Shape Stabilized Sodium Sulfate Decahydrate
Fin diameter	68 mm	Change in HTF temperature	<0.1 °C
Pipe diameter	8 mm	Mass flow rate	0.07 L/s
Pipe thickness	0.8 mm	Tank insulation	10 mm polyurethane with 0.03W/m.K
Pipe and fin material	Aluminum 6082	Number of fins	4
Outer diameter of shell	80 mm	Thickness of shell	3 mm
Total length of the finned pipe	160 mm		

The PCM utilized is a commercially available gelled salt-hydrate product [4], the material properties of which were tested and characterized with an in-house built testing facility based on an improved T-History method described by Chiu et al. [5]. The specific heat of the material in melting and in congealing (freezing) is measured between 5 °C and 40 °C, as depicted in Figure 1. The energy storage capacities measured in melting and congealing of the PCM are  $52 \pm 1$  Wh/kg ( $187 \pm 4$  kJ/kg). A proposed numerical curve fit function with the use of Dirac approximation and proposed parameters is presented in eq. (1). It is shown that melting latent heat extends over a range of 8 °C while the congealing  $c_p$  covers a temperature range slightly less than 4 °C. The use of correct material property data in modeling is essential in achieving representative results.

$$c_p(T) = c_{ps} + h * \frac{e^{-\frac{a^2}{b^2}}}{(\sqrt{\pi} * b)} \quad (1)$$

$$a = (T - T_{pc});$$

Melting

$$T_{pc} = 23.5 \text{ } ^\circ\text{C};$$

$$b = 1.830559547;$$

$$c_{ps} = 3600 \text{ J/kg.K};$$

$$h = 58800 \text{ J/kg};$$

Cooling

$$T_{pc} = 20.5 \text{ } ^\circ\text{C};$$

$$b = 0.9152797733;$$

$$c_{ps} = 3600 \text{ J/kg.K};$$

$$h = 64800 \text{ J/kg};$$

where "a" and "b" are cure fitting parameters that characterize the peak  $c_p$  temperature and the phase change temperature range. " $T_{pc}$ " is the phase change temperature with the peak  $c_p$ .  $c_{ps}$  corresponds to the sensible heat of the material; from the measurement, it is seen that the sensible heat is identical in both solid and liquid phases. "h" is the latent heat of the material with sensible heat deducted, it also corresponds to the surface area of the lobe in Figure 1.

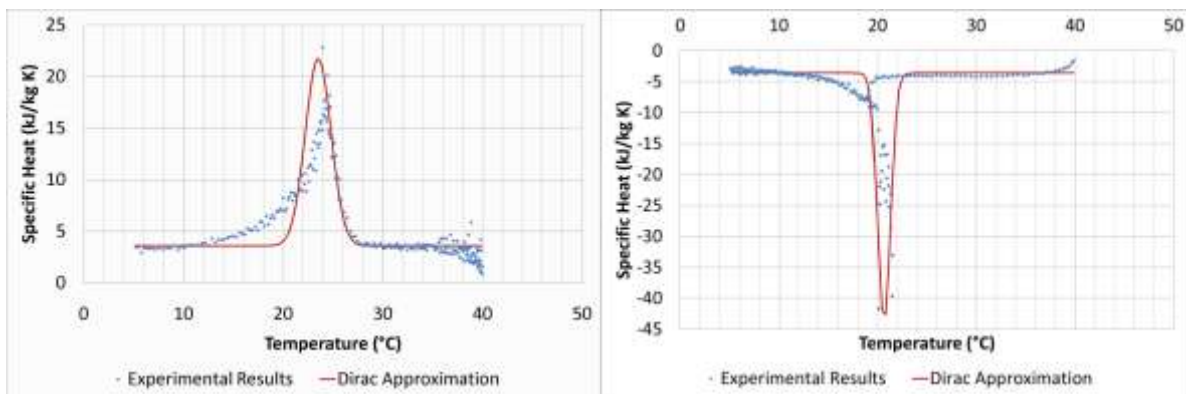


Figure 1 Thermal Property of PCM in Melting (left) and in Congealing (right) with Curve Fit Approximations

The schematic of the experimental setup is shown in Figure 2. Teflon insulated thermocouples are led out through the opening top of the TES unit. An 8 L water bath was served as the heat source and heat sink for charge and discharge of the TES unit. The experimental data were collected with a 16 bit multiplexer/ data logger and the data were recorded in a 32 bit computer. Temperature sensors are placed along the pipe, on the fins and in the center of the PCM, see Figure 2 (right).

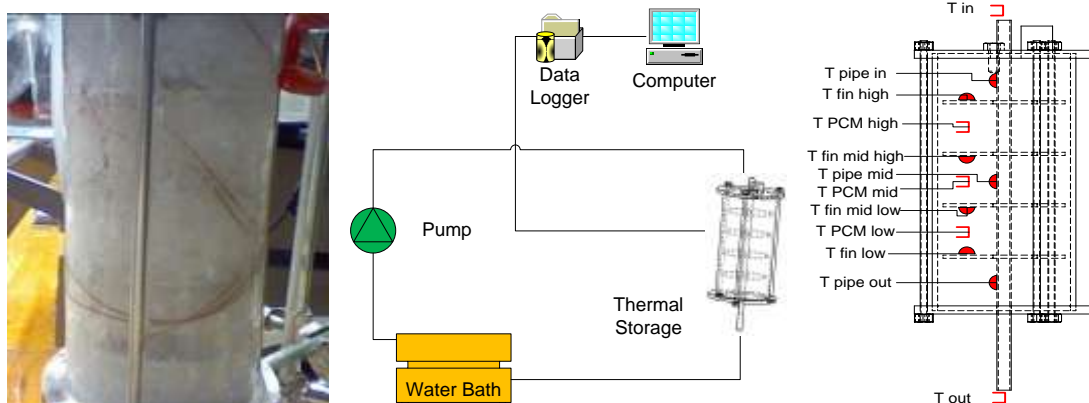


Figure 2 Submerged Finned Heat Exchanger (left); Schematic of the Setup (middle); Thermocouple Placement (right)

The charging of heat (melting process) was performed with initial temperature of 12 °C and HTF at 32 °C; the discharging of heat (freezing process) was performed with initial temperature of 31 °C and HTF at 11 °C. Data were recorded from 15 °C to 29 °C in the melting process and 29 °C to 15 °C in the congealing process.

## RESULTS AND DISCUSSION

Temperature readings obtained for the finned pipe heat exchanger submerged gelled PCM TES unit are appended to this article. The data are open for use to all for experimental comparisons and numerical validations by giving reference to this article. The fin temperature, PCM temperature, and pipe temperature presented in the appendices are the average fin temperatures, PCM temperatures and pipe temperatures measured. Averaging is possible due to the practically uniform HTF temperature throughout the heat exchanger tube and the symmetry of the storage.

The temperature profiles are presented in Figure 3, the shown temperatures are fin temperatures and PCM temperatures in run A, run B and run C. It is shown here that the PCM heating temperatures deviate 5% in terms of melting time at the upper bound of the testing temperature range, while the congealing temperature curves have more consistent readings through the 3 test runs.

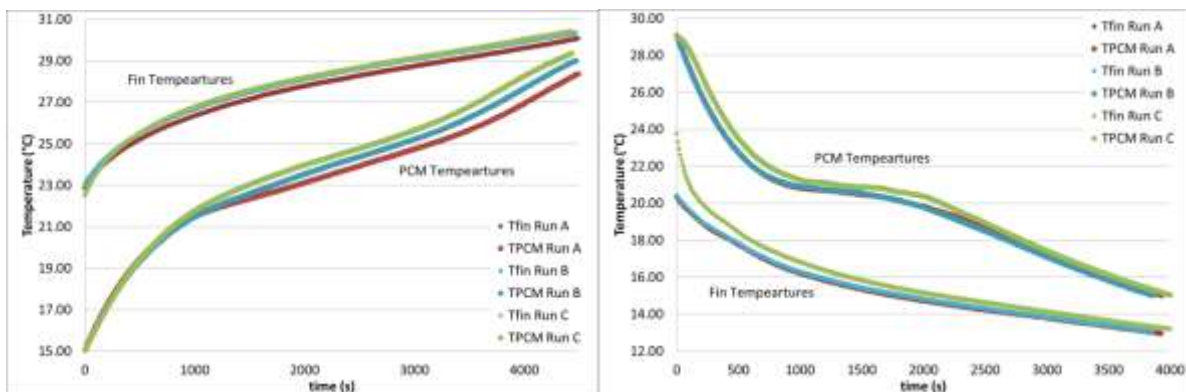


Figure 3 Temperature Profiles in Melting (left) and in Congealing (right)

## CLOSURE

A compilation of experimental results for a gelled PCM based submerged finned pipe heat exchanger TES is made available in this report for numerical validation. The material enthalpy data measured with T-history method, the temperature profiles of the gelled PCM and of the fins are appended to this report. The data are open for access to all, and we welcome the use of the data with reference to this report.

## Acknowledgement

The authors would like to acknowledge Swedish Energy Agency for providing funding for this project 31067-1.

## BIBLIOGRAPHY

- [1] A. Castell, M. Belusko, F. Bruno and L.F. Cabeza, Maximisation of heat transfer in a coil tank PCM cold storage system, *Applied Energy*, 88, pp. 4120-4127, 2011.
- [2] Li P.W. et al., "Similarity and generalized analysis of efficiencies of thermal energy storage systems," *Renewable Energy*, vol. 39, pp. 388-402, 2012.
- [3] Ye W.B., Zhu D.S., and Wang N., "Numerical simulation on phase-change thermal storage/release in a plate-fin unit," *Applied Thermal Engineering*, vol. 31, pp. 3871-3884, 2011.
- [4] Julin N. Climator. [Online]. [www.climator.com/](http://www.climator.com/)
- [5] Chiu NWJ. and Martin V., "Submerged finned heat exchanger latent heat storage design and its experimental verification," *Applied Energy*, vol. 93, pp. 507-516, 2012.

## EXPERIMENTAL RESULTS FOR PCM-AIR HEAT EXCHANGERS: MELTING AND SOLIDIFICATION IN FLAT PLATES (CSM PANELS FROM RUBITHERM)

P. DOLADO, A. LÁZARO, J.M. MARÍN, B. ZALBA; GITSE-I3A, Department of Mechanical Engineering, EINA, University of Zaragoza, Spain.

### INTRODUCTION

Experimental investigations are performed to test PCM-air heat exchange for macroencapsulated PCM in flat plates. The plates are commercially available as CSM panels from Rubitherm GmbH, and filled with RT27 (paraffin wax from Rubitherm GmbH as well). The set up of the heat exchange is shown in Fig. 1. The plates are arranged in walls of plates, allowing an air gap to let the air go through. The air flows parallel to the plates from the inlet in the top to the outlet in the bottom, exchanging heat with the plates and melting/solidifying the PCM inside them.

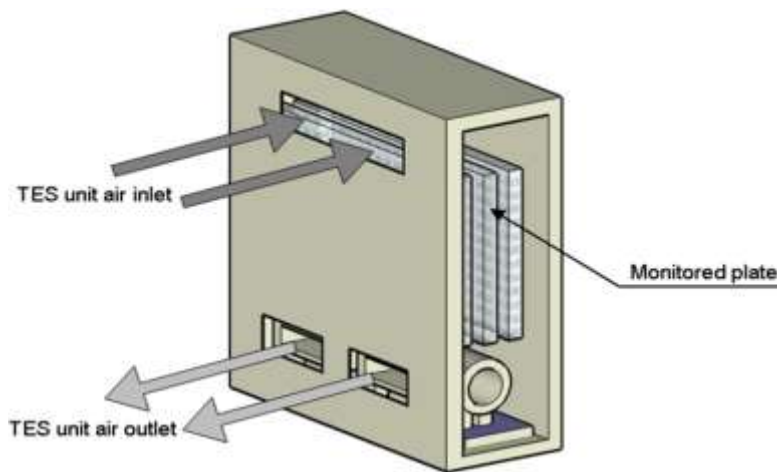


Figure 1: PCM-air heat exchanger set up

The experimental database involves:

- For the whole heat exchanger:
  - temperatures of different points at the surface of the plates
  - temperatures of the air in the air channels
  - temperature difference between the inlet and the outlet (measured with a thermopile, that was constructed based on the ANSI-ASHRAE standard [1])
  - pressure drop between the inlet and the outlet
  - air temperature at the inlet and at the outlet
  - relative humidity
  - ambient temperature
- For one single plate (see Fig. 2; the reader can find experimental data for one single plate monitoring in the corresponding Appendix):
  - temperature of three points at the surface of the plate
  - temperature of the PCM at the corresponding points inside the plate
  - temperature of the air at the inlet and the outlet of the corresponding air channel

The location of the sensors on the tested slab is shown in Figure 2. For the whole heat exchanger, 36 temperature sensors were distributed among air ducts and slab surfaces as shown in Figure 3.

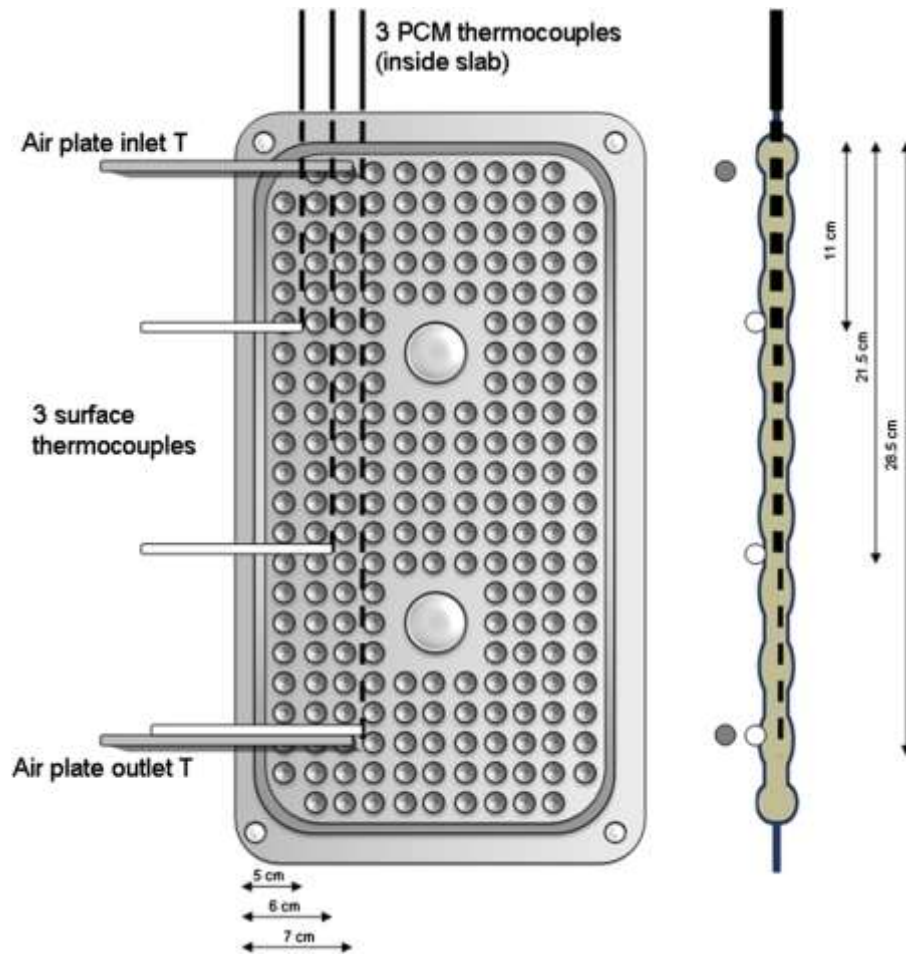


Figure 2: Compact Storage Modules by Rubitherm, layout of the T sensors over the plate

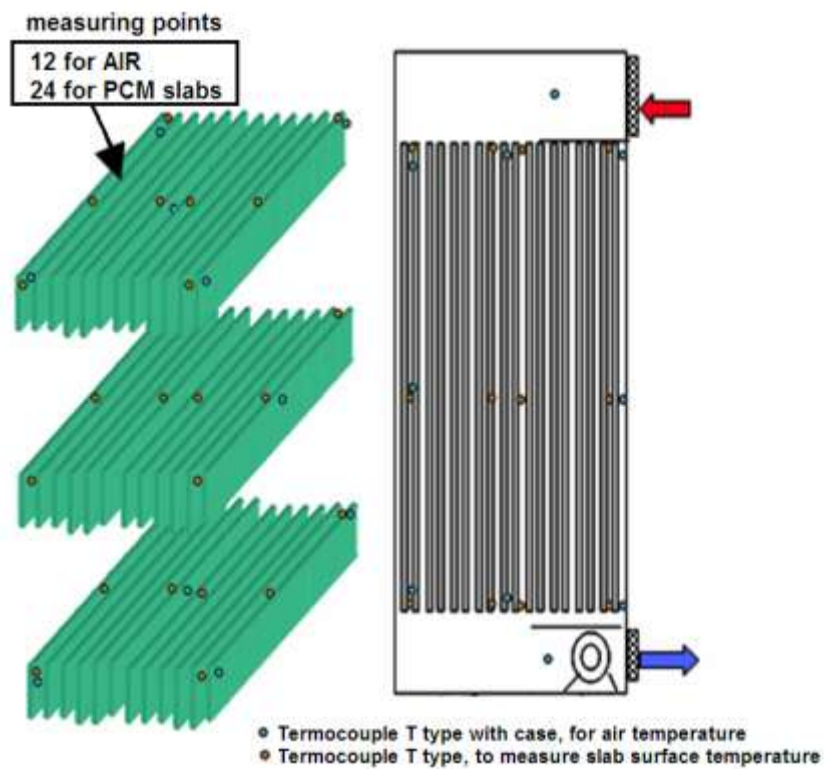


Figure 3: Temperature sensors distribution in the heat exchanger

### LAY-OUT OF THE EXPERIMENTAL SET-UP

The experimental set-up is shown in Fig. 4.

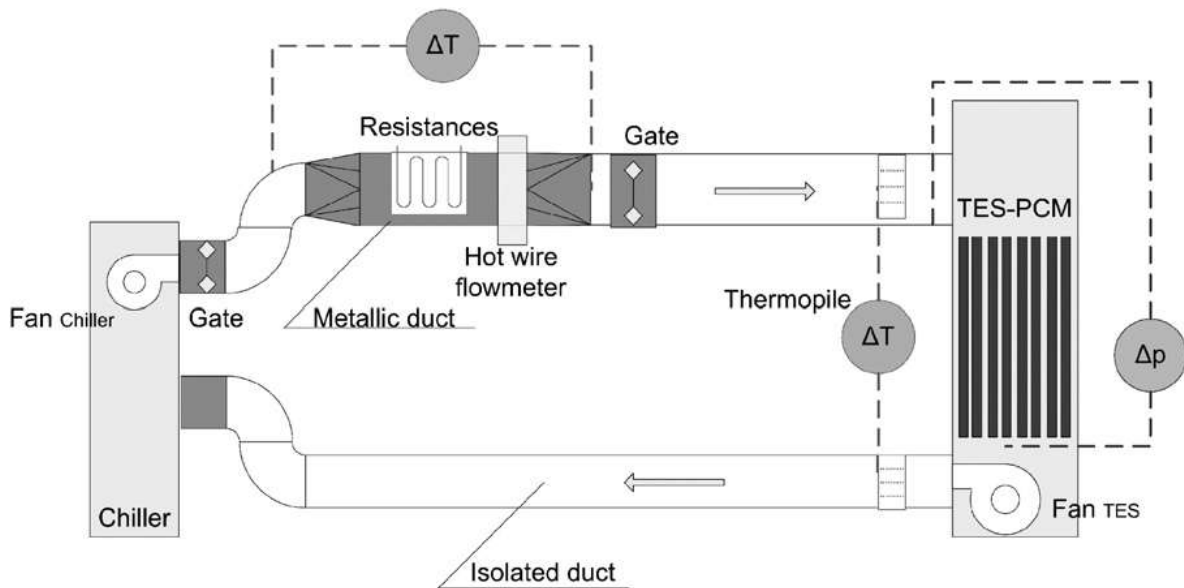


Figure 4: Experimental set-up

An experimental setup was designed to study different PCM-air heat exchangers. A closed air loop setup is used to simulate indoor conditions. Setup design was based on ANSI/ASHRAE STANDARD 94.1-2002 "Method of testing active latent-heat storage devices based on thermal performance" [1]. This setup is constituted of [2]:

- Inlet air conditioner allowing the simulation of different operating modes (5 kW air chiller and 4.4 kW electrical resistance)
- Air flow measurement
- Difference between inlet and outlet air temperatures measurement (thermopile)
- Inlet and outlet air temperature and humidity measurement
- PCM and air channels temperature measurement (over 20 thermocouples)
- Data logger and data screening
- Air ducts and gates
- PID controller

The total amount of PCM in TES is approximately 135 kg, contained in 216 plates. The outer dimensions of the plate are 450 mm per 300 mm, and 10 mm thick. The plates are arranged in walls of plates (3 plates high per 4 plates width). The 18 walls of plates are separated from each other by a 1 cm air gap. The chiller fan was single speed, while the TES unit fan had three speeds. In the energy balance the heat released by the fan is considered as a fixed quantity of watts, depending on the selected speed of the fan. Detailed information on the energy balance can be found in [6], section 3.3 (particularly page 69, Eq. 3.4). The air flow range varied from 675 m<sup>3</sup>/h to 1550 m<sup>3</sup>/h. Depending on the stage of the thermal cycling (melting or solidification of the PCM), the working equipment will be the electrical resistances (to heat the inlet air) or the chiller (to cool down the inlet air).

### **DESCRIPTION OF THE MEASURING PROCEDURE**

Measurements started after surface temperatures of the PCM slabs in the TES unit (average PCM temperature) had reached a stable value.

One of the main outputs of the PCM-air heat exchanger is the heat rate. This is determined applying an energy balance to the air between the inlet and the outlet of the heat exchanger.

$$\dot{Q}_{\text{TES}} = \dot{m} \cdot c_p \cdot (T_{\text{inlet}} - T_{\text{outlet}}) = \dot{m} \cdot c_p \cdot \Delta T$$

As the main parameters are the air flow and the air temperature difference between the inlet and the outlet, accuracy depends on the precision in measuring these parameters. The methods used are:

- Air temperature difference: Thermopile. There are three difficulties to solve in this measurement: a long period of time with small temperature difference, temperature distributions in air ducts because of its dimensions and accuracy is needed because it is a main parameter of evaluation. ANSI/ASHRAE standard recommends a thermopile to solve this problem. It was chosen because it solves these difficulties. Thermocouples are designed to measure direct temperature difference between two temperature junctions. Since a thermopile is constructed by using several junctions in series of calibrated thermocouple wire, the output signal is amplified by the number of junctions, so sensibility is increased. In this case, a six junction thermopile is used. In order to have representative measurements of air temperature difference, each junction is located at the centre of equal cross section areas. Therefore, the temperature difference is measured involving the complete sectional area. Precision is then 0.51 °C, better than when using two Pt100 (0.65 °C) and also sensibility and temperature distribution evaluation are improved.
- Air flow: energy balance of electrical resistances. Air temperature changes during a test, therefore most of air flow measurements methods are not suitable for transitory measurements. Mass flow depends only on fan velocity; therefore it is measured by applying an energy balance on electrical resistance. The maximum power is set to electrical resistances. The energy consumption is measured with a 1% uncertainty and air temperature difference caused in the air by passing through the electrical resistances is measured by a thermopile with an accuracy of 0.51 °C.
- Air humidity: two sensors are used to measured air humidity at the inlet and the outlet. The maximum air humidity variation during a test was 0.006 kg/kg<sub>da</sub>. It is lower than the 0.2% of total stored energy, therefore, it was confirmed that latent energy variation is negligible in energy balance of air for cooling power evaluation.

## **RESULTS**

As an example, the experimental results of a test using constant setpoint air inlet temperature are shown in Figs. 5 and 6. In these two plots different temperature measurements are shown, the first for the whole heat exchanger and the second for one single plate.

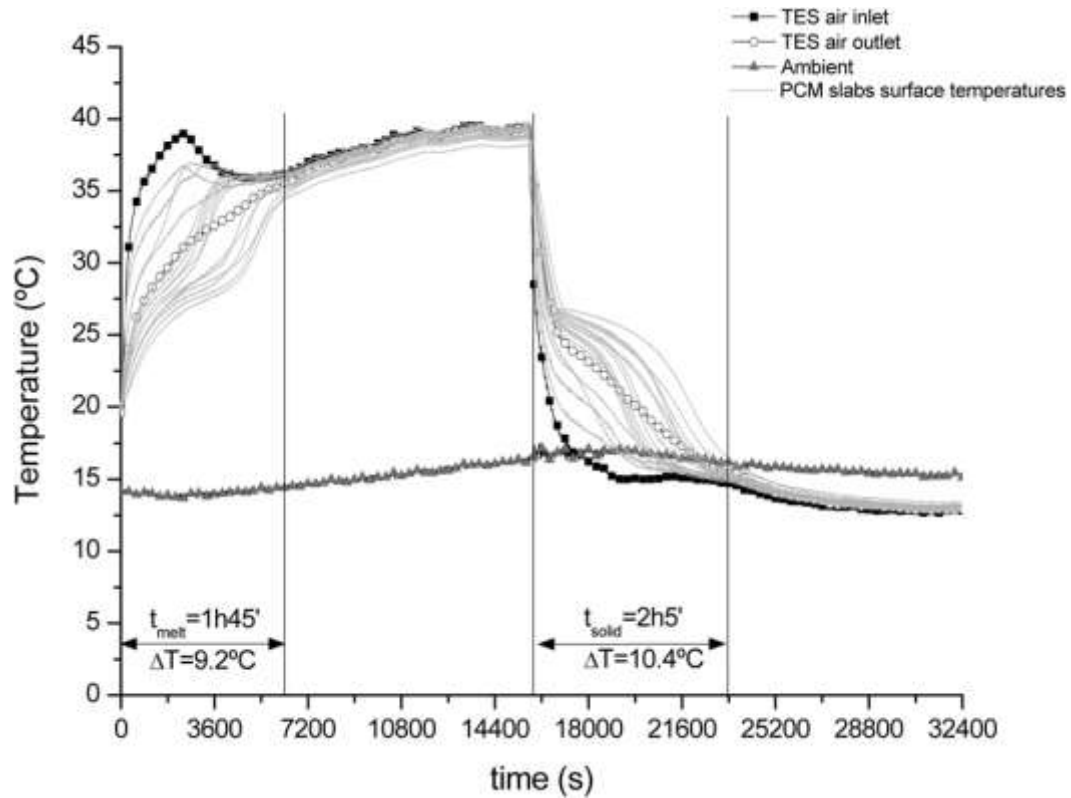


Figure 5: Experimental results for a full cycle: TES air inlet and outlet temperatures, ambient temperature, and surface temperature distribution of the plates inside TES

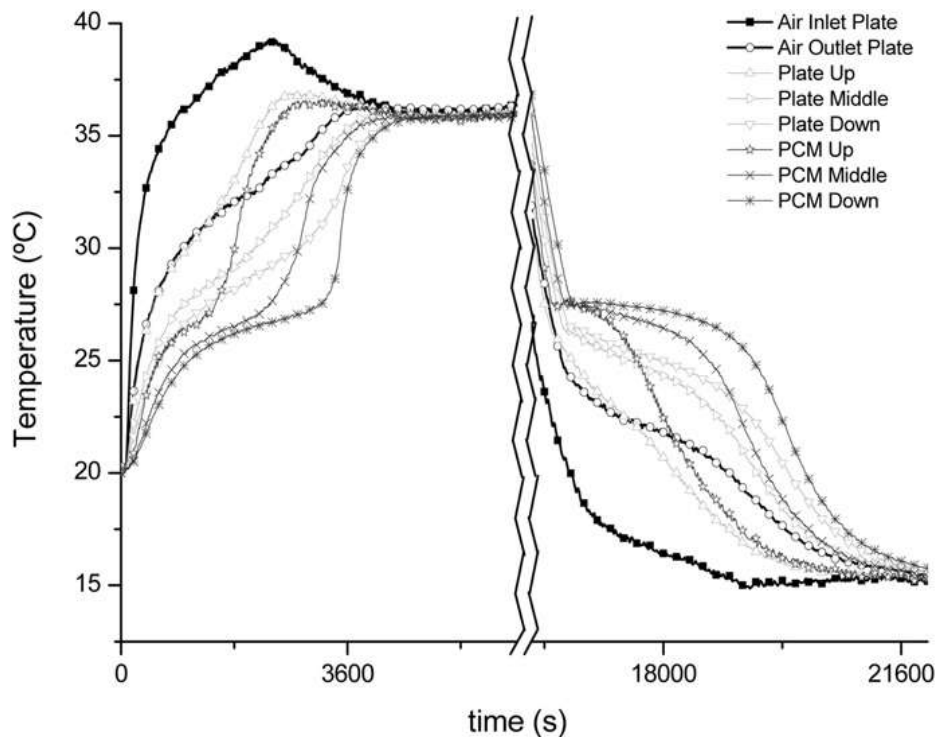


Figure 6: Experimental results for a full cycle, single-plate monitoring (air-plate surface-PCM temperatures)

In Fig. 7 the experimental heat rate (determined by means of the previous energy balance) is plotted as well as the total energy stored on each stage (melting or solidification).

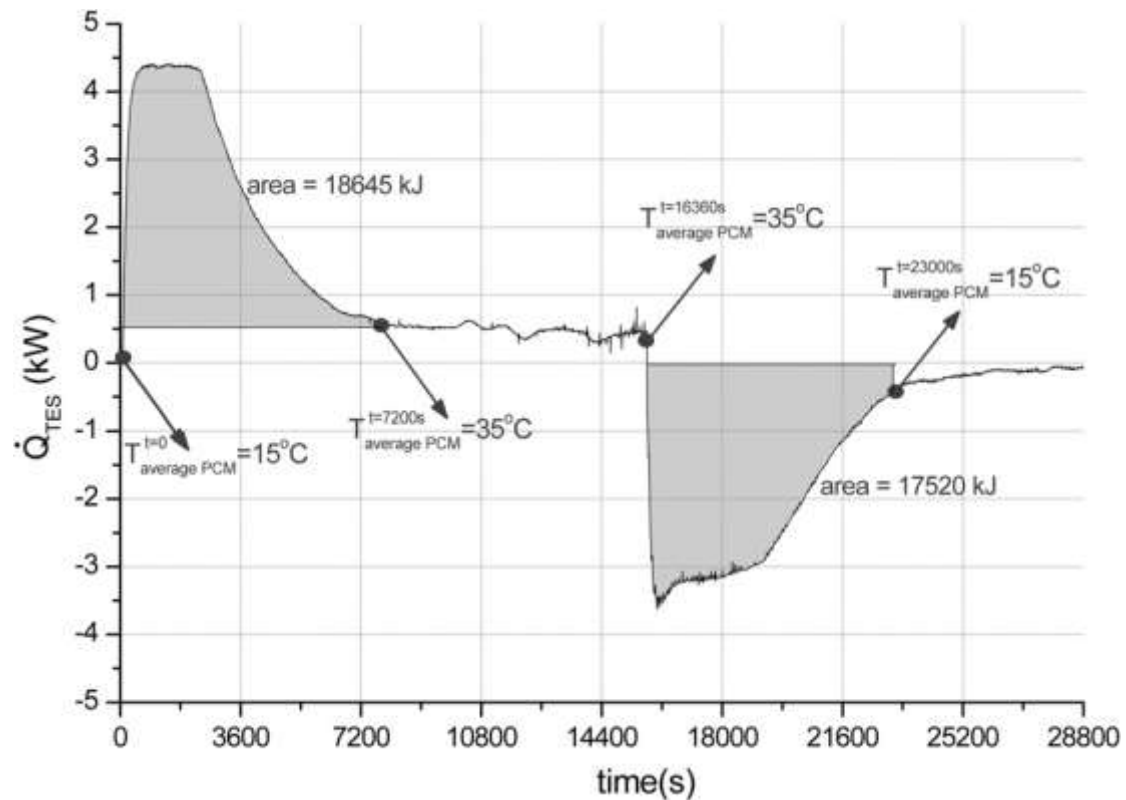


Figure 7: Heat rate curve and total energy exchanged

### CLOSURE

An experimental database has been created for melting and solidification of PCM in CSM panels exchanging heat with air as heat transfer fluid in a PCM-air heat exchanger. Thus, these data can be used for benchmarking. Further information is available (see the Bibliography section or contact [dolado@unizar.es](mailto:dolado@unizar.es)).

### BIBLIOGRAPHY

- [1] ANSI/ASHRAE STANDARD 94.1-2002 (updated by 94.1-2010). Method of testing active latent-heat storage devices based on thermal performance.
- [2] A. Lázaro, P. Dolado, J.M. Marín, B. Zalba, PCM-air heat exchangers for free-cooling applications in buildings: Experimental results of two real-scale prototypes, *Energy Conversion and Management*, vol. 50 (2009), no. 3, pp. 439-443.
- [3] A. Lázaro, P. Dolado, J.M. Marín, B. Zalba, PCM-air heat exchangers for free-cooling applications in buildings: Empirical model and application to design, *Energy Conversion and Management*, vol. 50 (2009), no. 3, pp. 444-449.
- [4] P. Dolado, A. Lázaro, J.M. Marín, B. Zalba, Characterization of melting and solidification in a real-scale PCM-air heat exchanger: Numerical model and experimental validation, *Energy Conversion and Management*, vol. 52 (2011), pp. 1890-1907.
- [5] P. Dolado, A. Lázaro, J.M. Marín, B. Zalba, Characterization of melting and solidification in a real scale PCM-air heat exchanger: Experimental results and empirical model, *Renewable Energy*, vol. 36 (2011), pp. 2096-2917.
- [6] P. Dolado, Thermal Energy Storage with phase change. Design and modelling of storage equipment to exchange heat with air, Ph.D. Thesis, University of Zaragoza, Spain, 2011.; ISBN: 978-84-694-6103-7. Available online (Spanish only) at: <http://zaguan.unizar.es/record/6153?ln=es>.

## HEAT STORAGE SYSTEM COUPLED WITH A PHOTOVOLTAIC PANEL

V. LO BRANO, G. CIULLA, M. CELLURA; Department of Energy, University of Palermo, Italy.

### INTRODUCTION

A key element of a wider dissemination of PV systems is represented by high power conversion efficiency. Concerning this point, the energy produced by a PV cell depends, apart materials, also on other two important parameters:

- the amount of the incident radiation;
- the temperature of the PV cell.

The performance of a PV panel in fact is defined by manufactures according to the "peak power", which identifies the maximum electric power supplied by the PV panel when it receives an insolation of  $1 \text{ kW/m}^2$  and the cell temperature is maintained at  $25 \text{ }^\circ\text{C}$ . These conditions are nominal only because solar radiation has a variable intensity and the panel is subjected to significant temperature changes, with temperature values higher than  $25 \text{ }^\circ\text{C}$ . In real conditions performances of a PV panel are different from those declared under the nominal conditions and the conversion efficiency decreases when temperature of the cell increases.

Among other measures aimed to increase the energy conversion, we investigated the application of PCMs (Phase Change Materials).

The idea to couple the PCMs with the photovoltaic technology arises from features of these materials to absorb large amounts of heat (keeping almost constant the temperature) when the heat is not required. Indeed overheating causes a drop in efficiency of the photovoltaic cells. The absorbed heat should be then released to the surrounding air during the night when the panel does not produce electrical power. The application of PCM in PV systems has been experimentally and numerically studied by several authors [1-6].

### PV-PCM Model

Considering a PV panel coupled with PCM system, the energy balance must take into account the presence of the phase-change material. Schematically, the energy exchanges in a PV-PCM system can be exemplified by the figure. Thanks to the presence of a simple geometry it was possible to choose a one-dimensional approach, considering only the heat flow orthogonal to the PV plane.

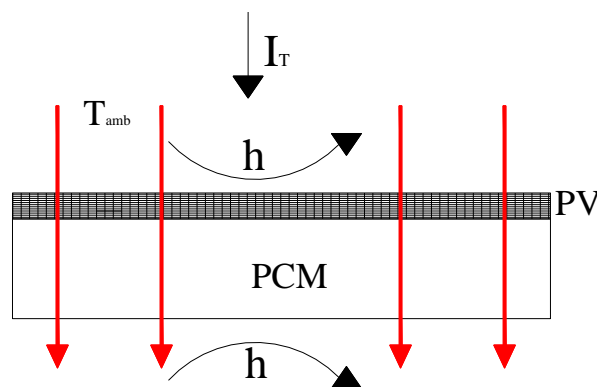


Figure 1: PV-PCM schema of the PV-PCM system

In detail, the system is composed by a:

- tempered glass sheet ( $\lambda = 1.3 \text{ W/mK}$ ) with a thickness of 3.2 mm (Glass layer);
- 1 mm of PET plastic panel ( $\lambda = 0.15 \text{ W/mK}$ ) on which are "printed" the silicon cells; the silicon cells are considered having negligible thickness (PET layer);
- an optional layer of air interposed between the panel and the heat storage system representing a possible imperfect contact (Air layer); a plastic layer ( $\lambda = 0.15$

W/mK) that takes into account the bag that contains the PCM (bag layer); this is a vacuum plastic bag of 20cm x30 cm.

- the PCM layer;

Figure 2 represents a section of the geometry along the thickness of the PV-PCM system where it is possible to identify all the involved layers: the glass panel, the PET panel, the layer of air due to the imperfect contact of the envelope of PCM with the PV, the thickness of the envelope containing the PCM and the PCM layer itself.

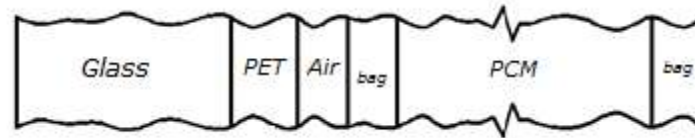


Figure 2: PV-PCM cross-section

The PV-PCM system is presented as a multi-layer plate invested by solar radiation and exchanging heat with the external environment by convection and radiation. Depending on the properties of the PCM and on the amount of energy captured from the panel, the layer of PCM can partially or totally melt during the maximum insolation, and returns that amount of energy, possibly solidifying again, during the night. The first hypothesis is that the phase change is isothermal. In case of non-isothermal transition, having the value of  $c_p$  with temperature, the problem is reduced to a heat conduction case. The occurrence of a phase change that keeps the temperature at a given value is a more interesting case and implies the determination of the PCM liquid fraction.

In general terms, commercial PCMs have a thermal window; only pure substances show an isothermal phase change

The balance equations were written by finite difference model considering a one-dimensional approach with constant thermo-physical properties and without internal heat generation. It was necessary to distinguish the energy balance of border nodes.

We developed an algorithm that can easily be implemented in a software procedure that uses a common programming language like VB.NET. Authors developed a software tool implementing the discussed algorithm shown in Fig. 3.

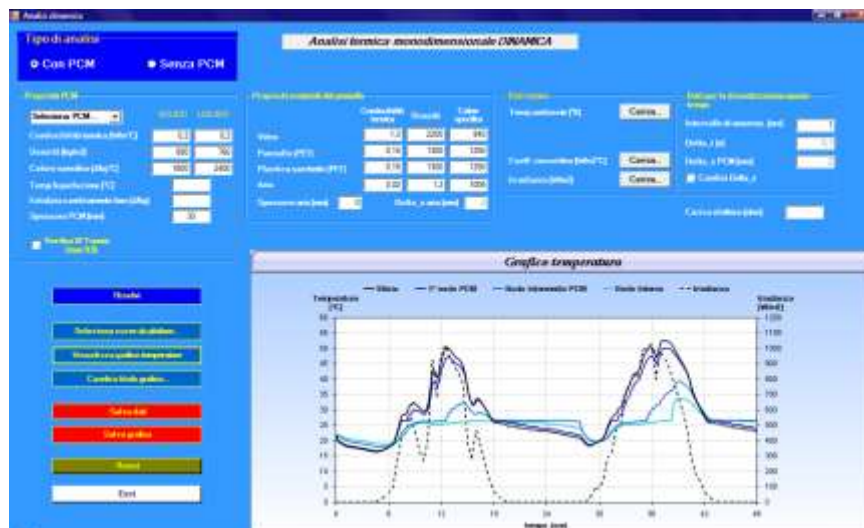


Figure 3: Front panel of the developed software

## EXPERIMENTAL SYSTEM

To perform the measurements, an experimental system was made up and situated on the top of the Energy Department of University of Palermo, (38°07' N, 13°22' E). Two

identical PV panels by Kyocera manufacturers' have been chosen (KC175GHT-2), one of which is coupled to PCM (Fig.4).

To secure a proper PV-PCM system configuration it was decided to install PCM in the bottom part of PV panel using a perforated metal mesh bolted into the frame of the panel. The silicon temperature was measured using thermocouples (type T, copper-constantan) installed into little holes made in the PET (Polyethylene Terephthalate) rear film of the panel, in order to improve the thermal contact with the cell silicon back face. To evaluate the real performance of PV panel, the electrical circuit has been linked to precision resistances (Vishay RH250) with a tolerance of  $\pm 1\%$  and a temperature coefficient of  $\pm 50$  ppm/ $^{\circ}\text{C}$ . To avoid that the presence of an ammeter altered the value of the electrical load connected to the panel, especially with the lowest values of electric resistances, the current was calculated on the basis of the measured voltage, accepting the error due to the precision resistances.



Figure 4: PV panel experimental system

### **SIMULATION AND RESULTS**

To study the influence of PCM, as previously described, two identical PV panels were monitored, one of which was applied to the PCM. The field measurements were launched in the summer months as these are characterized by higher irradiance values.

The electrical load also has been changed frequently in order to observe the system response to load variations. Therefore, numerical simulations were performed on different days. The results were compared with measured data. In detail, the comparison was made between temperature and electrical power, measured and calculated.

In the following table, the thermo-physical characteristics of the PCMs used in this work are listed. The graphs below show some of the results that were obtained comparing the trends of the measured and simulated temperatures.

Table1: Thermo-physical characteristics of the RT27 PCM

PCM		
Transition phase	25-28	$^{\circ}\text{C}$
Solid density	0.88	kg/l
Liquid density	0.76	kg/l
Specific enthalpy of phase change	184	kJ/kg
Thermal Conductivity	0.2	W/mK
Volumetric change	16	%

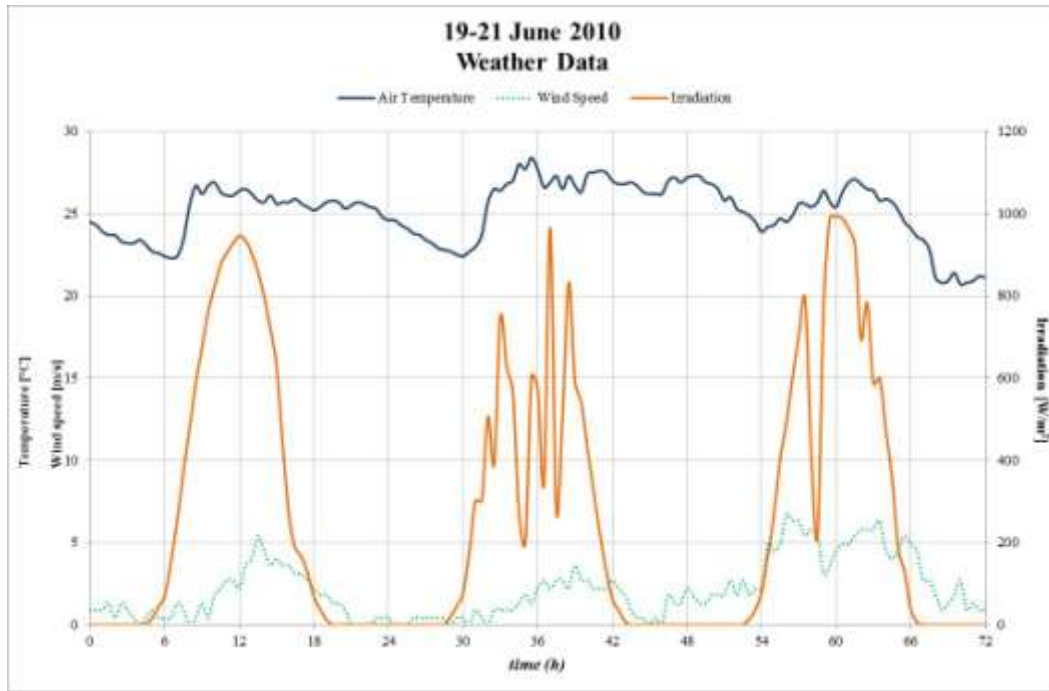


Figure 5: The figure represents the trends of climatic parameters in Palermo, June 19 to 21

Table 2: Climatic parameters in Palermo, June 19 to 21

Mean value		
Air Temperature	25.14	°C
Irradiation	264.75	W/m <sup>2</sup>
Wind Speed	2.1	m/s

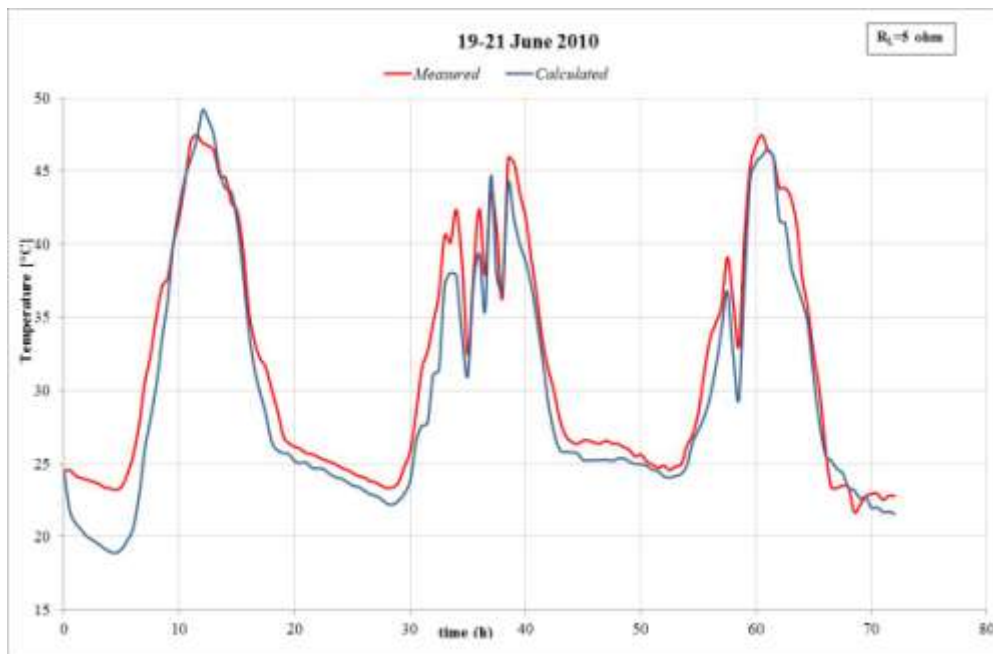


Figure 6: Temperature trend of the measured and simulated PV-PCM system, in Palermo, June 19 to 21

## COMMENTS AND CONCLUSIONS

Looking at the graphs represented before, it is possible to see as the calculated temperature trends are in good agreement with measured temperatures, validating the reliability of the calculation model.

The calculated temperatures at night are significantly lower than the comparable measured: this is an indication of an incorrect estimate irradiative heat exchange, which were estimated under the assumption of the sky always clear. Table 3 shows that the differences between the measured and calculated values are lower than 10% of average temperature. The comparison is based on the following definitions:

- Average gap:  $\sum_{i=1}^n \frac{(T_{mea} - T_{cal})}{n}$
- Absolute average gap:  $\sum_{i=1}^n \frac{|T_{mea} - T_{cal}|}{n}$
- Average Deviation:  $\sum_{i=1}^n \frac{|T_{cal} - T_{mea}|}{T_{mea}} / n$
- the maximum negative gap:  $\min \sum_{i=1}^n (T_{cal} - T_{mea}) ;$
- the maximum positive gap:  $\max \sum_{i=1}^n (T_{cal} - T_{mea}) ;$

where  $T_{mea}$  is the measured temperature [°C],  $T_{cal}$  is the calculated temperature [°C] and  $n$  in the number of samples.

Table 3: Comparison between measured and calculated temperatures

PV panel	
Average gap	2.32 [°C]
Absolute average gap	2.48 [°C]
Max negative gap	-2.72 [°C]
Max positive gap	8.51 [°C]
Average Deviation	7.39%
PCM	
Average gap	1.67 [°C]
Absolute average gap	1.87 [°C]
Max negative gap	-2.21 [°C]
Max positive gap	5.22 [°C]
Average Deviation	6.11%

The results show that the proposed model is valid and can be used to determine the thermal behaviour of a multilayer wall in which there is a phase change material. The model was validated by comparison with the analytical solution of the Voller and Cross problem and then by using an experimental setup with PV panel.

The good agreement between experimental measurements and numerical predictions have shown that the algorithm, although simplified and in one-dimensional geometry, can be used to determine the trend in temperature of a multilayer wall accompanied by a PCM

**BIBLIOGRAPHY**

- [1] Huang M.J., Eames P.C., Norton B., Thermal regulation of building-integrated photovoltaics using phase change materials, *International Journal of Heat and Mass Transfer* 47 (2004) 2715–2733.
- [2] Huang M.J., Eames P.C., Norton B., An experimental study into the application of phase change materials to limit the temperature rise in build integrated photovoltaic systems, *Proceedings of Renewable Energy in Maritime Island Climates*, September, Belfast, UK, 2001, 143-150.
- [3] Huang M.J., The application of CFD to predict the thermal performance of phase change materials for the control of photovoltaic cell temperature in buildings, *Proceedings of VI World Renewable Energy Congress*, July, Brighton, 2000, 2123-2126.
- [4] Huang M.J., Eames P.C., Norton B., Phase change materials for limiting temperature rise in building integrated photovoltaics, *Solar Energy* 80 (2006) 1121–1130.
- [5] Cellura M., Lo Brano V., Orioli A., et al., Miglioramento della resa energetica di un pannello fotovoltaico per mezzo di materiale a cambiamento di fase, *ATI 2009*, L'Aquila, Italy.
- [6] Cellura M., Lo Brano V., Orioli A., et al., A Photovoltaic panel coupled with a phase changing material heat storage system in hot climates, *DREAM University of Palermo, PLEA*, Dublin, 2008.
- [7] Frank P. Incropera, David P. DeWitt, *Fundamentals of Heat Mass Transfer*, 5<sup>th</sup> edition, ISBN 0471386502.
- [8] E V.R. Voller and M. Cross, Accurate Solutions of Moving Boundary Problems Using Enthalpy Method. *Int. J. Heat Mass Transfer* 24 (1981).
- [9] L. Rubenstein, *The Stefan Problem*, *Transactions in Mathematics Monograph No. 27*. American Mathematical Society, 1971

## Thermo-Chemical Material Models

### INTRODUCTION

Households use a large amount of their energy consumption for space heating and domestic hot water. The energy consumption in the built environment can be reduced by energy saving measures (improved insulation, heat recovery, etc.). A substantial part of the remaining energy demand can be fulfilled by using renewable energy sources such as solar energy. During summer, the heat demand can be completely covered using solar heat, but in winter the heat demand exceeds the solar supply. To accommodate this lag between the solar energy surplus in summer and the energy demand in winter, a seasonal thermal storage is needed.

Traditionally, water is used for storing solar heat (for example, solar boiler) for short time periods. However, water-based long-term heat storage will require a large tank ( $>50 \text{ m}^3$ ) that is often too large to be placed inside a building. As an alternative, it is possible to store energy by means of chemical processes, making use of the reversible reactions  $C + \text{heat} \leftrightarrow A + B$ .

In the charging mode during summer, solid C dissociates under the influence of solar heat into components A and B, which are stored separately. In the discharging mode during winter, the two components (A and B) react to form solid C while releasing the stored solar heat. No reactions occur as long as the two components A and B are stored separately. Preliminary calculations show that sensible heat losses comprise approximately 10% of the total energy storage; this means that the remaining energy can be stored loss-free.

The Table below gives a list of candidate Thermo-Chemical Materials which can be used for long-term heat storage, see [1]. Dependent on their loading temperatures, energy densities, power densities and recyclability, TCM-materials can be used for (long-term) heat storage in the built environment and/or industry. To gain more insight into the heat and mass transfer processes taking place in these materials during charging and discharging, numerical modeling is needed ranging from the molecular- and micro-scale up to the macro- and reactor-scale. This insight can be used in a later stage to optimize specific properties of the storage materials with respect to their usage. The next chapters present an overview of the state-of-the-art modeling techniques on the various scales.

*Candidate TCM-materials for long-term heat storage (from [1])*

C	$\leftrightarrow$	B	+	A	GJ/m <sup>3</sup>	T(°C)	score
MgSO <sub>4</sub> · 7H <sub>2</sub> O		MgSO <sub>4</sub>		7H <sub>2</sub> O	2.8	122	9.5%
SiO <sub>2</sub>		Si		O <sub>2</sub>	37.9	4065	9.0%
FeCO <sub>3</sub>		FeO (wustite)		CO <sub>2</sub>	2.6	180	6.3%
Fe(OH) <sub>2</sub>		FeO		H <sub>2</sub> O	2.2	150	4.8%
CaSO <sub>4</sub> · 2H <sub>2</sub> O		CaSO <sub>4</sub>		2H <sub>2</sub> O	1.4	89	4.3%
MgSO <sub>4</sub> · H <sub>2</sub> O		MgSO <sub>4</sub>		H <sub>2</sub> O	1.3	216	2.7%
ZnCO <sub>3</sub>		ZnO		CO <sub>2</sub>	2.5	133	1.6%
CaCl <sub>2</sub> · 2H <sub>2</sub> O		CaCl <sub>2</sub> · 1H <sub>2</sub> O		H <sub>2</sub> O	0.6	174	1.1%
MgSO <sub>4</sub> · 7H <sub>2</sub> O		MgSO <sub>4</sub> · 1H <sub>2</sub> O		H <sub>2</sub> O	2.3	105	1.1%

- [1] Visscher, K., Veldhuis, J. B. J., Oonk, H. A. J., van Ekeren, P. J., and Blok, J.G., 2004, "Compacte Chemische Seizoenopslag Van Zonnearmte; Eindrapportage," ECN Report No. ECN-C-04-074.

## HYDRATION AND DESHYDRATION OF SORPTION MATERIALS: EXPERIMENTS IN A SMALL-SCALE REACTOR

Camilo RINDT and Hadi RAJAEI, Eindhoven University of Technology, Eindhoven, The Netherlands.

### INTRODUCTION

In the present study a small-scale reactor is built in which controlled adsorption and desorption experiments are carried out. During the hydration and dehydration cycle temperature profiles are measured in the reactor to gain insight into the heat and mass transfer processes. Firstly a general description is given of the experimental set-up with special attention to the design of the reactor. Secondly some results are presented of adsorption and desorption experiments of zeolite 13X. Finally some conclusions are drawn and contact details are presented.

### LAY-OUT OF THE EXPERIMENTAL SET-UP

#### The setup

The main components of the experimental device are the reactor, a heater and an evaporator. Figure 1 shows a lay-out of the experimental setup. At the left hand side, compressed air is delivered at a pressure of 7.5 bar and a relative humidity of 2.5 % at 25°C. The incoming dried air flow is measured and regulated by a gas flow controller (GFC). During a desorption experiment this air flows at the bottom side of the setup through the heater into the reactor. During an adsorption experiment water is pressed out of the water vessel by the pressurized airflow and measured by the liquid flow controller (LFC), resulting in a water-air stream into the controlled evaporator mixer (CEM). By giving set points for the air and water flow, the absolute humidity can be controlled. Then the humidified air flows into the reactor. A relative humidity/temperature sensor is used to measure the humidity and temperature at the outflow and a thermocouple data logger is used to readout the temperature profiles in the reactor. A more detailed description of the experimental device can be found in Rajaei [2012].

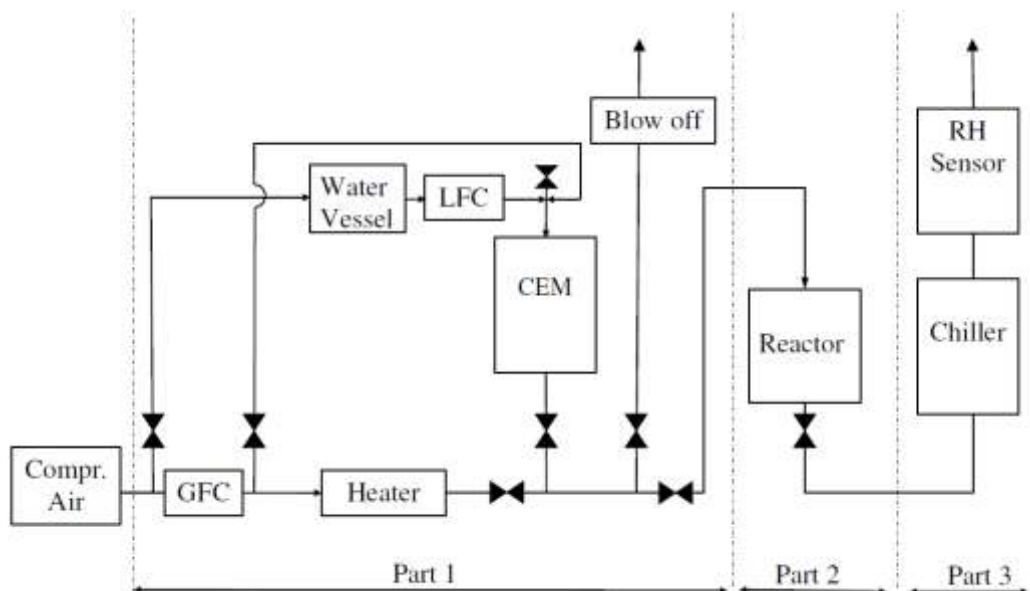


Figure 1: Lay-out of the experimental setup

#### Dimensions and design

Figure 2 shows a schematic view of the reactor and the positioning of the thermocouples and pressure gauges. The reactor is made of multiple materials. The inner shell is made of Teflon. The Teflon layer is used because of its low thermal conductivity characteristics, leading to large temperature differences over the wall, which are relatively easy to measure. The middle layer is made of stainless steel. A layer of insulation is applied at the outer part of the reactor. The outer side of the insulation is covered with a layer of

tape. The air enters the reactor from the top side and leaves the reactor at the bottom, preventing the particles to go to a fluidized state. At the bottom of the reactor a filter is applied with a pore size is 40 micron. Table 1 shows all material characteristics of the reactor. Total mass of the reactor (including bolts, nuts and flanges) is around 4.7 kg.

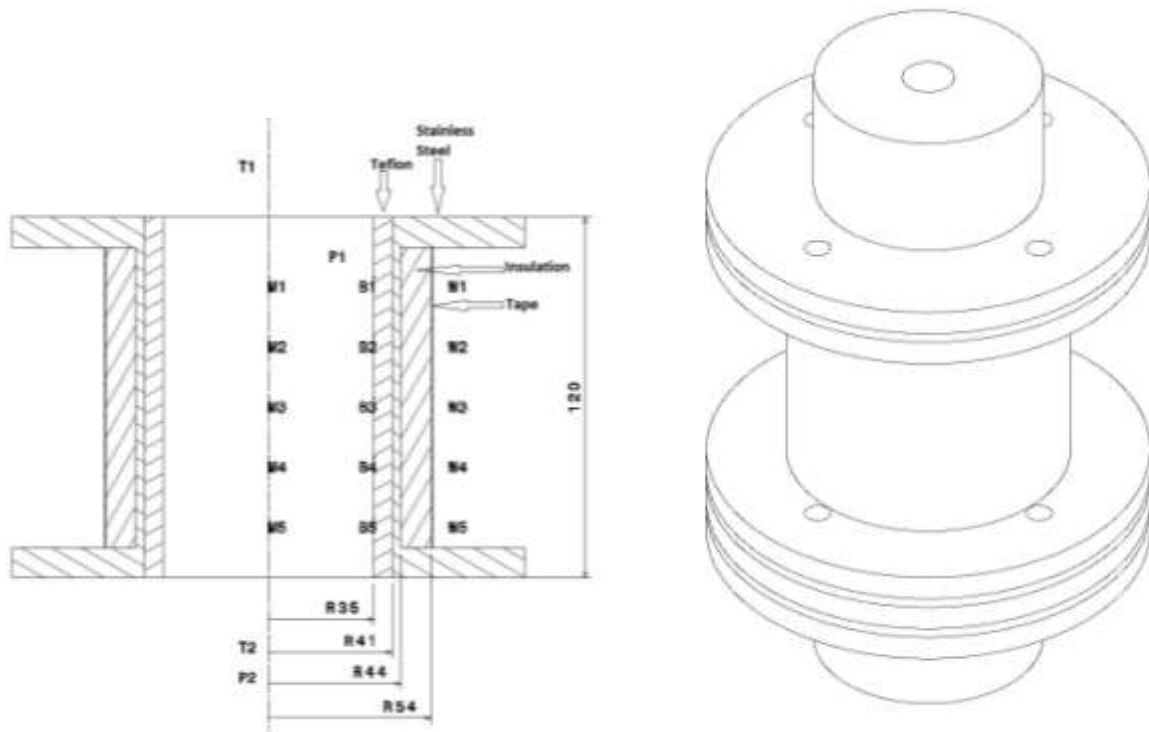


Figure 2: Schematic view of the reactor and the positioning of the thermocouples and pressure gauges (left). All dimensions are in mm. Perspective view of the reactor (right).

Table 1: Material characteristics of the reactor (not measured but taken from specifications or from literature)

Material	Density (kg/m <sup>3</sup> )	Heat Capacity (J/kg.K)	Thermal conductivity (W/m.K)
Teflon	2200	1005	0.25
Stainless steel	8238	468	13.4
Insulation	192	1000	0.04
PEEK (Filter)	1320	320	0.25

### Material properties

Around 248 grams (weighted at ambient temperature and humidity) zeolite 13X pre-dried (dried at a temperature of 200°C for two hours) was used for the adsorption and desorption experiments. Table 2 shows the properties of zeolite 13X.

*Table 2: Properties of zeolite 13X (not measured but taken from literature)*

Material	Diameter of pellets (mm)	Density (kg/m <sup>3</sup> )	Heat Capacity (J/kg.K)	Thermal conductivity (W/m.K)
Zeolite 13X	1.3-2.5	1876	1047	0.076

### **DETAILED DESCRIPTION OF THE MEASURING PROCEDURE**

17 thermocouples are attached to the reactor. T1 and T2 measure the inlet and outlet temperature, respectively. M1 up to M5 measure the temperature over the bed. B1 up to B5 are attached at the inner side of the Teflon wall, measuring the inner wall temperature. The thermocouples labeled W1 up to W5 are used to measure the outer wall temperatures. The thermocouples M and B are of type T. The thermocouples attached to the wall are of type K. In the reactor, every 2 cm a thermocouple is positioned. The filter is mounted at the bottom and has a thickness of 0.5 cm. The distance between bottom side of the reactor and M5 is 2.5 cm (total length of the reactor and filter is 12.5cm). Thermocouples T1 and T2 are positioned in the gas stream leading to typical measuring errors in the range of 2%. The humidity/temperature sensor has an accuracy of 1.5% on the relative humidity and 0.2°C on the temperature. It can measure from 0% to 100% of relative humidity and its response time is less than 15s. Since there are only 16 slots available at the data acquisition system, not all temperatures are measured simultaneously. Furthermore, two slots are required for measuring the humidity and temperature at the outlet. So, 14 slots remain available to measure temperatures in the reactor. To this end the 3 thermocouples labeled W1, W3 and W5 are not used in the presented measurements. Two pressure gauges are positioned at the inlet and outlet of the reactor to measure the pressure difference over the reactor. The reactor is filled with more or less spherical particles of zeolite 13X on top of the filter. The particle bed is not pressed, leading to a 'natural' porosity in the range of around 0.6 (not measured).

At the start of the experiment the reactor was in thermal equilibrium with the surroundings.

### **RESULTS**

#### Adsorption

During the adsorption experiment a regulated gas flow of 24 l/min and a liquid flow of 0.28 g/min enter the reactor. These numbers result in a relative humidity of 59%. The 248 grams of zeolite used in the adsorption experiment resulted in a bed height of 8.5 cm, covering M2. The experiment lasted 6 hours until the reaction ceased. Figure 3-top shows the temperature profiles in the reactor bed. The reactor inlet temperature is 17.5 °C which is different from the temperature of the compressed air (25°C). This difference comes from the required energy for evaporation of water droplets.

The maximum temperature reached was 54°C which occurred at the top of the bed. The outlet temperature remains constant for almost 4 hours at 42°C. The temperature profiles for T1 and M1 are identical. The thermocouples M2, M3, M4 and M5 show successive temperature peaks and this indicates a moving reaction front. The smaller this front, the more concentrated the energy released and so the higher the temperatures reached. Deeper in the reactor, the reaction front stretches out and the elevated temperatures last longer. This is caused by the fact that not all water vapor is consumed within the reaction front so material downstream the reaction front will hydrate in steps. So, deeper inside the reactor zeolite 13X loses some of its stored energy before the reaction front passes

and, as a consequence, less elevated temperatures are reached which last longer. The reaction ceased after 5 hours (300 min) when the outlet temperature drops close to the inlet temperature.

Figure 3-bottom shows the outlet humidity. The vapor inflow is kept constant by the liquid flow controller and has a value of 0.28 g/min during this experiment. The vapor outflow is not constant: at the start of the experiment it decreases to zero. In this period of time, all the supplied water vapor is consumed by the reaction. After 50 minutes it starts to rise and it stabilizes after 300 minutes. According to the measurements 56.3 grams H<sub>2</sub>O was absorbed in 300 minutes which is 22 %wt of the zeolite.

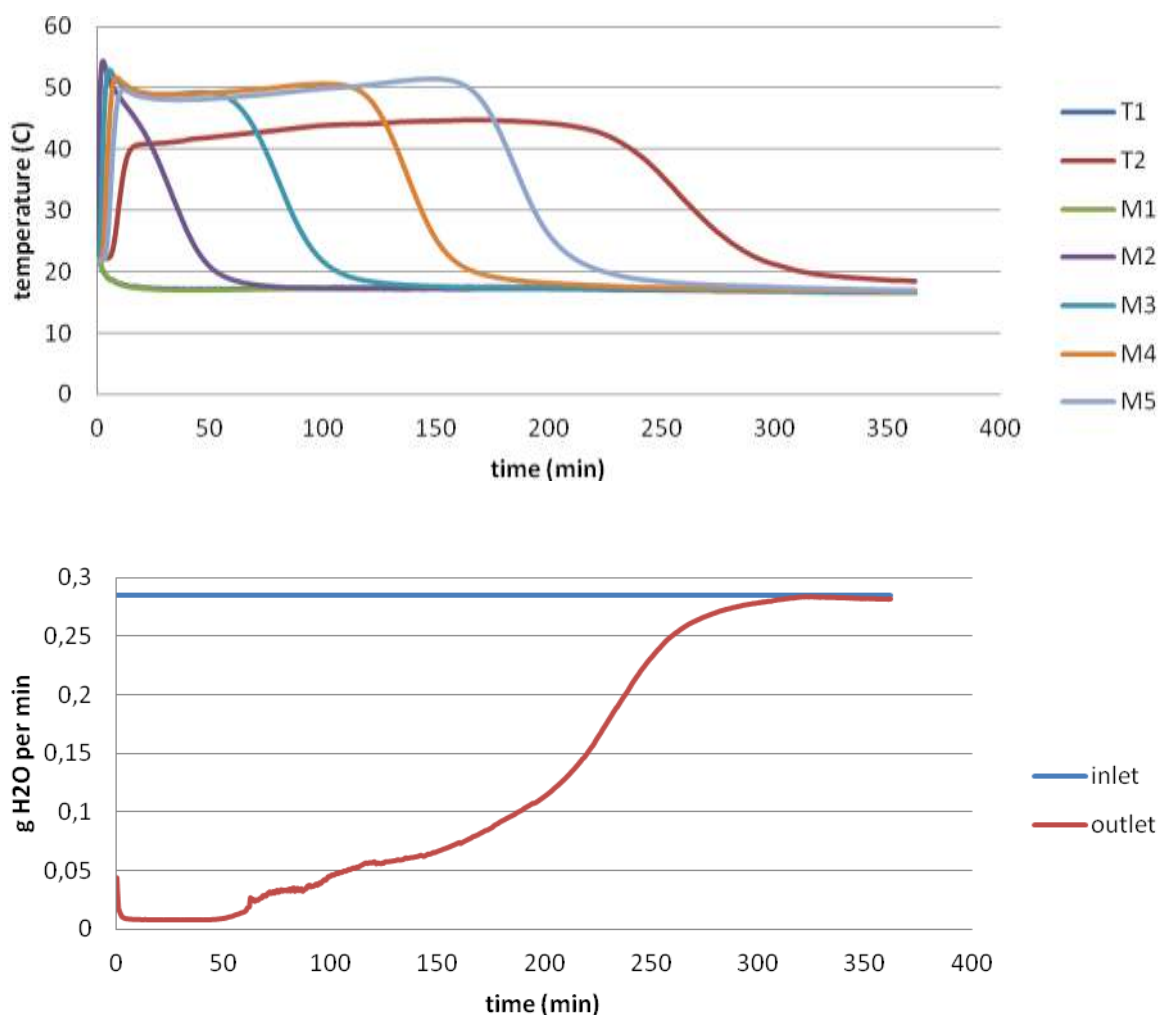


Figure 3: Temperature profile (top) and vapor in- and outflow (bottom) as function of time during the adsorption reaction of zeolite 13X

### Desorption

For the desorption experiment the heater was set to a heating rate of 1°C per minute. The maximum temperature was set to 200°C and the heater kept the maximum temperature for 2 hours. Figure 4-top shows the temperature profiles during the desorption experiment. At the beginning of the experiment the temperature at several positions drops a few degrees below the inlet temperature because water is expelled and process absorbs heat. As the inlet flow gradually heats up, the reactor temperature increases as well.

The outlet humidity graph shows that at the beginning of the desorption, a huge amount of water is expelled. Zeolite 13X has a maximum water uptake of 30 wt%. Figure 4-bottom shows that the vapor content decreases in time. The water vapor content starts at 1 g/min and decreases quickly in the first 10 minutes. The incoming dry air causes the

weakly bonded water molecules to separate from the zeolite. By further heating the air, more vapor is released from the zeolite (second peak at  $t = 45$  min). The vapor content that is released from the zeolite gradually reduces, but is more or less constant between  $t = 100$  min and  $t = 170$  min. In this time interval the temperature of the incoming air is ranging between  $70^{\circ}\text{C}$  and  $130^{\circ}\text{C}$ . The total amount of water expelled from the zeolite during the experiment was 70 grams, which is 28 wt%. The zeolite apparently released more water than it took up in the adsorption experiment as described above. Possibly the zeolite was not fully dehydrated before the start of the adsorption experiment. The vapor content of the incoming heated air stream was  $0.038$  g/min.

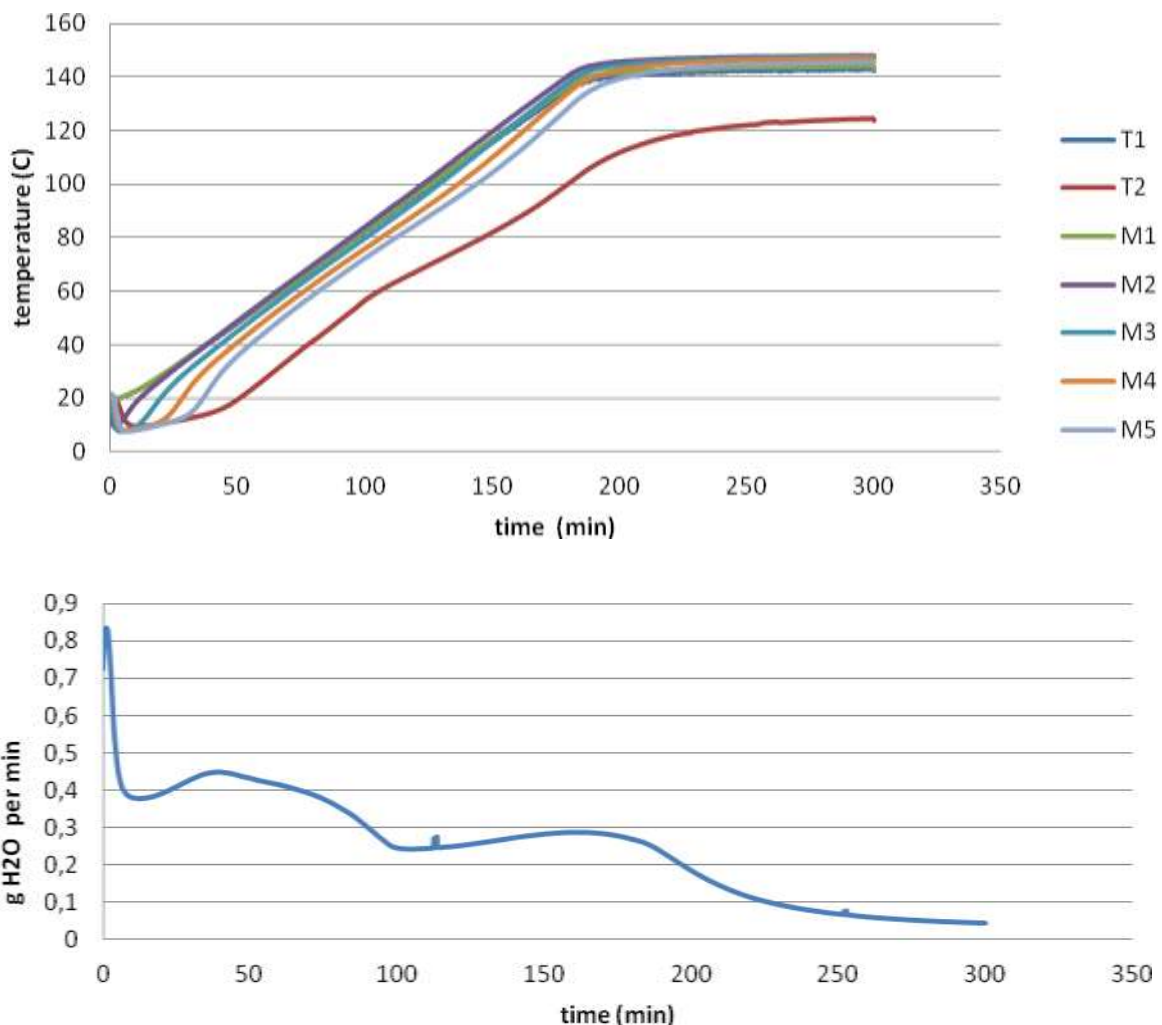


Figure 4: Temperature profiles in the reactor (top) and vapor outflow (bottom) as function of time during the desorption reaction of zeolite 13X.

### CLOSURE

An experimental database has been created for adsorption and desorption of zeolite 13X using a small-scale reactor. Temperature profiles in the reactor are shown as function of time. The data can be used for benchmarking. For further information please contact [c.c.m.rindt@tue.nl](mailto:c.c.m.rindt@tue.nl).

### BIBLIOGRAPHY

- [1] A.J. Brouwer, *Development of an experimental device for the investigation of seasonal heat storage by thermo-chemical materials*, M.Sc. Thesis, WET 2008.07, Eindhoven University of Technology, Eindhoven, the Netherlands, (2008)

- [2] P.J. van Kimmenade, *Design of a test reactor for thermo-chemical heat storage materials*, M.Sc. Thesis, WET 2010.13, Eindhoven University of Technology, Eindhoven, the Netherlands, (2010)
- [3] E.C.J.A Dukers, *Fixed bed reactor analysis for thermochemical heat storage*, M.Sc. Thesis, WET 2012.01, Eindhoven University of Technology, Eindhoven, the Netherlands, (2012)
- [4] H. Rajaei, *Fixed bed reactor analysis for seasonal heat storage by thermochemical materials* , M.Sc. Internship Report, WET 2012.16, Eindhoven University of Technology, Eindhoven, the Netherlands, (2012)

## ADSORPTION HEAT STORAGE: DYNAMIC PROPERTIES

Gerrit FUELDNER, Fraunhofer Institute Solar Energy Systems, Freiburg, Germany.

### INTRODUCTION

Adsorption heat storage uses the exothermal process of physical adsorption of a gas (e.g. water vapor) on highly porous materials such as zeolites or silicagel. The storage can be loaded by drying the material with high temperature (100-250°C) heat. If kept dry, it only cools down sensibly, and when exposed to water vapor will release the heat of adsorption at a medium temperature level (35-70°C). The storage can be built as an open system where hot air flows through an adsorbent bed for desorption and cool air is heated by adsorption of its water content. It can also be built as a closed (vacuum) system with pure water vapor atmosphere. In this case an additional heat exchanger is needed to bring in and out the heat. As well, a low temperature (0-20°C) evaporation source is necessary for the adsorption process in a closed system adsorption storage.

Porous adsorbent materials can be characterized in various ways. The typical physical properties which are of importance when considering a material in the context of thermal energy storage are mass/volume specific working fluid uptake (isobars/isotherms), heat capacity, heat conductivity, diffusivity, porosity and density. There are different characterization techniques for all these parameters. All of them have an influence on both the energy storage density and on the possible power of the storage, i.e. how fast can the storage be (un-)loaded. Of course, also the complete storage setup with casing, heat exchangers etc. will influence both, and it is often not easily possible to find the limiting factors.

### LAY-OUT OF THE EXPERIMENTAL SET-UP

To evaluate the dynamic properties of different heat-exchanger/adsorbent setups a volumetric adsorption kinetics measurement facility will be presented. In this the transient adsorption process is measured. Physical parameters like heat transfer resistances or diffusivities can be drawn from such measurements by comparison to a detailed model.

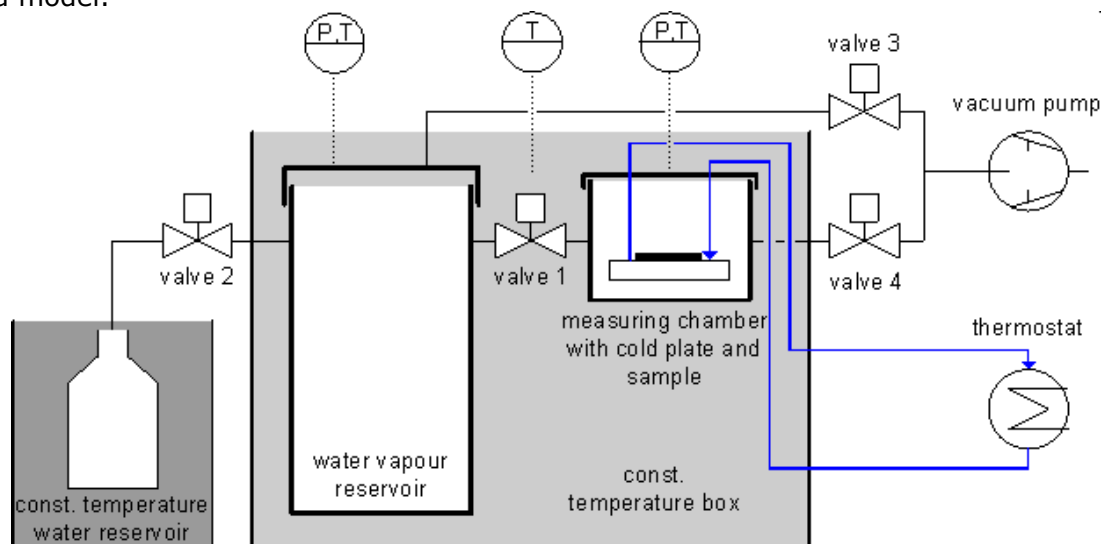


Figure 1: Scheme of the measurement setup for adsorption kinetics (most important parts).

The dosing chamber (water vapour reservoir, Volume 42.888 liters) with a defined quantity of pure water vapor (given by the saturation pressure at water bottle temperature) and the measuring chamber (Volume 0.7.. litres) are put in a thermostated rack (40°C). The sample is put on a coldplate thermostated by a water flow at constant temperature.

### Sample properties

The exemplary sample presented in this report is a composite adsorbent material in a thin layer (thickness 0.72 mm) that is glued to an aluminum plate (thickness 0.4 mm) representing the heat exchanger. The material consists of a rare earth exchanged Y-zeolite in a polymer fibre matrix (UOP DDZ-70) [1]. The sample size is 5x5 cm<sup>2</sup>, the density of the dry material is 650 kg/m<sup>3</sup> (dry adsorbent mass 1.12 g) and the porosity is 57% [2]. The mean intercrystalline poresize between the zeolite crystals (from permeability and mercury intrusion) is approximately 3-5 µm, the pore tortuosity factor is about 7 [3].

The heat capacity is 1000 J/(kg K), the heat conductivity of the dry material about 0.12 W/(m K) [2]. The adsorption equilibrium can be described by a generalized form of Dubinin's characteristic curve giving the adsorbed volume  $W$  [cm<sup>3</sup> of adsorbate/kg of dry adsorbent] as a function of the adsorption potential  $A=RT \ln p_{\text{sat}}(T)/p$  [J/g of adsorbate].

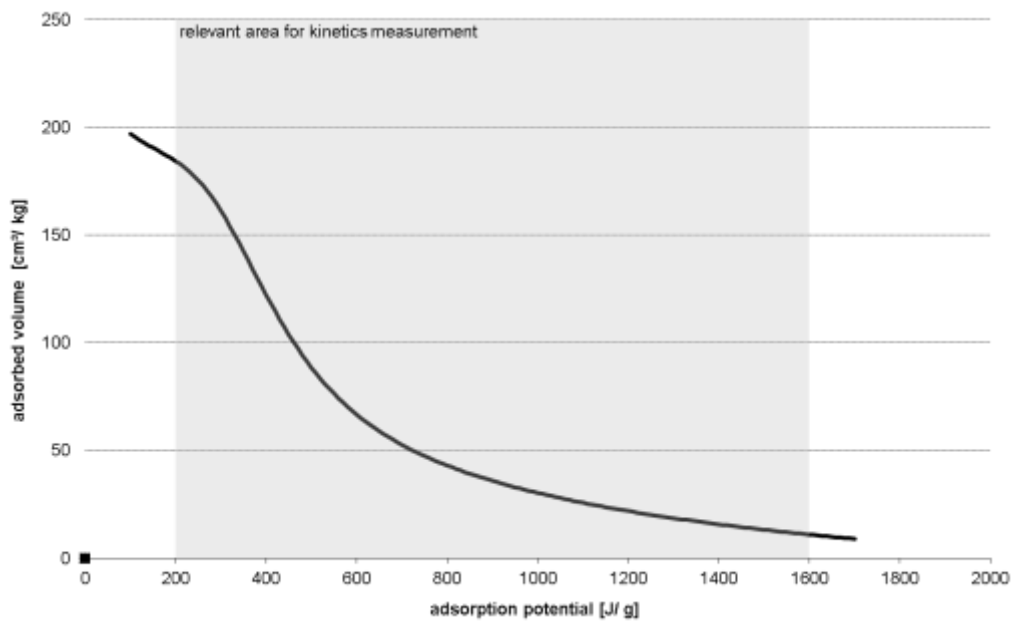


Figure 2: Characteristic curve UOP DDZ-70 with 20% of polymeric binder.

$$W = (a + cA + eA^2 + gA^3) / (1 + bA + dA^2 + fA^3) \quad [4,2]$$

with the parameters

a	221,160732
b	-2,01E-03
c	-7,91E-01
d	-2,22E-06
e	1,48E-03
f	1,65E-08
g	-5,13E-07

### **DETAILED DESCRIPTION OF THE MEASURING PROCEDURE**

To measure the transient adsorption process, the desorbed (activated) sample is cooled to 40°C and then exposed to water vapor atmosphere by opening valve 1. The sample immediately starts to adsorb.

The possible measurements vary with respect to the activation (desorption) conditions and with respect to the actual adsorption process.

### **Desorption Conditions**

For desorption two different conditions are applied:

1. The sample is heated to 95°C and the measurement cell is evacuated to ending pressure of a two stage vacuum pump (about 0.1 mbar).
2. For conditions closer to real working conditions in an adsorption storage, the desorption is against a condenser (the thermostated water reservoir) at e.g. 30°C.

In both conditions one has to keep in mind that the starting point (equilibrium uptake at  $t=0$ ) is not directly defined by the desorption conditions (e.g. 95°C and 42 mbar condenser pressure), since the sample is cooled down after the desorption phase and takes up some water from the small but not negligible volume of the measurement cell.

### **Canonical Measurement**

„Canonical“ in this context means that we have a closed system so the amount of water molecules in the system stays constant during the measurement. After opening valve 1 it is possible to calculate the absolute uptake of the sample by the drop in pressure (knowing the exact volume of measurement cell + dosing chamber). As starting pressure usually either 12.3 mbar (evaporator 10°C) or 17 mbar (evaporator 15°C) are chosen.

### **Coupling of the Sample to Coldplate/HF-Sensor**

The sample has been characterized in three different coupling variants. First, the sample has only been pressed to the coldplate without Thermigrease and without heat flux (HF) sensor to get the pressure drop without the danger of polluting the sample with the thermigrease. Then, to get the fastest possible adsorption kinetics, the sample is coupled to the coldplate with a thin layer of Thermigrease but without HF sensor. Finally the samples can be characterized with the HF sensor included in the setup.

## **RESULTS**

The measurement gives data on the surface temperature, the pressure in the measurement chamber and – if included – on the heat flux to the coldplate. Figure 3 shows 4 measurements, two measured with heatflux sensor and two without.

To evaluate the measurements, a detailed model of the non-isothermal adsorption kinetics taking into account heat transfer in the adsorbent and the metal, heat transfer resistances both between the adsorbent and the metal as well as between the metal and the coldplate and of course also mass transfer through macro- and micropores is fitted to the experiment [5]. The blue marks show the fitted model results.

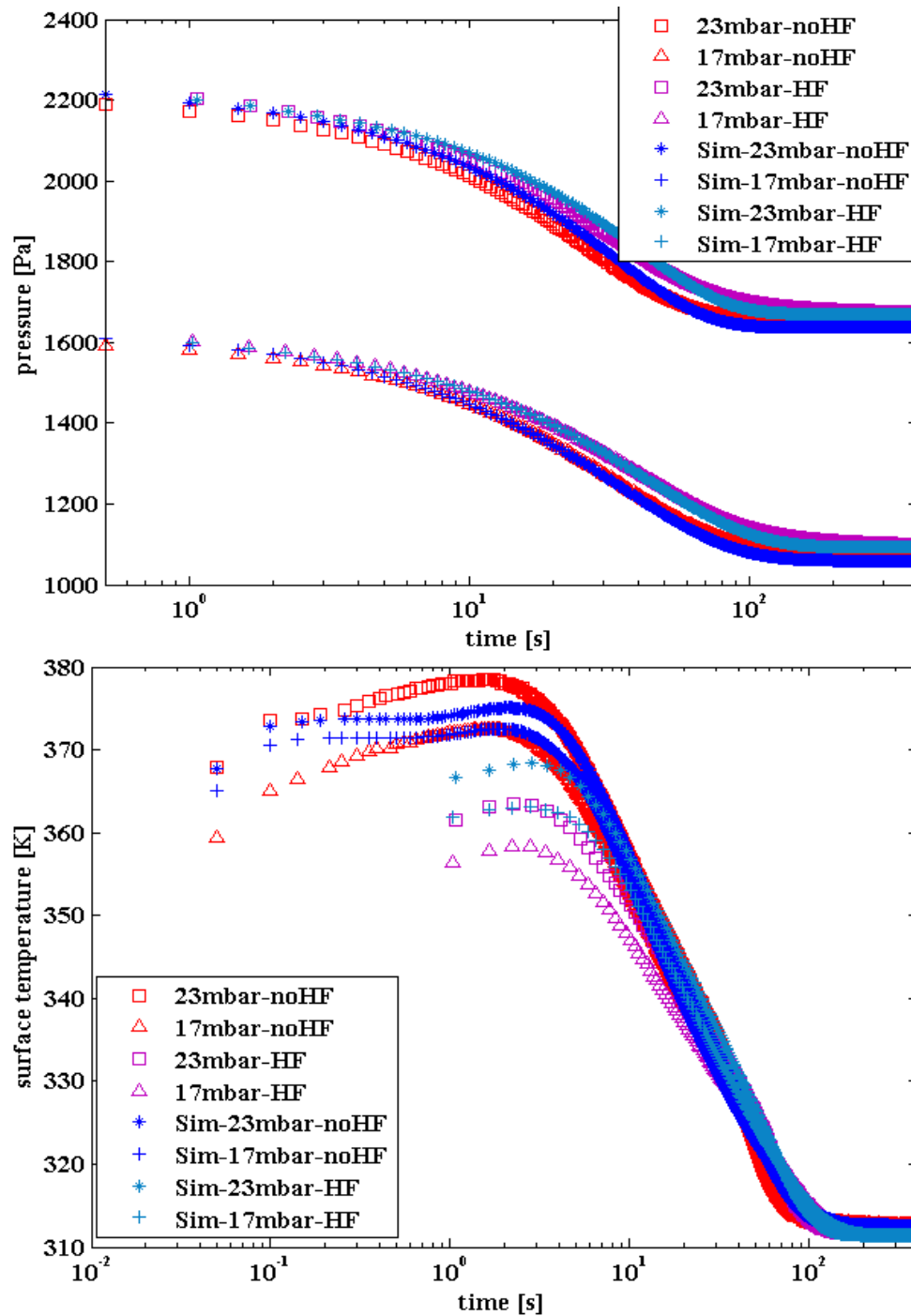


Figure 3: Pressure in measurement chamber (upper) and surface temperature of the sample after step change in pressure to 17 or 23 mbar after desorption and cooling. The measurements have been carried out with and without a heat flux (HF) sensor. For the measurements with HF, data on the heat flux is available as well. The HF introduces an additional heat transfer resistance which slows down the kinetics and thus has to be taken into account when modeling the transient uptake.

### CLOSURE

By measuring the uptake kinetics of macroscopic composite samples, heat and mass transfer parameters relevant for designing adsorption heat storages can be extracted. Using these parameters in simulation of the cyclic ad- and desorption process allows to predict the performance of different storage designs and materials [6,7].

For further information and detailed experimental data, please contact [gerrit.fueldner@ise.fraunhofer.de](mailto:gerrit.fueldner@ise.fraunhofer.de)

### **BIBLIOGRAPHY**

- [1] Dawoud, B., Vedder, U., Amer, E. and Dunne, S., *Non-isothermal adsorption kinetics of water vapour into a consolidated zeolite layer*, International Journal of Heat and Mass Transfer, **50**, 2190 – 2199, (2007)
- [2] Schnabel, L., *Experimentelle und numerische Untersuchung der Adsorptionskinetik an Adsorbens-Metall-Verbundstrukturen*, PhD Thesis Faculty III - Process Sciences, Technical University Berlin, Germany, (2009)
- [3] Földner G., Permeability of composite adsorbent layer, Unpublished measurements, (2008-2010)
- [4] Núñez, T., *Charakterisierung und Bewertung von Adsorbentien für Wärmetransformationsanwendungen*, PhD Thesis Faculty of Physics, University of Freiburg, Germany, (2001)
- [5] Földner G. and Schnabel L., Non-isothermal kinetics of water adsorption in compact adsorbent layers on a metal support, Proc. of the Int. COMSOL Conf., Hannover, Germany, (2008)
- [6] Schnabel L. and Földner G., Water Adsorption in Compact Adsorbent Layers – Kinetic Measurements and Numerical Layer Optimization, *Proc. of Heat Powered Cycles 2009*, TU Berlin, Germany: 520, (2009)
- [7] Földner, G.; Schnabel, L.; Wittstadt, U.; Henning, H. & Schmidt, *Numerical layer optimization of aluminium fibre/Sapo-34 composites for the application in adsorptive heat exchangers*, F. Lazzarin, R.; Longo, G. & Noro, M. (ed.), Proceedings of the International Sorption Heat Pump Conference, Padua Italy, 533-542, (2011)

## FIXED BED REACTOR FOR HYDRATION / DEHYDRATION OR ADSORPTION / DESORPTION EXPERIMENTS

Barbara METTE, Florian BERTSCH, Henner KERSKES, Institute for Thermodynamic and Thermal Engineering, Stuttgart University, Stuttgart, Germany.

### INTRODUCTION

Experiments on the hydration and dehydration or adsorption and desorption behavior of thermochemical energy storage materials are carried out in a small-scale fixed bed reactor. The experiments are performed under controlled inlet conditions of the airflow (humidity, temperature and mass flow). During the experiments, the temperature profile inside of the material bed is measured at five different axial positions. In addition, the inlet and outlet temperature, the inlet and outlet humidity and the mass flow of the airflow are measured.

### LAY-OUT OF THE EXPERIMENTAL SET-UP

Figure 1 depicts the experimental set up of the fixed bed reactor. Compressed air is filtered, additionally dried and then entering the fixed bed reactor test rig. For the drying process of the compressed air, the air is conducted through a bulk of zeolite 13X particles which has been dried at a temperature of  $\vartheta = 180\text{ °C}$ . This drying process further reduces the air humidity to values of  $p_{\text{H}_2\text{O}} < 0.3\text{ mbar}$ .

The mass flow rate of the air is measured and regulated with a mass flow controller (Bronkhorst, El-Flow, control range:  $0 \dots 0.16 \dots 8\text{ m}^3/\text{h}$ ). During the hydration / adsorption experiments, the air is humidified by directing part of the air flow through the air humidifier and part of it through the bypass. Afterward, the two air flows are mixed together again and the air humidity is measured with a dew points sensor (EdgeTech Dew Master, dew point range:  $-20$  to  $95\text{ °C}$ , accuracy  $\pm 0.2\text{ K}$ ). A pneumatic control valve regulates the volume flow through the bypass so that the resulting combined flow has the desired air humidity. During the dehydration / desorption experiments the complete air flow is passing through the bypass.

In an electrically heated pipe the air is heated to the desired reactor inlet temperature. The electrical power of the heating coils can be regulated so that the variation in the inlet temperature is less than  $\pm 0.3\text{ K}$ .

The reactor inlet and outlet temperature of the airflow and the temperature of the material bed at five different axial positions ( $T_{R,1} = 20\text{ mm}$ ,  $T_{R,2} = 40\text{ mm}$ ,  $T_{R,3} = 60\text{ mm}$ ,  $T_{R,4} = 80\text{ mm}$ ,  $T_{R,5} = 120\text{ mm}$ ) of the reactor are measured with thermocouples (type K, diameter  $1\text{ mm}$ , accuracy  $\pm 1\text{ K}$ ). The air humidity at the reactor inlet and outlet are measured with dew point sensors.

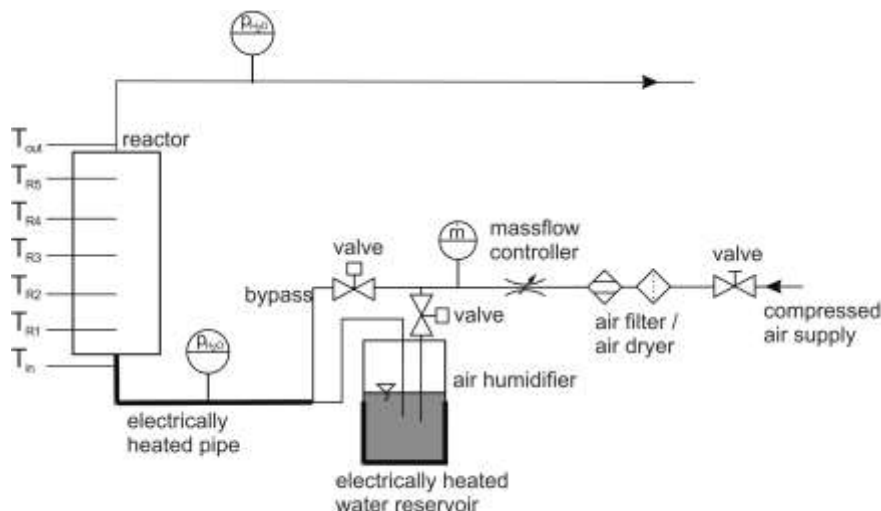


Figure 1: Experimental set up of the fixed-bed reactor test rig

A more detailed sketch of the fixed bed reactor is given in figure 2. The reactor is made of stainless steel (wall thickness of 3 mm) and has a volume of approximately 165 ml (reactor height = 125 mm, reactor diameter = 40.5 mm). The reactor is insulated with glass wool of a thickness of approximately 50 mm.

The temperature sensors for measuring the material bed temperatures are not in direct contact with the material bed. The sensors are inserted in brass tubes (inner diameter of 1 mm, outer diameter of 1.4 mm) which are horizontally passed through the reactor. This set up allows an easy and reproducible measurement of the bed temperature in many experiments.

A clamp ring connection allows an easy installation and removal of the reactor. A reducer pipe from the reactor diameter to 20 mm is installed before and behind the fixed bed reactor. Two filters (sintered bronze, pore size of 1 mm), which are positioned in the top and bottom flange, are fixing the material inside the reactor.

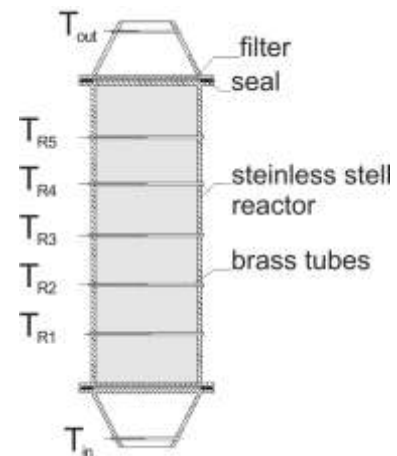


Figure 2: Sketch of the fixed bed reactor.

The following inlet conditions of the air flow can be set:

- Mass flow (dry air): 100 ... 3000 g/h
- Air humidity: 5 ... 100 mbar
- Reactor inlet temperature: 25 ... 190 °C

### **DETAILED DESCRIPTION OF THE MEASURING PROCEDURE**

A measuring cycle in general consists of at least three steps which are all conducted in the fixed bed reactor: Desorption / dehydration of the material, cooling down the material, adsorption / hydration of the material. In all three phases air at a defined mass flow is flowing through the material bed.

The different steps will be described in more details by the example of an adsorption / desorption cycle of binder-free zeolite 13X and a hydration / dehydration cycle of a composite of calcium chloride on a mineral clay matrix.

#### Binder-free zeolite 13X

The reactor is filled with binder-free zeolite 13X (Köstrolith® 13XBFK) of the company *Chemiewerke Bad Köstritz* up to the fifth temperature sensor (approximately 88 g). The particles are spherical and have a grain size of 1.6 – 2.0 mm.

During the desorption process the material is dried in the reactor with a dry air flow of the following reactor inlet conditions: air mass flow rate  $\dot{m} = 1000$  g/h, reactor inlet temperature  $\vartheta = 180$  °C, reactor inlet air humidity  $p_{\text{H}_2\text{O}} < 0.3$  mbar. Due to heat losses over the reactor length no uniform temperature distribution over the reactor length is achieved in steady-state conditions. A temperature drop of  $\Delta T = T_{\text{in}} - T_{\text{out}} = 30$  K is measured over the reactor length.

In the cooling phase the material (and also the periphery to and from the reactor) is cooled down by air flow through the fixed bed reactor. The reactor inlet temperature is set to the desired temperature of the adsorption phase. The mass flow rate and air humidity remain constant.

For the adsorption process the air flow is humidified to the desired inlet air humidity. Due to the control algorithm of the pneumatic valve it takes a few minutes (up to 8 minutes) until the air humidity is constant at the desired set point value. A bypassing of the reactor is not possible so that during the first minutes of the measurements the inflow conditions are not stationary.

The adsorption is performed at an inlet temperature of the air flow of  $\vartheta = 35$  °C and an inlet humidity of  $p_{\text{H}_2\text{O}} = 20$  mbar.

### Composite of calcium chloride on a mineral clay matrix

The composite of calcium chloride and mineral clay was prepared at ITW by impregnating mineral clay (grain size of 2 to 5 mm) in a salt solution of calcium chloride. Afterwards the sample was dried in an oven at 150 °C. The uptake of calcium chloride into the mineral clay matrix was approximately 34 weight-% (related to the mineral clay mass). Afterwards the sample was stored under room conditions.

For investigating the hydration behavior of this composite 71 g of the material was filled in the fixed bed reactor, just covering the fifth temperature sensor.

For the dehydration of the composite, the temperature of the airflow is stepwise increased: 4 hours at 50 °C, 5 hours at 100 °C, 6 hours at 150 °C. The mass flow is set constant to  $\dot{m} = 1000$  g/h, the reactor inlet air humidity is  $p_{\text{H}_2\text{O}} < 0.3$  mbar. Due to heat losses over the reactor length a temperature drop over the reactor of  $\Delta T = 22$  K is measured at a reactor inlet temperature of  $\vartheta = 150$  °C.

The cooling and the hydration phase were conducted in the same manner as for the binder-free zeolite 13X.

## **Results**

### Binder-free zeolite 13X

Figure 3 depicts the temperature profile in the material bed, the reactor inlet and outlet temperatures and the reactor inlet and outlet water vapor pressures of the airflow during the adsorption process.

Successively the temperatures measured at the five thermocouples  $T_{R1}$  to  $T_{R5}$  are increasing to a maximum temperature of around  $\vartheta = 80$  °C and are then decreasing again. The sharp temperature peaks indicate a sharp reaction front which is moving through the reactor.

Over almost 1.5 hours the air humidity at the reactor outlet is almost zero. This indicates a high affinity of this zeolite towards water. During the next 40 minutes, the reactor outlet water vapor pressure is comparatively rapidly increasing to 18.5 mbar and then over a long period of roughly 30 to 40 minutes slowly approaching the value of the water vapor pressure of the reactor inlet of 20 mbar. The total amount of water vapor adsorbed is measured to 23 g, equivalent to 26.4 weight-% (related to the dry material mass).

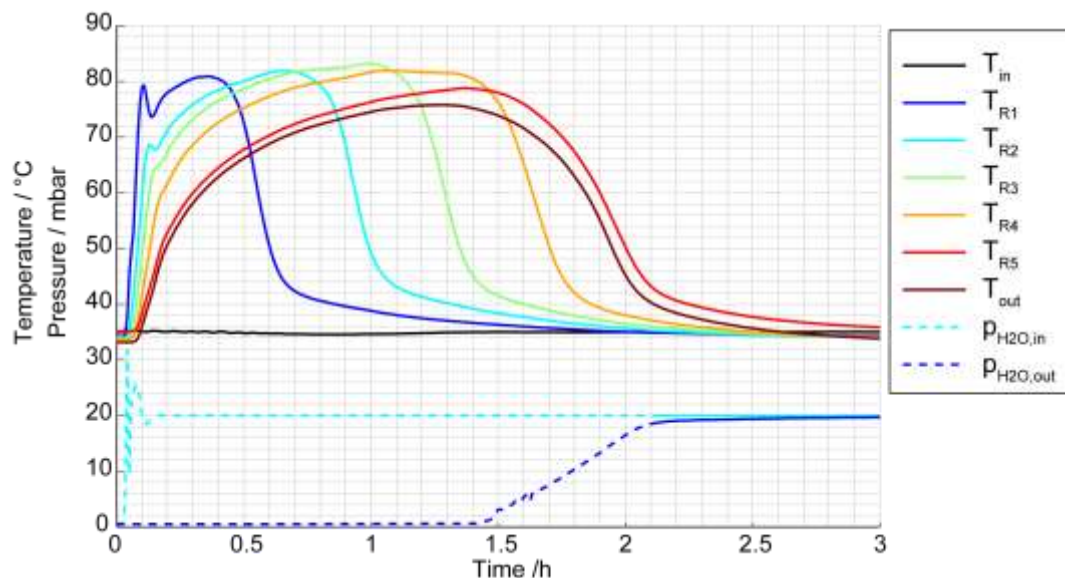


Figure 3: Temperature distribution over the reactor length, reactor inlet and outlet air temperatures and reactor inlet and outlet water vapor pressures depicted over the reaction time during the adsorption of binder-free zeolite 13X

### Composite of calcium chloride on a mineral clay matrix

In figure 4 the temperature profile in the material bed, the reactor inlet and outlet temperatures and the reactor inlet and outlet water vapor pressures of the airflow during the hydration phase are depicted.

As soon as water vapor is given to the airflow a temperature increase at all temperature sensors is measured immediately. After 6 minutes, a maximum temperature of about  $\vartheta = 60\text{ }^{\circ}\text{C}$  is reached at temperature sensor  $T_{R3}$  and  $T_{R4}$ . Afterwards, the temperature in the whole material bed is first dropping quickly to around  $\vartheta = 45\text{ }^{\circ}\text{C}$ , then only slightly decreasing for a quite long period and then decreasing faster again to the air flow inlet temperature. For example, the temperature at sensor  $T_{R3}$  is first dropping by 15 K (from  $\vartheta = 60\text{ }^{\circ}\text{C}$  to  $\vartheta = 45\text{ }^{\circ}\text{C}$ ) in 1.5 hours, then only dropping by 3 K (to  $\vartheta = 42\text{ }^{\circ}\text{C}$ ) during the next 3.5 hours and then by 5 K again (to  $\vartheta = 37\text{ }^{\circ}\text{C}$ ) in 2.5 hours.

The curve of the partial pressure of the water vapor at the reactor outlet can be classified in four phases: a very quick increase from  $p_{\text{H}_2\text{O}} = 0$  to  $p_{\text{H}_2\text{O}} = 12.5\text{ mbar}$  in the first hour, then a slow increase to  $p_{\text{H}_2\text{O}} = 14\text{ mbar}$  in the next 4 hours, and then a faster increase to  $p_{\text{H}_2\text{O}} = 17.5\text{ mbar}$  in the next 2.5 hours. Afterwards, the water vapor at the reactor outlet only approaches very slowly the water vapor inlet pressure. Even after 10 hours of reaction only a water vapor pressure of  $p_{\text{H}_2\text{O}} = 19\text{ mbar}$  is measured at the reactor outlet. In total, the water uptake of the composite was measured to be 31.7 weight-% (related to the dry material) during 10 hours of hydration.

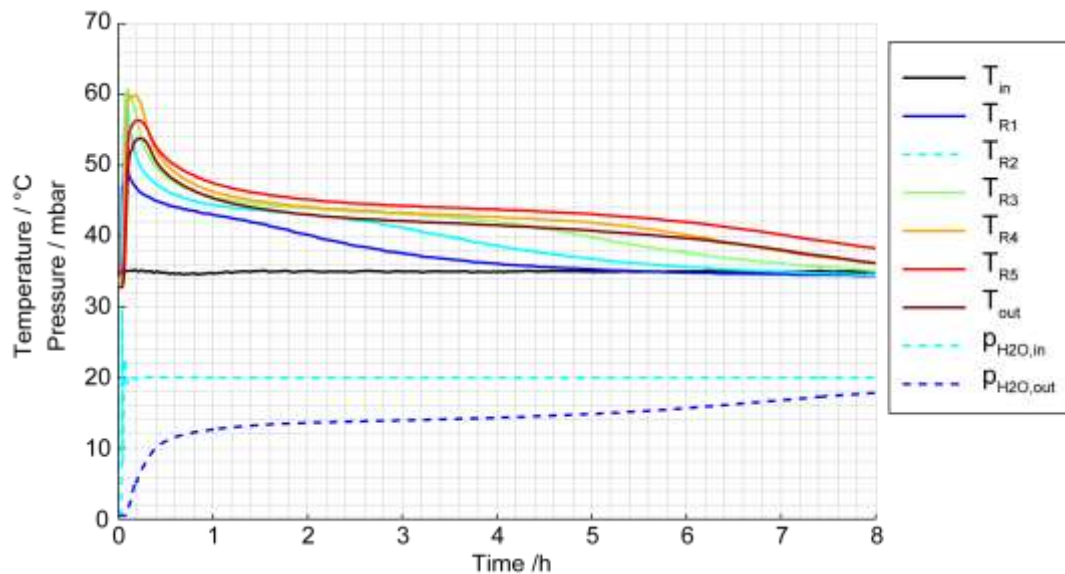


*Figure 4: Temperature distribution over the reactor length, reactor inlet and outlet air temperatures and reactor inlet and outlet water vapor pressures depicted over the reaction time during the hydration of the composite of mineral clay and calcium-chloride.*

An explanation for the fast increase in temperature in the beginning of the hydration experiment is that the anhydrous salt first reacts comparatively quickly with the water vapor. Due to the superposition of two effects, the maximum temperature is measured at the temperature sensors  $T_{R3}$  and  $T_{R4}$ : 1) the air flow transports the heat of reaction from further upstream in this area and preheats the material and 2) the material in this area is reacting with the water vapor which is transported via the air flow, heat is released and further increases the material's temperature.

Further downstream the water vapor in the air flow is consumed and no further reaction takes place. Hence, no further heat is produced and the air flow is slowly cooled down by preheating the material.

As soon as a first hydration of the material has occurred the reaction rate rapidly decreases. This explains the fast temperature decrease over the whole reactor length after the first peak.

Now, the reaction front is distributed over the whole reactor length and even at the reactor outlet not the whole water vapor is consumed but blown out with the air flow. The almost constant temperature plateau inside the reactor which is measured over a long time period of 3 to 5 hours especially at the temperature sensors TR4 and TR5 can be explained by the fact that over the whole reactor length an almost constant heat of reaction is produced. This explanation is supported by the measurement of the water vapor pressure at the reactor outlet which is also only very slightly increasing during this time period.

With increasing material hydration the reaction rate further decreases. After 4 hours of reaction the temperature measured at the temperature sensor TR1, after 6 and 7 hours the temperature measured at temperature sensor TR2 and TR3 has dropped almost to the air inlet temperature. This indicates that the hydration reaction has almost stopped in this area. Due to a slower hydration reaction of the material also further downstream, less water vapor is consumed in the reactor and the water vapor outlet pressure is increasing more rapidly. This is also associated with less heat production inside the reactor. Less or no preheating of the material further downstream is possible. The temperatures at the temperature sensors TR4 and TR5 are dropping faster again.

**CLOSURE**

The experimental investigations in the fixed bed reactor allow to gain insight in the overall heat and mass transport phenomena during a desorption / dehydration and adsorption / hydration reaction of thermochemical energy storage materials. Information on the energy density of the material and the material loading can be determined.

The measured data can be used to determine the heat and mass transport parameters which are needed for a mathematical description of the reaction and to validate numerical codes. Information on the equilibrium data cannot be obtained from these experiments and have to be determined by other means.

The validated simulation software can be used to investigate the heat and mass transport phenomena of different thermochemical energy storage materials under arbitrary boundary conditions. In addition different reactor designs and different operations of the reactor can be investigated in great detail which forms the basis for the designing process of a thermochemical energy storage.

For further information and detailed experimental data contact Barbara Mette, University of Stuttgart, Institute for Thermodynamic and Thermal Engineering, Pfaffenwaldring 6, 70550 Stuttgart, Germany.

# ADSORPTION HEAT STORAGE: EQUILIBRIUM PROPERTIES DETERMINATION WITH COMPARISON TO MOLECULAR SIMULATIONS

Stefan HENNINGER, Fraunhofer Institut Solar Energy Systems, Freiburg, Germany.

## INTRODUCTION

As written above, adsorption heat storage uses the exothermal process of physical adsorption of a gas (e.g. water vapor) on highly porous materials such as zeolites or silicagel.

Therefore, the determination of the water adsorption equilibrium on sorption materials is the first step for evaluation of the materials to be used in adsorption heat storage. Unfortunately measurement procedures are up today not standardized and therefore hardly comparable. Several measurements are published, but even for the same materials they may be dissimilar due to different measurement techniques and boundary conditions. Beside different measurement methods like thermogravimetry or volumetric characterization, the pre-treatment and the measuring procedure have a great influence on the results (see fig. 1) [1].

The pre-treatment, more precisely the drying or desorption temperature previous to the measurement leads to different results. Obviously, a higher desorption temperature may lead to less residual water within the sample and therefore higher water uptake capacity. In addition, the atmospheric conditions (drying under continuous evacuation or under inert gas flow) play another important role for the initial state or the net weight of the sample and the measurement. Further important points are the heating or scanning rate for continuous measurements or the equilibration time for non-continuous, true equilibrium measurements. Depending on the material used, a difference between the adsorption and desorption path can be observed. This hysteresis leads to significant errors in comparison with computer simulations like e.g. Monte Carlo simulation.



Figure1: Influencing factors for water adsorption measurements [1].

## GENERAL OVERVIEW

The characterization of micro- and mesoporous materials in terms of working fluid uptake for several combinations of adsorbent/adsorbate with regard to the application in heat transformation processes has been and still is a field of intensive investigations [2-5]. Different measurement methods are used, with thermogravimetry and volumetry being the most common methods. In case of thermogravimetric measurements there are in principle three possibilities.

Commonly used in chemistry are open flow systems mainly using nitrogen as carrier gas. There exist several publications with thermogravimetric analysis (TGA), performing a desorption curve under an inert carrier gas flow with a defined temperature-scanning rate. Previous to the measurement the samples are prepared under a more or less defined humid atmosphere.

Unfortunately the shape of the curve and therefore the differential thermogravimetric (DTG) signal to determine the temperature on set point for the released water strongly depends on the used heating rate. Furthermore comparison of materials measured with

this method leads to large discrepancies as the initial state, which is room temperature, is not well defined and therefore difficult to reproduce. In addition without a possibility to perform adsorption curves, possible hysteresis effects cannot be detected.

Another possibility in case of open systems is to use a well defined humidified carrier gas (e.g. Setaram WetSys) which flows around the sample. To prevent condensation, the transfer line and the measurement cell has to be temperature controlled in an accurate way.

The third possibilities are systems with closed working fluid atmosphere. As shown in Henninger et al. [6] measurements with open and closed systems are comparable if using the same reference conditions. Beside the differences in the apparatuses an additional uncertainty is the difference in isobaric versus isothermal measurements. Isothermal measurement in principle allows the determination of the heat of adsorption, by calculation for at least two isotherms or direct measurement within a simultaneous TG/DSC. In addition, especially with regard to the Dubinin transformation, the temperature independency can be verified.

Isobaric measurement can in principle be performed in a broader temperature range therefore covering a larger range of the adsorption potential  $A = RT \ln p/p_0$ . Furthermore as the real cycle (ideally) consists of two isobaric phases of desorption and adsorption at condenser and evaporator pressure, the isothermal measured data is not directly adoptable to the operating device. An overview on the adsorption equilibrium characterization is given in fig. 2.

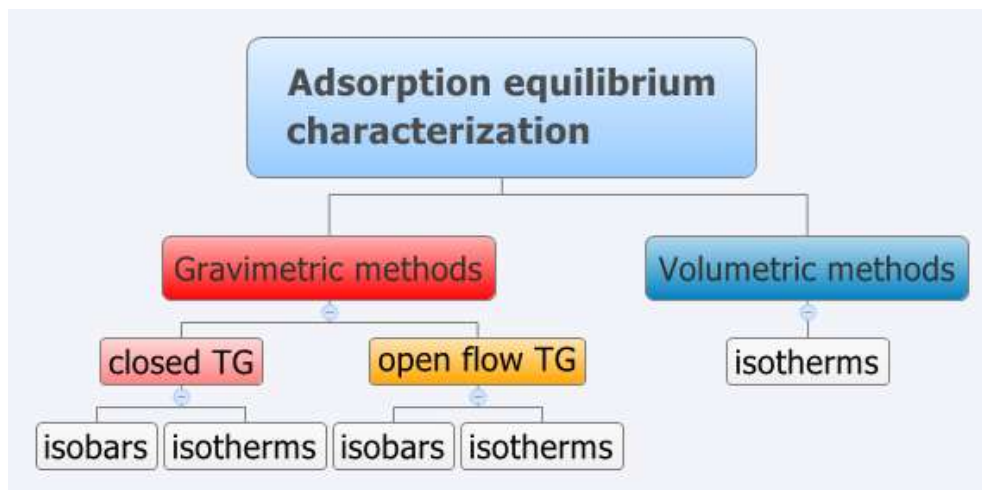


Figure 1: Overview on possible adsorption equilibrium characterization methods. This list is not exhaustive.

### MEASUREMENT PROCEDURES

As a result of the consideration described above a common method for determination of water adsorption characteristics with focus on adsorption heat transformation must be defined.

Within this Task a round robin test (RRT) consisting of two isothermal measurements has been performed. The results of this RRT will be described within another report.

Beside this proposed procedure here another procedure is described, allowing for comparison of measurement with simulation were isotherms are difficult to be performed [1]. As defined below, in case of grand canonical simulations the definition of the temperature is more straight forward than the definition of a pressure via the fugacity.

The procedure consists of a pre-treatment of the sample under continuous evacuation (vacuum level:  $1e-4$  kPa) or dry carrier gas flow.

The optimal sample pre-treatment temperature should be selected according to the hydrophilicity of the samples.

- Strongly hydrophilic zeolites (4A, 13X): pre-treatment  $T = 300^{\circ}\text{C}$ .
- Hydrophilic aluminosilicates (NaY): pre-treatment  $T = 200^{\circ}\text{C}$

- Hydrophobic aluminosilicates (silicalites, ZSM5):  $T=150^{\circ}\text{C}$
- Aluminophosphates (AIPO, SAPO):  $T=150^{\circ}\text{C}$
- Others (silica gels, activated carbons):  $T=150^{\circ}\text{C}$

The sample is heated starting from ambient conditions with a heating rate of 1K/min followed by an isothermal drying step for another 8 hours. In the following step, isobar measurement at a water vapour pressure of 1.2 and 5.6 kPa takes place.

The selection of the two pressure levels is motivated with respect to the possible applications. The pressure level of 1.2 kPa corresponds to an evaporation temperature of  $10^{\circ}\text{C}$ , which marks a useful temperature level for low temperature heat source. The second pressure level of 5.6 kPa corresponds to  $35^{\circ}\text{C}$  which either marks the temperature where heat can be rejected (in desorption case) or can be used for low temperature heating (heat pumping application).

For each pressure level the sample temperature is varied in 5 or 10 K steps between  $150^{\circ}\text{C}$  and  $40^{\circ}\text{C}$  (for 5.6 kPa) or  $20^{\circ}\text{C}$  (for 1.2 kPa) respectively. In addition at least one adsorption and desorption measurements should be performed in order to detect possible hysteresis effects.

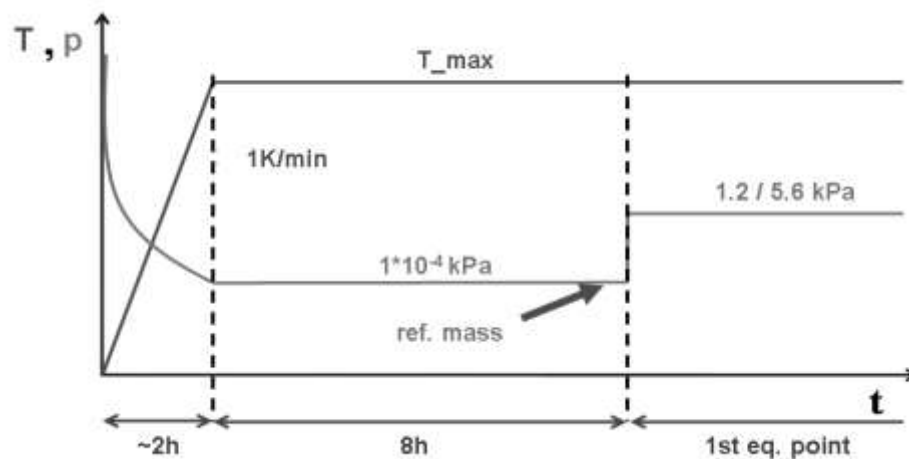


Figure 2: Proposed measurement procedure, including sample pre-treatment and the first isobaric step.

This procedure has successfully been used within the IEA annex 34 "Thermally driven heat pumps". First promising results with a good agreement between measurements performed at Fraunhofer ISE and at CNR-ITAE, using different techniques were performed. As first two candidates of a standard material to be used in a round robin test, a silica gel 127 B and a SAPO-34 have been chosen.

### **CALIBRATION AND COMPARISON WITH MODELLING RESULT**

New materials are necessary in order to improve the adsorption characteristics for these applications. Molecular simulations are seen as a promising tool to investigate the influence of molecular structure on the adsorption characteristics and thus to provide means for future improvements of such materials for application in heat transformation. The field of molecular simulation enfolds a broad range, from model systems of generally theoretical interest to real fluids or solids in material science up to applications in life science, e.g. drug design.

Within a recently published work, a simulation program specially tailored to the problem has been developed [7]. The program uses the grand canonical ensemble and the simple point charge model (SPC) and the enhanced version (SPC/E) developed by Berendsen et al. [7,8]. Calculation of long-range electrostatic interactions is realised by the use of the Ewald summation technique [9,10] in combination with periodic boundary conditions respecting the minimum image convention [11]. The accurate implementation of the long ranged coulomb interactions has been examined by calculation of the Madelung constant

for a NaCl ion lattice. Furthermore the combined interaction energy for water within a zeolite structure has been confirmed for a fixed water configuration with the molecular dynamic program MOSCITO [12].

For comparison with experimental data the chemical potential is converted according to the ideal gas law

$$\beta \cdot \mu = \beta \cdot \mu_{ideal} + \ln(\beta \cdot P\phi)$$

with the fugacity  $f = P\phi$  and  $\beta = 1/k_B T$ .

Calculation of the isosteric adsorption enthalpy is achieved by the ensemble fluctuation method [13-15].

As result of the simulations, the number of water molecules adsorbed in thermodynamic equilibrium under given conditions of temperature and chemical potential (pressure) are compared with the experimental data. To assure thermodynamic equilibrium, all simulations start with an equilibration phase followed by a production phase. The number of required equilibration cycles varies strongly with the different simulated frameworks, depending on size and number of water molecules within the unit cell. As an average two million equilibration cycles have been chosen for the equilibration phase. Within one cycle there is one attempt for a displacement, five attempts for exchange and one attempt for a rotation of a water molecule. Simulation results out of the production cycles are analysed and simulation errors are calculated according to the block transformation method of Flyvbjerg and Petersen [16].

As shown in Fig. 3, the simulated and experimental isobars are in very good agreement.

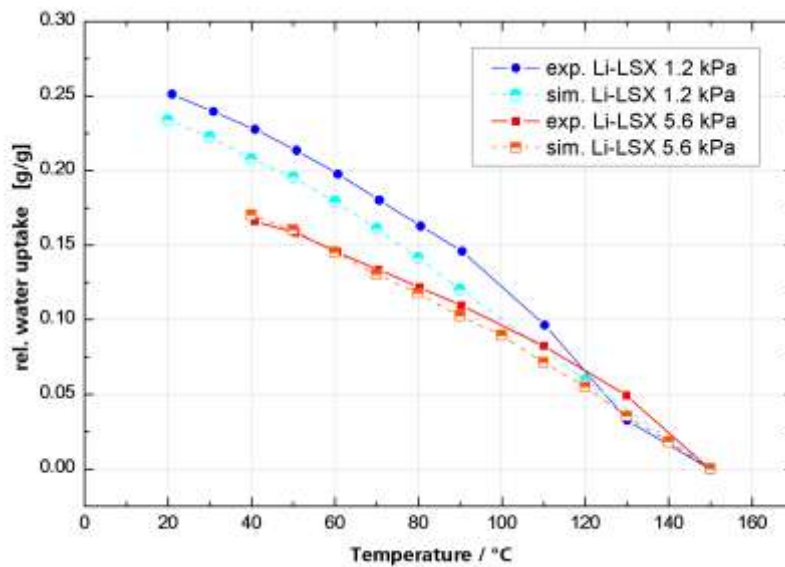


Figure 3: Comparison of simulated (dashed line) and experimental (solid line) adsorption isobars at 1.2 and 5.6 kPa.

The relative water uptake (absolute water uptake normalized by the reference mass at 150°C) is shown for the water vapour pressure at 1.2 kPa or 5.6 kPa. The reason for choosing this reference mass is due to the fact that the real adsorbent sample in the experimental case is different to the ideal crystalline framework (see Fig.4). Whereas in the simulation there is only the pure crystal, the real sample contains potentially a binding agent, amorphous phases and residual water content.

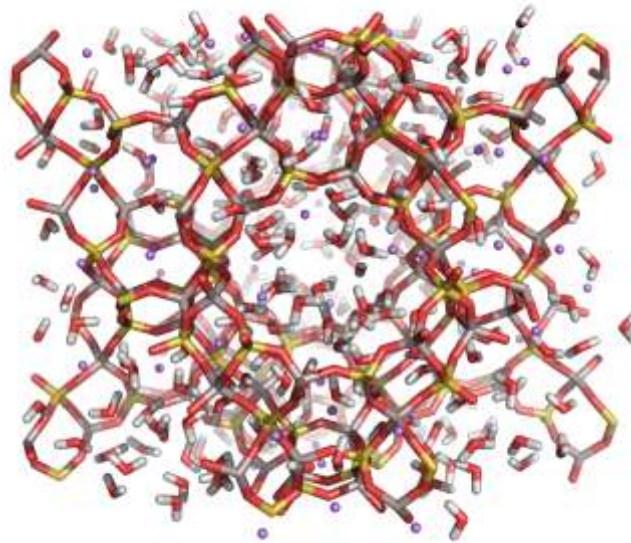


Figure 4: Snapshot of the simulation showing 214 water molecules in a Li-LSX host at 383 K, 5.6 kPa.

### **CLOSURE**

To measure equilibrium adsorption characteristic several important influencing factors have to be taken into account. This includes for example the sample preparation. Here the outgassing temperature and surrounding has the greatest impact on the results. With regard to the measurement procedure isobaric vs. isothermal measurements may show different results. By a proper choice of reference mass and illustration this can be overcome.

The apparatus itself also has a great influence on the experimental data. As written above, differences between open flow and closed system can be eliminated by a proper choice of the reference mass.

All these factors have to be taken into account comparing simulated results with experimental data.

However, evaluation of sorption materials on basis of experimental characterisation and molecular simulation methods can give deeper insight into the underlying adsorption mechanism. According to the molecular simulation results, various recommendations on the improvement of sorption materials for heat transformation can be given.

### **BIBLIOGRAPHY**

- [1] Henninger, S. K., Freni, A., Schnabel, L., Schossig, P., & Restuccia, G. (2011). Unified water adsorption measurement procedure for sorption materials. *Proc. of International Sorption Heat Pump Conference* (Vol. 4, pp. 513 - 522). Padova, Italy. doi:ISBN: 978-2-913149-84-7
- [2] Srivastava, N. C., & Eames, I. W. (1998). A review of adsorbents and adsorbates in solid-vapour adsorption heat pump systems. *Applied Thermal Engineering*, 18, 707-714.
- [3] Aristov, Y. I., Restuccia, G., Cacciola, G., & Parmon, V. (2002). A family of new working materials for solid sorption air conditioning systems. *Applied Thermal Engineering*, 22(2), 191-204. Elsevier

- [4] Jänchen, J., Ackermann, D., & Stach, H. (2002). Adsorption Properties of Aluminophosphate Molecular Sieves-Potential Applications for Low Temperature Heat Utilization. *Proceedings of the International Sorption Heat Pump Conference Shanghai, PR China* (pp. 2-5).
- [5] Critoph, R. E., & Zhong, Y. (2005). Review of trends in solid sorption refrigeration and heat pumping technology. *Proceedings of the Institution of Mechanical Engineers, Part E: Journal of Process Mechanical Engineering*, 219(3), 285-300. doi: 10.1243/095440805X6982.
- [6] Henninger, S.K., Schmidt, F. P., & Henning, H.-M. (2010). Water adsorption characteristics of novel materials for heat transformation applications. *Applied Thermal Engineering*, 30(13), 1692-1702. Elsevier Ltd. doi: 10.1016/j.applthermaleng.2010.03.028.
- [6] Henninger, S., Schmidt, F., & Henning, H.-M. (2011). Characterisation and improvement of sorption materials with molecular modeling for the use in heat transformation applications. *Adsorption*, 17(5), 833-843. Springer. doi:10.1007/s10450-011-9342-6
- [7] Berendsen H. J. C. et al.: Interaction models for water in relation to protein hydration, Pullmann B. (Ed.), *Intermolecular Forces*, Reidel, Dordrecht. 1981, pp. 331-342
- [8] Berendsen H. J. C., Grigera J. R. and Straatsma T. P.:The Missing Term in Effective Pair Potentials, *J. Phys. Chem.*, Vol 91, No. 24, 1987, pp. 6269-6271
- [9] Kolafa Jiri and Perram John W., Cutoff errors in the ewald summation formulae for point charge systems, *Molecular Simulation*, 1992, pp. 351-368
- [10] Frenkel Daan and Smit Berend: *Understanding Molecular Simulation*, Academic Press, San Diego (2002).
- [11] Allen M. P. und Tildesley D. J., *Computer Simulation of Liquids*, Clarendon Press, Oxford, 1986
- [12] Paschek Dietmar and Geiger Alfons, User's Guide and Manual MOSCITO 4 Performing Molecular Dynamics Simulations, <http://ganter.chemie.uni-dortmund.de/MOSCITO/index.shtml>, Accessed April 7, 2003.
- [13] Karavias F. and Myers A.L., Isosteric Heats of Multicomponent Adsorption - Thermodynamics and Computer-Simulations, *Langmuir*, 7, No. 12, 1991, pp. 3118-3126
- [14] Pellenq RJM et al., Grand canonical Monte Carlo simulations of adsorption of polar and nonpolar molecules in NaY zeolites, *Langmuir*, 12, 1996, pp. 4768-4783
- [15] Woods G.B. and Rowlinson J.S., Computer-Simulations of Fluids in Zeolite-X and Zeolite-Y, *Journal of the Chemical Society - Faraday Transactions II*, 85, 1989, pp. 765-781
- [16] Flyvbjerg H. und Petersen H. G., Error Estimates on Averages of Correlated Data, *J. Chem. Phys.*, 91, 1989, pp. 461-466

## CHARACTERIZATION OF THE DEHYDRATION REACTION OF SEVERAL CRYSTALLINE SALT HYDRATES UNDER THE CONDITIONS OF THE SEASONAL HEAT STORAGE

Claire FERCHAUD<sup>1</sup> and Herbert ZONDAG<sup>1,2</sup>

<sup>1</sup> Energy Research Center of the Netherland (ECN),

<sup>2</sup> Eindhoven University of Technology, Eindhoven, The Netherlands.

### INTRODUCTION

At ECN, research is carried out into seasonal solar heat storage for individual houses, based on the reversible sorption reaction of water vapor. During summer, salt hydrates can be dehydrated by solar heat provided by the solar thermal collectors at a temperature below 150°C. In the present work, the dehydration reactions of four salt hydrate materials,  $\text{Li}_2\text{SO}_4 \cdot \text{H}_2\text{O}$ ,  $\text{CuSO}_4 \cdot 5\text{H}_2\text{O}$ ,  $\text{MgSO}_4 \cdot 7\text{H}_2\text{O}$  and  $\text{MgCl}_2 \cdot 6\text{H}_2\text{O}$ , have been studied by thermal analysis to determine the reaction data for these materials for seasonal heat storage. The dehydration was carried out at a water vapor pressure of 13 mbar, which is a typical value for the Dutch summer.

### LAY-OUT OF THE EXPERIMENTAL SET-UP

#### Dimensions

The thermal analysis has been carried out with a Simultaneous Thermal Analysis apparatus (STA 409 PC). This allows measuring the mass loss and the heat flow of the sample, observed for each phase transition of the material by Thermogravimetry (TG) and Differential Scanning Calorimetry (DSC). The inlet air at the entrance of the apparatus has been set at a water vapor pressure of 13 mbar. A moist air flow of 100 ml/min was applied from the bottom to the top of the apparatus surrounding the open pan of 25  $\mu\text{l}$  (5 mm diameter) containing the salt hydrate sample (fig. 1).

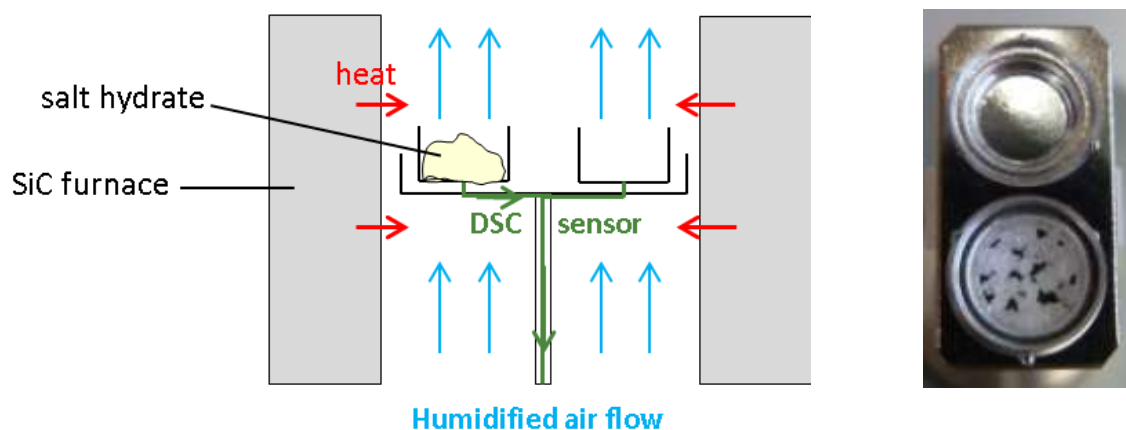


Figure 1: Scheme of the STA system and picture of the 25  $\mu\text{l}$  aluminum cups used during the thermal analyses measurements

#### Material properties

Commercial crystalline powders sieved with a particle size distribution of 100-200  $\mu\text{m}$  have been used for these experiments. The weight of the salt hydrate sample used for each measurement was around 10.2 mg with  $\pm 0.2$  mg. It corresponds to a homogeneous mono-layer thickness (maximum 200  $\mu\text{m}$ ) over the bottom of the aluminium cup. This quantity of material has been taken as reference to be able to compare one material to another, in order to avoid a gradient of gas diffusion through the sample during the measurements.

### DETAILED DESCRIPTION OF THE MEASURING PROCEDURE

The dehydration of the salt hydrates has been carried out in dynamic mode with a slow heating rate of 0.5 K/min to approach the equilibrium conditions of the materials. For the sulfates, the dehydration reaction was carried out between 25 and 150°C. A different temperature range between 40 and 130°C has been chosen for  $\text{MgCl}_2 \cdot 6\text{H}_2\text{O}$  for practical reasons. *In-situ* X-ray diffraction analyses performed at 13 mbar have shown an overhydration of  $\text{MgCl}_2 \cdot 6\text{H}_2\text{O}$  for temperatures below 40°C and a decomposition of the material in  $\text{MgOHCl}$  by release of  $\text{HCl}$  vapors above the temperature of 130°C. The TG and DSC curves of the dehydration of the four salt hydrates are presented in this study. Additionally, the temperature of the dehydration reactions (peak temperature), the reaction enthalpy values and energy density values obtained for these materials under the practical conditions of the heat storage have been summarized and compared with the values determined from the NBS data [1]. The energy density values were calculated with the material density values of the reactant phase of each reaction.

### RESULTS

The TG and DSC results in figure 2 shows that the four salt hydrates presented in this study can store heat under the operational conditions of seasonal heat storage by removal of water molecules in their material structure, thereby reaching lower hydrated or anhydrous composition.

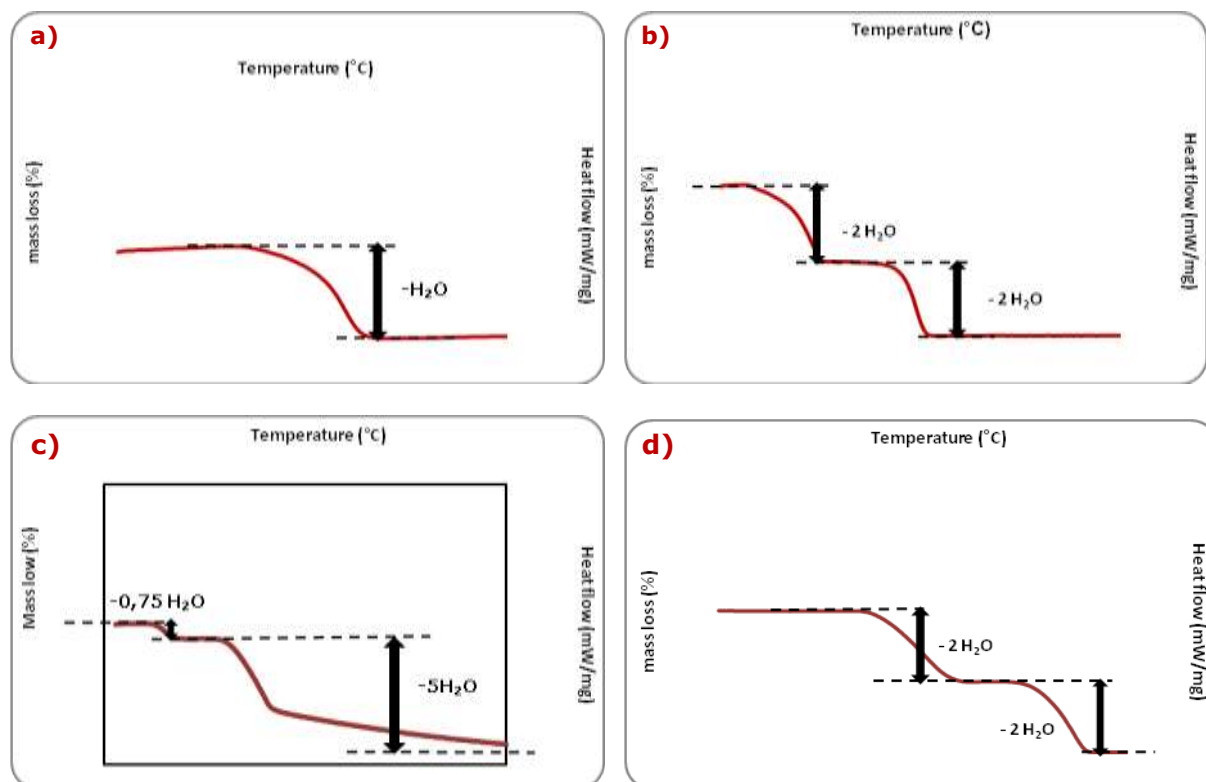


Figure 2 : TG (in red) and DSC (in blue) curves of the dehydration reaction at 13 mbar water vapor pressure and a heating rate of 0.5 K/min of (a)  $\text{Li}_2\text{SO}_4 \cdot \text{H}_2\text{O}$ , (b)  $\text{CuSO}_4 \cdot 5\text{H}_2\text{O}$ , (c)  $\text{MgSO}_4 \cdot 7\text{H}_2\text{O}$  and (d)  $\text{MgCl}_2 \cdot 6\text{H}_2\text{O}$  powders sieved at 100-200  $\mu\text{m}$

The summary of the temperature of the dehydration reactions (peak temperature), the reaction enthalpy values and energy density values obtained from the thermal analysis measurements are presented in table 1. The initial composition of magnesium sulfate hydrate powder has been estimated at  $\text{MgSO}_4 \cdot 6.75\text{H}_2\text{O}$  instead of  $\text{MgSO}_4 \cdot 7\text{H}_2\text{O}$ , because the material was already partially dried as shown on the figure 2c. This phenomenon can be explained by the fact that the transition of  $\text{MgSO}_4 \cdot 7\text{H}_2\text{O}$  to  $\text{MgSO}_4 \cdot 6\text{H}_2\text{O}$  starts at nearly ambient temperature (25-30°C). Therefore, during the storage and the sieving step performed before the measurement, 25% of the  $\text{MgSO}_4 \cdot 7\text{H}_2\text{O}$  powder was

dehydrated and the initial composition of the powder is a mix of  $\text{MgSO}_4 \cdot 7\text{H}_2\text{O}$  and  $\text{MgSO}_4 \cdot 6\text{H}_2\text{O}$  materials. The reaction enthalpy and the energy density values obtained for the loss of 0.75 water molecule have been recalculated for 1 molecule of water in table 1. The energy density of the dehydration reaction of  $\text{MgSO}_4 \cdot 6.75\text{H}_2\text{O}$  in  $\text{MgSO}_4 \cdot 6\text{H}_2\text{O}$  has been calculated with the density values of  $\text{MgSO}_4 \cdot 7\text{H}_2\text{O}$  because the density of  $\text{MgSO}_4 \cdot 6.75\text{H}_2\text{O}$  does not exist in the literature (indicated by an \* in table 1).

*Table 1 : Temperature of transition and enthalpy values of the phase transition observed during the dehydration reactions of sieved powders of  $\text{Li}_2\text{SO}_4 \cdot \text{H}_2\text{O}$ ,  $\text{CuSO}_4 \cdot 5\text{H}_2\text{O}$ ,  $\text{MgSO}_4 \cdot 7\text{H}_2\text{O}$  and  $\text{MgCl}_2 \cdot 6\text{H}_2\text{O}$  at 13 mbar water vapor pressure and 0.5 K/min heating rate.*

Dehydration reactions	Experimental data			NBS data [1]	
	$T_{\text{peak DSC}}$ (°C)	$\Delta rH$ [kJ/mol]	Energy density GJ/m <sup>3</sup>	$\Delta rH$ [kJ/mol]	Energy density GJ/m <sup>3</sup>
$\text{Li}_2\text{SO}_4 \cdot \text{H}_2\text{O} (s) \rightarrow \text{Li}_2\text{SO}_4 (s) + \text{H}_2\text{O} (g)$	97	41.01	0.71	57.18	0.99
$\text{CuSO}_4 \cdot 5\text{H}_2\text{O} (s) \rightarrow \text{CuSO}_4 \cdot 3\text{H}_2\text{O} (s) + 2\text{H}_2\text{O} (g)$	52	89.07	0.81	111.68	1.02
$\text{CuSO}_4 \cdot 3\text{H}_2\text{O} (s) \rightarrow \text{CuSO}_4 \cdot \text{H}_2\text{O} (s) + 2\text{H}_2\text{O} (g)$	86	89.44	1.12	114.82	1.44
$\text{MgSO}_4 \cdot 6.75\text{H}_2\text{O} (s) \rightarrow \text{MgSO}_4 \cdot 6\text{H}_2\text{O}(s) + 0.75\text{H}_2\text{O} (g)$ [ $\text{MgSO}_4 \cdot 7\text{H}_2\text{O} (s) \rightarrow \text{MgSO}_4 \cdot 6\text{H}_2\text{O} (s) + \text{H}_2\text{O} (g)$ ]	39	42.97 (0.75) 58.07 (1)	0.29 (0.75) * 0.39 (1)	59.88	0.41
$\text{MgSO}_4 \cdot 6\text{H}_2\text{O} (s) \rightarrow \text{MgSO}_4 \cdot \text{H}_2\text{O} (s) + 5\text{H}_2\text{O} (g)$	72	249.88	1.83	275.75	2.37
$\text{MgCl}_2 \cdot 6\text{H}_2\text{O} (s) \rightarrow \text{MgCl}_2 \cdot 4\text{H}_2\text{O} (s) + 2\text{H}_2\text{O} (g)$	85	102.61	0.79	116.37	0.89
$\text{MgCl}_2 \cdot 4\text{H}_2\text{O} (s) \rightarrow \text{MgCl}_2 \cdot 2\text{H}_2\text{O} (s) + 2\text{H}_2\text{O} (g)$	118	117.41	1.10	135.61	1.27

The energy density found for each material is directly related to the thermochemical reactions taking place in the material during the dehydration process. According to the present results, the crystal energy density of these materials is between 4 times ( $\text{Li}_2\text{SO}_4 \cdot \text{H}_2\text{O}$ ) to 11 times ( $\text{MgSO}_4 \cdot 7\text{H}_2\text{O}$ ) higher than the energy density in water (0.25 GJ/m<sup>3</sup>). Note however, that the energy density as presented above will be reduced in practical systems because of the porosity in the packed bed required for the vapor transport.

An additional disclaimer has to be made about the temperatures of reaction presented in this paper to model the water vapor sorption process of these materials. The temperature data presented correspond to the temperatures at which the chemical reactions take place during the dehydration process. Additional experiments showed that these temperatures depend on the heating rate applied to the system during the dehydration process. Then, these temperature results should be only considered to model a system set with a heating rate at 0.5 K/min. Moreover, the reaction temperatures presented in this paper should not be taken as reaction temperatures for the hydration process of these materials. As represented in fig. 3, the temperature of reaction of the dehydration process is commonly higher than the equilibrium temperature of the chemical reaction, while the temperature of reaction for the reversible hydration process is lower.

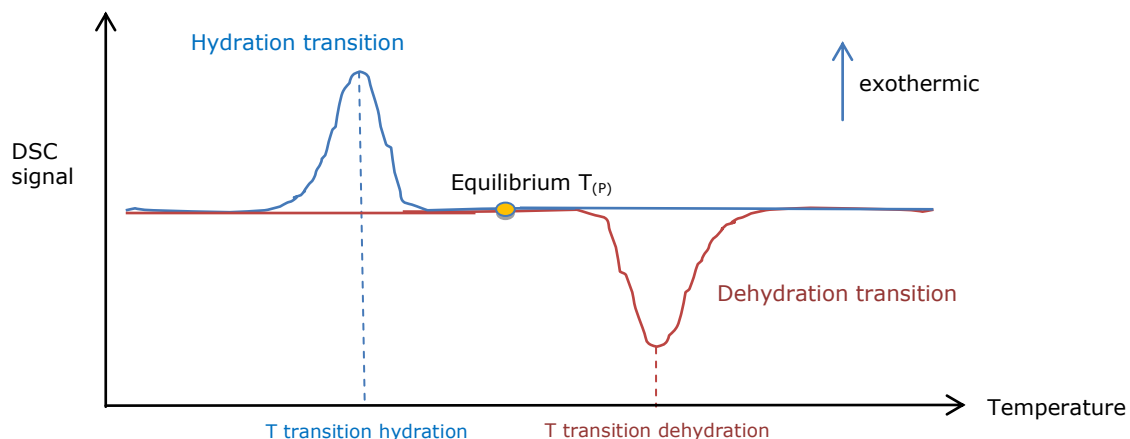


Figure 3: Theoretical representation of the DSC signal obtained for a phase transition during the dehydration and hydration reactions

### **CLOSURE**

Additional measurements performed with faster heating rates (1, 5, 10 K/min) have also been carried out for these materials, showing a constant energy density but an increase of the temperature of the phase transitions. Information on these measurements can be obtained by contacting Herbert Zondag, ECN – department Thermal Systems, P.O. Box 1, 1755 ZG Petten, The Netherlands, Tel : +31 224 56 4941, email : zondag@ecn.nl.

### **BIBLIOGRAPHY**

- [1] D. D. Wagman, W. H. Evans, V. B. Parker, R. H. Schumm, I. Halow, S. M. Balley, K. L. Churney, R. L. Nuttall, The NBS tables of chemical thermodynamic properties : selected values for inorganic and C<sub>1</sub> and C<sub>2</sub> organic substances in SI units, Journal of physical and chemical reference data, **11** (2), (1982)

## **SHORT DESCRIPTION OF TASK 42/ ANNEX 24**

From past IEA SHC and ECES tasks it was concluded that a broad and basic research and development initiative is needed to find and improve compact thermal energy storage materials. The IEA joint Task/Annex 42/24 brings together experts from both the materials development field and the systems integration fields. In four years, the task aims at having finished the first steps towards a new generation of thermal storage technologies.

## **OBJECTIVE**

The overall objective of this task is to develop advanced materials and systems for the compact storage of thermal energy. This can be subdivided into seven specific objectives:

- to identify, design and develop new materials and composites for compact thermal energy storage,
- to develop measuring and testing procedures to characterise new storage materials reliably and reproducibly,
- to improve the performance, stability, and cost-effectiveness of new storage materials,
- to develop multi-scale numerical models, describing and predicting the performance of new materials in thermal storage systems,
- to develop and demonstrate novel compact thermal energy storage systems employing the advanced materials,
- to assess the impact of new materials on the performance of thermal energy storage in the different applications considered, and
- to disseminate the knowledge and experience acquired in this task.

A secondary objective of this task is to create an active and effective research network in which researchers and industry working in the field of thermal energy storage can collaborate.

## **SCOPE**

This task deals with advanced materials for latent and chemical thermal energy storage, and excludes materials related to sensible heat storage. The task deals with these materials on three different scales:

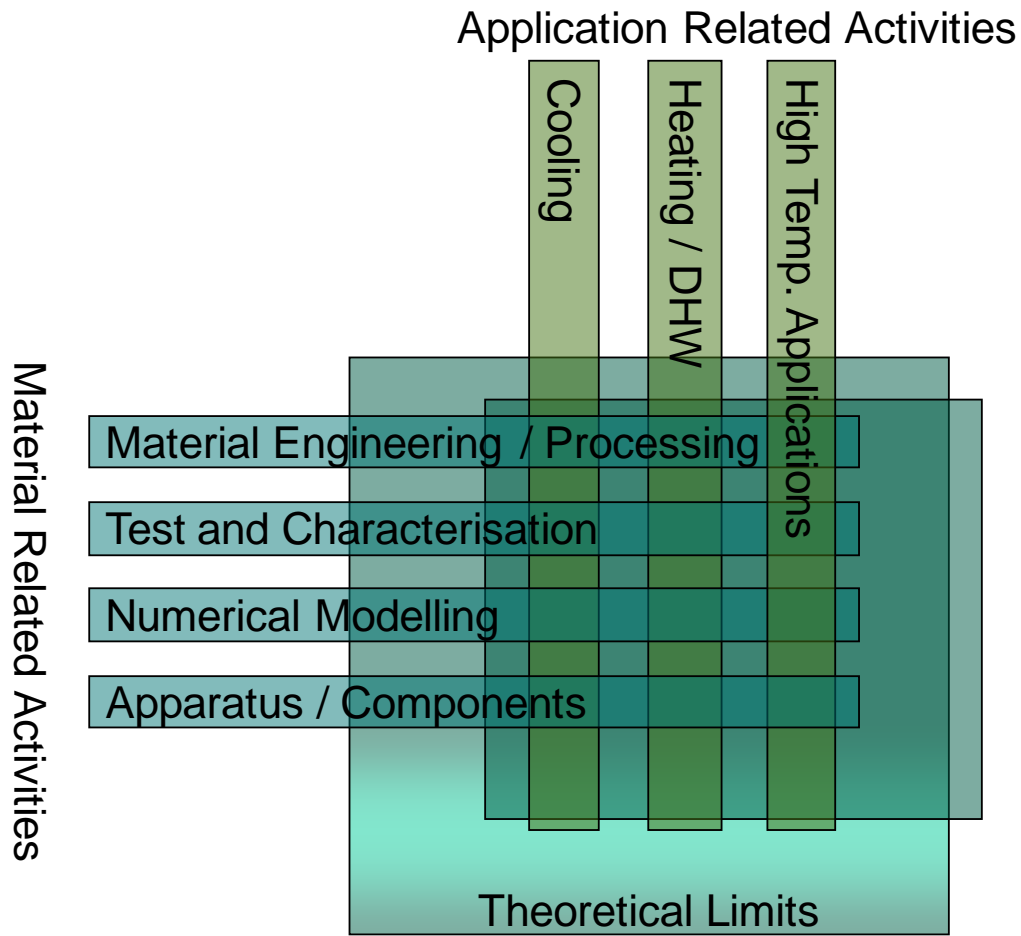
- material scale, focused on the behaviour of materials from the molecular to the 'few particles' scale, including e.g. material synthesis, micro-scale mass transport, and sorption reactions;
- bulk scale, focused on bulk behaviour of materials and the performance of the storage in itself, including e.g. heat, mass, and vapour transport, wall-wall and wall-material interactions, and reactor design;
- system scale, focused on the performance of a storage within a heating or cooling system, including e.g. economical feasibility studies, case studies, and system tests.

Because seasonal storage of solar heat for solar assisted heating of buildings is the main focus of the SHC IA, this will be one of the primary topics of this task. However, because there are many more relevant applications for TES, and because materials research is not and can not be limited to one application only, this task will focus on multiple application areas.

In the Task kick-off meeting it was decided to subdivide the Applications Subtask into three Working Groups, corresponding to three different temperature levels of thermal energy storage, as depicted below.

## **STRUCTURE**

To achieve the maximum amount of cross-fertilisation between the different backgrounds of the two Implementing Agreements and experts in this Joint Task, the Task is organised in a matrix-like structure (see diagram below).





## IEA Solar Heating and Cooling Programme

The *International Energy Agency* (IEA) is an autonomous body within the framework of the Organization for Economic Co-operation and Development (OECD) based in Paris. Established in 1974 after the first “oil shock,” the IEA is committed to carrying out a comprehensive program of energy cooperation among its members and the Commission of the European Communities.

The IEA provides a legal framework, through IEA Implementing Agreements such as the *Solar Heating and Cooling Agreement*, for international collaboration in energy technology research and development (R&D) and deployment. This IEA experience has proved that such collaboration contributes significantly to faster technological progress, while reducing costs; to eliminating technological risks and duplication of efforts; and to creating numerous other benefits, such as swifter expansion of the knowledge base and easier harmonization of standards.

The *Solar Heating and Cooling Programme* was one of the first IEA Implementing Agreements to be established. Since 1977, its members have been collaborating to advance active solar and passive solar and their application in buildings and other areas, such as agriculture and industry. Current members are:

Australia	Finland	Portugal
Austria	France	South Africa
Belgium	Italy	Spain
Canada	Mexico	Sweden
Denmark	Netherlands	Switzerland
European Commission	New Zealand	United States
Germany	Norway	

A total of 44 Tasks have been initiated, 33 of which have been completed. Each Task is managed by an Operating Agent from one of the participating countries. Overall control of the program rests with an Executive Committee comprised of one representative from each contracting party to the Implementing Agreement. In addition to the Task work, a number of special activities—Memorandum of Understanding with solar thermal trade organizations, statistics collection and analysis, conferences and workshops—have been undertaken.

To find Solar Heating and Cooling Programme publications and learn more about the Programme visit [www.iea-shc.org](http://www.iea-shc.org) or contact the SHC Secretariat, Pamela Murphy, e-mail: pmurphy@kmgrp.net.

**C**urrent Tasks & Working Group:

- Task 36 *Solar Resource Knowledge Management*
- Task 39 *Polymeric Materials for Solar Thermal Applications*
- Task 40 *Towards Net Zero Energy Solar Buildings*
- Task 41 *Solar Energy and Architecture*
- Task 42 *Compact Thermal Energy Storage*
- Task 43 *Solar Rating and Certification Procedures*
- Task 44 *Solar and Heat Pump Systems*
- Task 45 *Large Systems: Solar Heating/Cooling Systems, Seasonal Storages, Heat Pumps*
- Task 46 *Solar Resource Assessment and Forecasting*
- Task 47 *Renovation of Non-Residential Buildings Towards Sustainable Standards*
- Task 48 *Quality Assurance and Support Measures for Solar Cooling*
- Task 49 *Solar Process Heat for Production and Advanced Applications*

**C**ompleted Tasks:

- Task 1 *Investigation of the Performance of Solar Heating and Cooling Systems*
- Task 2 *Coordination of Solar Heating and Cooling R&D*
- Task 3 *Performance Testing of Solar Collectors*
- Task 4 *Development of an Insolation Handbook and Instrument Package*
- Task 5 *Use of Existing Meteorological Information for Solar Energy Application*
- Task 6 *Performance of Solar Systems Using Evacuated Collectors*
- Task 7 *Central Solar Heating Plants with Seasonal Storage*
- Task 8 *Passive and Hybrid Solar Low Energy Buildings*
- Task 9 *Solar Radiation and Pyranometry Studies*
- Task 10 *Solar Materials R&D*
- Task 11 *Passive and Hybrid Solar Commercial Buildings*
- Task 12 *Building Energy Analysis and Design Tools for Solar Applications*
- Task 13 *Advanced Solar Low Energy Buildings*
- Task 14 *Advanced Active Solar Energy Systems*
- Task 16 *Photovoltaics in Buildings*
- Task 17 *Measuring and Modeling Spectral Radiation*
- Task 18 *Advanced Glazing and Associated Materials for Solar and Building Applications*
- Task 19 *Solar Air Systems*
- Task 20 *Solar Energy in Building Renovation*
- Task 21 *Daylight in Buildings*
- Task 22 *Building Energy Analysis Tools*
- Task 23 *Optimization of Solar Energy Use in Large Buildings*
- Task 24 *Solar Procurement*
- Task 25 *Solar Assisted Air Conditioning of Buildings*
- Task 26 *Solar Combisystems*
- Task 27 *Performance of Solar Facade Components*
- Task 28 *Solar Sustainable Housing*
- Task 29 *Solar Crop Drying*
- Task 31 *Daylighting Buildings in the 21<sup>st</sup> Century*
- Task 32 *Advanced Storage Concepts for Solar and Low Energy Buildings*
- Task 33 *Solar Heat for Industrial Processes*
- Task 34 *Testing and Validation of Building Energy Simulation Tools*
- Task 35 *PV/Thermal Solar Systems*
- Task 37 *Advanced Housing Renovation with Solar & Conservation*
- Task 38 *Solar Thermal Cooling and Air Conditioning*

**C**ompleted Working Groups:

*CSHPSS; ISOLDE; Materials in Solar Thermal Collectors; Evaluation of Task 13 Houses; Daylight Research*



## IEA Energy Conservation Through Energy Storage Programme

The *International Energy Agency* (IEA), based in Paris, is an autonomous agency linked with the *Organisation for Economic Co-operation and Development* (OECD). The IEA is the energy forum for 26 Member countries. IEA Member governments are committed to taking joint measures to meet oil supply emergencies. They have also agreed to share energy information, to co-ordinate their energy policies and to co-operate in the development of rational energy programmes.

The R&D programme *Efficient Energy End-Use Technologies* contains 14 different *Implementing Agreements* (IAs) of which one is the IA on energy storage. The full name of this IA is *Energy Conservation through Energy Storage* (ECES IA). This IA was founded in 2004 and intends to promote co-operative research, development, demonstrations and exchanges of information regarding energy conservation through energy storage.

The continued development, application and deployment of energy efficient end-use technologies has the potential to significantly reduce energy consumption and greenhouse gases in the buildings, electricity generation, industry, and transport sectors. Energy storage technologies can overcome the temporal mismatch between energy supply and demand, especially regarding renewable energy technologies, the use of waste energy and energy from ambient sources such as cold from the natural environment.

Active participants in ECES IA are at present:

Belgium	Germany	Sweden
Canada	Italy	USA
China	Japan	Turkey
Finland	Korea	
France	Norway	

Three sponsors are participating in the ECES at the moment:

IF Technology B.V. (Netherlands)  
 Institute of Heat Engineering, University of Technology of Warsaw (Poland)  
 Energesis Ingeniería, S.L. (Spain).

Other countries have signed the agreement but are not presently engaged in the activities. Further countries have recently shown interest in participating in the near future, including countries from Eastern Europe.

The work within the ECES IA is lead by an *Executive Committee* (XC) and the work undertaken by this XC is done by mutual agreements defined in Annexes as listed on the next page. The work is led by Chairman Halime Paksoy (Turkey) and Secretary Hunay Evliya (Turkey).

To find ECES publications and learn more about the Programme visit <http://www.iea-eces.org> or contact the ECES Secretariat, Hunay Evliya, e-mail: hevliya@cu.edu.tr

**Ongoing Annexes:**

- Annex 20 *Sustainable Cooling with Thermal Energy Storage*
- Annex 21 *Thermal Response Test for Underground Thermal Energy Storages*
- Annex 22 *Thermal Energy Storage Applications in Closed Greenhouses*
- Annex 23 *Applying Energy Storage in Ultra-low Energy Buildings*
- Annex 24 *Material Development for Improved Thermal Energy Storage Systems*
- Annex 25 *Surplus Heat Management using Advanced TES for CO<sub>2</sub> mitigation*
- Annex 26 *Electric Energy Storage: Future Energy Storage Demand*

**Completed Annexes:**

- Annex 1 *Large Scale Thermal Storage Systems Evaluation*
- Annex 2 *Lake Storage Demonstration Plant in Mannheim*
- Annex 3 *Aquifer Storage Demonstration Plant in Lausanne Dorigny*
- Annex 4 *Short Term Water Heat Storage Systems*
- Annex 5 *Full Scale Latent Heat Storage Installations*
- Annex 6 *Environmental and Chemical aspects of Thermal Energy Storage in Aquifers and Research and Development of Water Treatment Methods*
- Annex 7 *Innovative and Cost Effective Seasonal Cold Storage Applications*
- Annex 8 *Implementing Underground Thermal Energy Storage Systems*
- Annex 9 *Electrical Energy Storage Technologies for Utility Network Optimization*
- Annex 10 *Phase Change Materials and Chemical Reactions for Thermal Energy Storage*
- Annex 12 *High-Temperature Underground Thermal Energy Storage (HT UTES)*
- Annex 13 *Design, Construction and Maintenance of UTES Wells and Boreholes*
- Annex 14 *Cooling with TES in all Climates*
- Annex 17 *Advanced Thermal Energy Storage Techniques – Feasibility Studies and Demonstration Projects*
- Annex 18 *Transportation of Thermal Energy Utilizing Thermal Energy Storage Technology*
- Annex 19 *Optimised Industrial Process Heat and Power Generation with Thermal Energy Storage*

**APPENDIX "DETAILED EXPERIMENTAL RESULTS FOR SUBMERGED FINNED HEAT EXCHANGER IN PCM BASED THERMAL ENERGY STORAGE" BY NM. J. CHIU AND V. MARTIN**

**Congeaing Process**

Inlet T 11 °C								
Freezing	Run A		Freezing	Run B		Freezing	Run C	
Time (s)	Tfin (°C)	Tpcm (°C)	Time (s)	Tfin (°C)	Tpcm (°C)	Time (s)	Tfin (°C)	Tpcm (°C)
0	20.31	29.08	0	20.42	29.03	0	23.74	29.01
10	20.22	28.91	10	20.33	28.85	10	23.32	28.99
20	20.12	28.73	20	20.24	28.68	20	22.94	28.95
30	20.05	28.56	30	20.15	28.49	30	22.61	28.91
40	19.96	28.37	40	20.08	28.32	40	22.31	28.86
50	19.88	28.21	50	20.02	28.16	50	22.06	28.79
60	19.81	28.05	60	19.94	27.98	60	21.81	28.71
70	19.73	27.87	70	19.86	27.80	70	21.59	28.63
80	19.68	27.71	80	19.80	27.64	80	21.38	28.52
90	19.62	27.54	90	19.72	27.47	90	21.21	28.42
100	19.55	27.37	100	19.66	27.32	100	21.04	28.31
110	19.49	27.22	110	19.60	27.15	110	20.89	28.19
120	19.43	27.05	120	19.54	27.00	120	20.76	28.06
130	19.37	26.91	130	19.47	26.86	130	20.65	27.93
140	19.30	26.75	140	19.41	26.70	140	20.53	27.81
150	19.25	26.60	150	19.35	26.55	150	20.44	27.65
160	19.19	26.44	160	19.28	26.39	160	20.36	27.52
170	19.12	26.29	170	19.21	26.26	170	20.27	27.38
180	19.07	26.16	180	19.16	26.12	180	20.19	27.23
190	19.00	26.01	190	19.08	25.97	190	20.09	27.10
200	18.95	25.87	200	19.03	25.84	200	20.03	26.95
210	18.90	25.74	210	18.97	25.68	210	19.97	26.82
220	18.84	25.61	220	18.92	25.55	220	19.90	26.67
230	18.78	25.48	230	18.86	25.42	230	19.82	26.51
240	18.73	25.35	240	18.81	25.29	240	19.75	26.38
250	18.69	25.22	250	18.78	25.17	250	19.70	26.25
260	18.64	25.10	260	18.76	25.05	260	19.62	26.11
270	18.59	24.97	270	18.71	24.93	270	19.58	25.99
280	18.55	24.85	280	18.67	24.81	280	19.50	25.85
290	18.51	24.75	290	18.64	24.69	290	19.45	25.72
300	18.48	24.62	300	18.59	24.58	300	19.41	25.60
310	18.44	24.52	310	18.52	24.45	310	19.35	25.46
320	18.40	24.39	320	18.51	24.36	320	19.30	25.35
330	18.37	24.29	330	18.46	24.24	330	19.25	25.22
340	18.33	24.17	340	18.43	24.15	340	19.21	25.11
350	18.30	24.08	350	18.40	24.05	350	19.18	24.99

360	18.26	23.98		360	18.35	23.95		360	19.13	24.88
370	18.23	23.88		370	18.31	23.84		370	19.09	24.77
380	18.20	23.79		380	18.29	23.75		380	19.04	24.65
390	18.16	23.68		390	18.25	23.66		390	19.00	24.55
400	18.14	23.58		400	18.19	23.57		400	18.95	24.46
410	18.11	23.51		410	18.17	23.48		410	18.89	24.35
420	18.06	23.41		420	18.12	23.38		420	18.84	24.25
430	18.02	23.33		430	18.08	23.30		430	18.80	24.14
440	17.98	23.23		440	18.04	23.22		440	18.75	24.05
450	17.94	23.15		450	18.01	23.12		450	18.68	23.95
460	17.91	23.08		460	17.97	23.04		460	18.65	23.86
470	17.87	22.99		470	17.94	22.97		470	18.59	23.77
480	17.82	22.92		480	17.90	22.90		480	18.53	23.68
490	17.78	22.83		490	17.87	22.82		490	18.49	23.58
500	17.74	22.76		500	17.84	22.74		500	18.44	23.51
510	17.70	22.67		510	17.78	22.65		510	18.38	23.42
520	17.67	22.61		520	17.75	22.58		520	18.34	23.35
530	17.64	22.54		530	17.71	22.53		530	18.30	23.28
540	17.61	22.48		540	17.67	22.46		540	18.24	23.20
550	17.57	22.42		550	17.63	22.39		550	18.20	23.13
560	17.53	22.33		560	17.59	22.32		560	18.16	23.06
570	17.48	22.27		570	17.55	22.25		570	18.12	22.98
580	17.44	22.21		580	17.51	22.20		580	18.08	22.93
590	17.40	22.15		590	17.46	22.13		590	18.03	22.85
600	17.35	22.08		600	17.43	22.07		600	17.99	22.77
610	17.32	22.02		610	17.38	22.02		610	17.95	22.71
620	17.28	21.97		620	17.36	21.96		620	17.92	22.65
630	17.24	21.91		630	17.32	21.91		630	17.88	22.58
640	17.22	21.86		640	17.28	21.86		640	17.84	22.51
650	17.18	21.83		650	17.25	21.81		650	17.82	22.47
660	17.14	21.76		660	17.22	21.76		660	17.78	22.42
670	17.09	21.72		670	17.18	21.72		670	17.75	22.34
680	17.06	21.67		680	17.17	21.69		680	17.70	22.30
690	17.03	21.62		690	17.12	21.62		690	17.68	22.26
700	17.01	21.58		700	17.10	21.61		700	17.64	22.20
710	16.98	21.53		710	17.06	21.55		710	17.62	22.14
720	16.93	21.49		720	17.02	21.52		720	17.58	22.11
730	16.90	21.46		730	17.00	21.49		730	17.54	22.06
740	16.87	21.42		740	16.98	21.46		740	17.52	22.02
750	16.84	21.38		750	16.93	21.42		750	17.49	21.97
760	16.81	21.35		760	16.91	21.40		760	17.46	21.94
770	16.78	21.31		770	16.86	21.36		770	17.43	21.89
780	16.75	21.28		780	16.83	21.33		780	17.40	21.86
790	16.72	21.24		790	16.80	21.30		790	17.37	21.83

800	16.68	21.23		800	16.78	21.28		800	17.34	21.78
810	16.65	21.19		810	16.74	21.25		810	17.31	21.77
820	16.62	21.17		820	16.72	21.23		820	17.29	21.73
830	16.60	21.13		830	16.69	21.20		830	17.27	21.69
840	16.58	21.12		840	16.66	21.17		840	17.23	21.67
850	16.56	21.09		850	16.65	21.15		850	17.20	21.64
860	16.53	21.06		860	16.63	21.14		860	17.17	21.60
870	16.51	21.04		870	16.60	21.12		870	17.14	21.57
880	16.48	21.02		880	16.58	21.09		880	17.12	21.54
890	16.44	20.99		890	16.54	21.08		890	17.09	21.52
900	16.42	20.97		900	16.53	21.04		900	17.07	21.50
910	16.40	20.97		910	16.50	21.04		910	17.04	21.48
920	16.38	20.94		920	16.45	21.00		920	17.01	21.44
930	16.35	20.92		930	16.44	20.98		930	17.00	21.42
940	16.34	20.90		940	16.41	20.98		940	16.96	21.40
950	16.32	20.88		950	16.39	20.96		950	16.95	21.37
960	16.30	20.88		960	16.38	20.95		960	16.91	21.35
970	16.26	20.87		970	16.35	20.94		970	16.89	21.33
980	16.24	20.87		980	16.33	20.94		980	16.86	21.29
990	16.22	20.84		990	16.31	20.93		990	16.84	21.28
1000	16.19	20.82		1000	16.29	20.90		1000	16.82	21.25
1010	16.18	20.81		1010	16.26	20.90		1010	16.80	21.24
1020	16.17	20.82		1020	16.24	20.88		1020	16.77	21.22
1030	16.15	20.80		1030	16.22	20.88		1030	16.74	21.21
1040	16.11	20.79		1040	16.21	20.87		1040	16.72	21.20
1050	16.11	20.80		1050	16.18	20.86		1050	16.70	21.19
1060	16.08	20.78		1060	16.18	20.85		1060	16.68	21.17
1070	16.05	20.77		1070	16.15	20.85		1070	16.64	21.17
1080	16.04	20.76		1080	16.14	20.84		1080	16.62	21.17
1090	16.03	20.75		1090	16.11	20.82		1090	16.61	21.16
1100	15.99	20.74		1100	16.08	20.82		1100	16.58	21.15
1110	15.99	20.76		1110	16.07	20.82		1110	16.56	21.15
1120	15.96	20.74		1120	16.06	20.81		1120	16.53	21.15
1130	15.95	20.73		1130	16.05	20.79		1130	16.52	21.13
1140	15.93	20.75		1140	16.01	20.79		1140	16.48	21.14
1150	15.91	20.72		1150	16.00	20.78		1150	16.47	21.13
1160	15.88	20.72		1160	15.98	20.77		1160	16.43	21.13
1170	15.86	20.71		1170	15.97	20.77		1170	16.44	21.12
1180	15.85	20.71		1180	15.95	20.76		1180	16.41	21.12
1190	15.82	20.71		1190	15.94	20.75		1190	16.40	21.12
1200	15.82	20.70		1200	15.92	20.74		1200	16.37	21.10
1210	15.79	20.69		1210	15.89	20.74		1210	16.34	21.10
1220	15.78	20.69		1220	15.88	20.73		1220	16.34	21.09
1230	15.74	20.69		1230	15.86	20.72		1230	16.30	21.07

1240	15.74	20.69		1240	15.86	20.73		1240	16.29	21.07
1250	15.73	20.67		1250	15.84	20.72		1250	16.28	21.07
1260	15.70	20.67		1260	15.80	20.70		1260	16.25	21.03
1270	15.69	20.66		1270	15.79	20.70		1270	16.24	21.02
1280	15.69	20.65		1280	15.77	20.69		1280	16.21	21.01
1290	15.66	20.64		1290	15.75	20.68		1290	16.19	21.02
1300	15.65	20.65		1300	15.73	20.67		1300	16.17	21.00
1310	15.64	20.62		1310	15.73	20.67		1310	16.15	20.99
1320	15.62	20.61		1320	15.70	20.65		1320	16.14	20.97
1330	15.58	20.60		1330	15.67	20.65		1330	16.11	20.97
1340	15.57	20.59		1340	15.67	20.65		1340	16.09	20.96
1350	15.56	20.59		1350	15.65	20.63		1350	16.09	20.95
1360	15.54	20.58		1360	15.64	20.63		1360	16.06	20.94
1370	15.53	20.58		1370	15.62	20.62		1370	16.05	20.94
1380	15.52	20.56		1380	15.61	20.63		1380	16.04	20.95
1390	15.51	20.56		1390	15.59	20.62		1390	16.01	20.93
1400	15.50	20.54		1400	15.58	20.61		1400	16.00	20.91
1410	15.47	20.54		1410	15.55	20.61		1410	15.98	20.93
1420	15.45	20.55		1420	15.53	20.61		1420	15.96	20.91
1430	15.44	20.54		1430	15.51	20.60		1430	15.94	20.91
1440	15.41	20.53		1440	15.50	20.62		1440	15.93	20.91
1450	15.41	20.51		1450	15.49	20.60		1450	15.92	20.91
1460	15.40	20.50		1460	15.47	20.58		1460	15.89	20.88
1470	15.39	20.49		1470	15.46	20.57		1470	15.87	20.89
1480	15.37	20.49		1480	15.45	20.57		1480	15.86	20.88
1490	15.36	20.48		1490	15.42	20.57		1490	15.85	20.88
1500	15.33	20.46		1500	15.42	20.54		1500	15.83	20.89
1510	15.32	20.47		1510	15.40	20.54		1510	15.82	20.91
1520	15.31	20.46		1520	15.39	20.52		1520	15.80	20.90
1530	15.28	20.44		1530	15.37	20.50		1530	15.78	20.88
1540	15.27	20.45		1540	15.37	20.49		1540	15.76	20.88
1550	15.26	20.44		1550	15.35	20.49		1550	15.76	20.87
1560	15.24	20.44		1560	15.33	20.47		1560	15.74	20.85
1570	15.23	20.43		1570	15.32	20.45		1570	15.71	20.85
1580	15.22	20.42		1580	15.31	20.44		1580	15.70	20.85
1590	15.19	20.42		1590	15.29	20.43		1590	15.69	20.84
1600	15.20	20.43		1600	15.29	20.42		1600	15.67	20.84
1610	15.17	20.42		1610	15.27	20.40		1610	15.65	20.84
1620	15.16	20.41		1620	15.26	20.38		1620	15.65	20.84
1630	15.15	20.39		1630	15.24	20.37		1630	15.62	20.83
1640	15.13	20.37		1640	15.23	20.36		1640	15.62	20.83
1650	15.12	20.36		1650	15.22	20.33		1650	15.60	20.81
1660	15.11	20.36		1660	15.21	20.33		1660	15.58	20.80
1670	15.09	20.34		1670	15.18	20.33		1670	15.56	20.80

1680	15.08	20.33		1680	15.18	20.32		1680	15.55	20.78
1690	15.06	20.32		1690	15.16	20.31		1690	15.55	20.77
1700	15.06	20.29		1700	15.15	20.31		1700	15.53	20.75
1710	15.05	20.29		1710	15.13	20.28		1710	15.51	20.73
1720	15.04	20.27		1720	15.13	20.28		1720	15.49	20.73
1730	15.02	20.26		1730	15.12	20.26		1730	15.49	20.69
1740	15.01	20.24		1740	15.11	20.25		1740	15.48	20.69
1750	15.00	20.21		1750	15.11	20.25		1750	15.46	20.67
1760	14.99	20.21		1760	15.09	20.23		1760	15.46	20.64
1770	14.97	20.21		1770	15.06	20.21		1770	15.42	20.64
1780	14.96	20.18		1780	15.06	20.18		1780	15.42	20.63
1790	14.94	20.15		1790	15.06	20.17		1790	15.40	20.62
1800	14.94	20.14		1800	15.05	20.16		1800	15.40	20.61
1810	14.94	20.14		1810	15.03	20.16		1810	15.37	20.61
1820	14.91	20.11		1820	15.02	20.11		1820	15.36	20.59
1830	14.90	20.10		1830	15.00	20.09		1830	15.35	20.59
1840	14.89	20.09		1840	14.99	20.07		1840	15.34	20.59
1850	14.89	20.05		1850	14.99	20.06		1850	15.32	20.58
1860	14.88	20.05		1860	14.97	20.04		1860	15.31	20.56
1870	14.86	20.03		1870	14.95	20.03		1870	15.30	20.55
1880	14.84	20.01		1880	14.95	20.01		1880	15.29	20.52
1890	14.85	19.99		1890	14.93	19.99		1890	15.28	20.50
1900	14.84	19.97		1900	14.93	19.97		1900	15.26	20.50
1910	14.81	19.95		1910	14.91	19.97		1910	15.26	20.49
1920	14.81	19.93		1920	14.90	19.96		1920	15.25	20.47
1930	14.79	19.92		1930	14.89	19.93		1930	15.23	20.47
1940	14.79	19.90		1940	14.88	19.92		1940	15.22	20.46
1950	14.77	19.90		1950	14.86	19.89		1950	15.20	20.45
1960	14.75	19.87		1960	14.86	19.87		1960	15.19	20.43
1970	14.75	19.86		1970	14.85	19.86		1970	15.18	20.41
1980	14.73	19.84		1980	14.84	19.83		1980	15.16	20.41
1990	14.72	19.84		1990	14.81	19.80		1990	15.15	20.38
2000	14.72	19.83		2000	14.82	19.78		2000	15.14	20.38
2010	14.71	19.81		2010	14.79	19.77		2010	15.13	20.36
2020	14.69	19.79		2020	14.78	19.73		2020	15.12	20.34
2030	14.68	19.76		2030	14.78	19.70		2030	15.11	20.32
2040	14.68	19.75		2040	14.76	19.68		2040	15.11	20.29
2050	14.67	19.73		2050	14.76	19.66		2050	15.08	20.27
2060	14.66	19.71		2060	14.74	19.64		2060	15.07	20.24
2070	14.64	19.67		2070	14.74	19.60		2070	15.06	20.22
2080	14.64	19.66		2080	14.73	19.58		2080	15.05	20.18
2090	14.62	19.63		2090	14.71	19.55		2090	15.05	20.16
2100	14.62	19.61		2100	14.70	19.52		2100	15.03	20.14
2110	14.60	19.59		2110	14.69	19.50		2110	15.02	20.10

2120	14.59	19.58		2120	14.68	19.49		2120	15.02	20.08
2130	14.58	19.56		2130	14.66	19.45		2130	15.00	20.06
2140	14.57	19.55		2140	14.66	19.43		2140	14.99	20.02
2150	14.56	19.52		2150	14.64	19.41		2150	14.98	19.99
2160	14.55	19.50		2160	14.63	19.38		2160	14.98	19.96
2170	14.54	19.48		2170	14.62	19.35		2170	14.96	19.94
2180	14.54	19.45		2180	14.61	19.34		2180	14.95	19.90
2190	14.52	19.42		2190	14.61	19.32		2190	14.94	19.88
2200	14.51	19.40		2200	14.60	19.29		2200	14.92	19.84
2210	14.50	19.37		2210	14.58	19.25		2210	14.91	19.80
2220	14.50	19.36		2220	14.58	19.22		2220	14.90	19.78
2230	14.48	19.34		2230	14.56	19.20		2230	14.89	19.74
2240	14.47	19.34		2240	14.55	19.17		2240	14.89	19.70
2250	14.46	19.31		2250	14.55	19.16		2250	14.87	19.67
2260	14.45	19.29		2260	14.54	19.13		2260	14.86	19.66
2270	14.44	19.26		2270	14.53	19.11		2270	14.85	19.63
2280	14.43	19.25		2280	14.51	19.06		2280	14.84	19.60
2290	14.42	19.21		2290	14.50	19.02		2290	14.83	19.56
2300	14.40	19.19		2300	14.50	19.03		2300	14.82	19.52
2310	14.41	19.16		2310	14.49	18.99		2310	14.82	19.50
2320	14.39	19.13		2320	14.49	18.97		2320	14.80	19.48
2330	14.39	19.11		2330	14.47	18.93		2330	14.80	19.45
2340	14.37	19.07		2340	14.46	18.92		2340	14.78	19.40
2350	14.37	19.05		2350	14.45	18.90		2350	14.78	19.38
2360	14.35	19.02		2360	14.43	18.86		2360	14.76	19.35
2370	14.34	19.00		2370	14.43	18.83		2370	14.76	19.31
2380	14.32	18.97		2380	14.41	18.80		2380	14.74	19.30
2390	14.31	18.95		2390	14.39	18.78		2390	14.73	19.26
2400	14.31	18.91		2400	14.39	18.74		2400	14.71	19.22
2410	14.31	18.90		2410	14.38	18.73		2410	14.70	19.20
2420	14.28	18.85		2420	14.37	18.70		2420	14.70	19.17
2430	14.28	18.83		2430	14.37	18.68		2430	14.70	19.16
2440	14.27	18.81		2440	14.36	18.65		2440	14.68	19.12
2450	14.26	18.77		2450	14.36	18.62		2450	14.67	19.09
2460	14.25	18.74		2460	14.35	18.60		2460	14.66	19.06
2470	14.25	18.73		2470	14.32	18.57		2470	14.66	19.04
2480	14.23	18.69		2480	14.31	18.54		2480	14.64	19.00
2490	14.22	18.66		2490	14.30	18.53		2490	14.64	18.98
2500	14.21	18.65		2500	14.31	18.49		2500	14.61	18.95
2510	14.21	18.61		2510	14.29	18.47		2510	14.61	18.92
2520	14.20	18.59		2520	14.28	18.43		2520	14.60	18.88
2530	14.20	18.57		2530	14.27	18.41		2530	14.60	18.85
2540	14.19	18.53		2540	14.26	18.39		2540	14.59	18.81
2550	14.18	18.51		2550	14.25	18.36		2550	14.58	18.78

2560	14.17	18.49		2560	14.24	18.33		2560	14.56	18.75
2570	14.16	18.45		2570	14.23	18.31		2570	14.55	18.72
2580	14.16	18.43		2580	14.22	18.29		2580	14.54	18.69
2590	14.14	18.39		2590	14.21	18.25		2590	14.53	18.66
2600	14.15	18.37		2600	14.21	18.22		2600	14.52	18.63
2610	14.12	18.35		2610	14.18	18.18		2610	14.52	18.58
2620	14.13	18.31		2620	14.16	18.15		2620	14.50	18.56
2630	14.10	18.28		2630	14.18	18.14		2630	14.49	18.53
2640	14.09	18.26		2640	14.16	18.10		2640	14.48	18.50
2650	14.08	18.23		2650	14.15	18.08		2650	14.48	18.46
2660	14.08	18.21		2660	14.14	18.04		2660	14.46	18.44
2670	14.07	18.19		2670	14.14	18.02		2670	14.45	18.40
2680	14.06	18.16		2680	14.12	18.00		2680	14.43	18.38
2690	14.05	18.11		2690	14.11	17.97		2690	14.44	18.35
2700	14.05	18.10		2700	14.11	17.94		2700	14.42	18.32
2710	14.04	18.07		2710	14.10	17.92		2710	14.41	18.28
2720	14.04	18.06		2720	14.10	17.88		2720	14.40	18.26
2730	14.01	18.02		2730	14.07	17.85		2730	14.39	18.23
2740	14.01	17.99		2740	14.07	17.82		2740	14.38	18.20
2750	13.99	17.97		2750	14.05	17.79		2750	14.37	18.17
2760	13.99	17.93		2760	14.05	17.75		2760	14.37	18.14
2770	13.97	17.91		2770	14.04	17.73		2770	14.36	18.11
2780	13.98	17.89		2780	14.03	17.71		2780	14.34	18.07
2790	13.98	17.87		2790	14.03	17.68		2790	14.32	18.05
2800	13.96	17.83		2800	14.01	17.65		2800	14.32	18.01
2810	13.95	17.81		2810	14.00	17.63		2810	14.30	17.98
2820	13.94	17.78		2820	14.00	17.62		2820	14.30	17.95
2830	13.95	17.75		2830	13.99	17.57		2830	14.29	17.93
2840	13.93	17.72		2840	13.98	17.53		2840	14.28	17.90
2850	13.92	17.69		2850	13.96	17.51		2850	14.27	17.86
2860	13.92	17.67		2860	13.96	17.48		2860	14.26	17.83
2870	13.91	17.64		2870	13.95	17.47		2870	14.25	17.80
2880	13.89	17.63		2880	13.94	17.43		2880	14.24	17.78
2890	13.87	17.58		2890	13.94	17.40		2890	14.24	17.75
2900	13.88	17.56		2900	13.93	17.37		2900	14.22	17.72
2910	13.86	17.53		2910	13.92	17.35		2910	14.21	17.70
2920	13.85	17.50		2920	13.91	17.32		2920	14.20	17.64
2930	13.85	17.48		2930	13.90	17.29		2930	14.19	17.63
2940	13.84	17.45		2940	13.89	17.28		2940	14.18	17.60
2950	13.83	17.40		2950	13.88	17.24		2950	14.18	17.58
2960	13.84	17.39		2960	13.87	17.21		2960	14.16	17.54
2970	13.81	17.37		2970	13.85	17.19		2970	14.16	17.52
2980	13.81	17.34		2980	13.84	17.14		2980	14.14	17.49
2990	13.78	17.30		2990	13.85	17.11		2990	14.13	17.45

3000	13.78	17.29		3000	13.83	17.10		3000	14.13	17.44
3010	13.78	17.25		3010	13.81	17.07		3010	14.13	17.40
3020	13.77	17.24		3020	13.80	17.04		3020	14.11	17.37
3030	13.76	17.19		3030	13.80	17.02		3030	14.09	17.33
3040	13.74	17.17		3040	13.80	16.99		3040	14.08	17.32
3050	13.73	17.15		3050	13.78	16.96		3050	14.08	17.28
3060	13.73	17.12		3060	13.79	16.94		3060	14.07	17.27
3070	13.71	17.10		3070	13.77	16.90		3070	14.06	17.23
3080	13.71	17.07		3080	13.76	16.88		3080	14.05	17.21
3090	13.69	17.05		3090	13.76	16.86		3090	14.04	17.18
3100	13.69	17.01		3100	13.74	16.83		3100	14.03	17.15
3110	13.68	16.99		3110	13.74	16.80		3110	14.02	17.12
3120	13.67	16.96		3120	13.73	16.77		3120	14.01	17.09
3130	13.66	16.94		3130	13.71	16.74		3130	14.00	17.06
3140	13.65	16.91		3140	13.70	16.72		3140	13.99	17.05
3150	13.64	16.88		3150	13.70	16.69		3150	13.98	17.01
3160	13.63	16.85		3160	13.68	16.67		3160	13.96	17.00
3170	13.62	16.82		3170	13.68	16.63		3170	13.96	16.96
3180	13.62	16.81		3180	13.68	16.63		3180	13.95	16.94
3190	13.60	16.77		3190	13.67	16.58		3190	13.95	16.91
3200	13.59	16.77		3200	13.65	16.56		3200	13.92	16.89
3210	13.58	16.72		3210	13.64	16.54		3210	13.91	16.85
3220	13.59	16.71		3220	13.64	16.52		3220	13.92	16.83
3230	13.57	16.67		3230	13.62	16.49		3230	13.90	16.80
3240	13.55	16.66		3240	13.61	16.44		3240	13.90	16.78
3250	13.55	16.64		3250	13.61	16.43		3250	13.88	16.76
3260	13.54	16.60		3260	13.59	16.40		3260	13.88	16.73
3270	13.54	16.58		3270	13.58	16.38		3270	13.86	16.69
3280	13.51	16.54		3280	13.57	16.36		3280	13.86	16.67
3290	13.51	16.51		3290	13.56	16.34		3290	13.83	16.65
3300	13.51	16.50		3300	13.56	16.31		3300	13.84	16.62
3310	13.50	16.47		3310	13.54	16.29		3310	13.83	16.59
3320	13.48	16.44		3320	13.54	16.25		3320	13.80	16.57
3330	13.49	16.42		3330	13.53	16.24		3330	13.82	16.55
3340	13.48	16.40		3340	13.50	16.21		3340	13.78	16.52
3350	13.45	16.37		3350	13.49	16.17		3350	13.79	16.50
3360	13.47	16.35		3360	13.48	16.16		3360	13.78	16.46
3370	13.45	16.33		3370	13.47	16.11		3370	13.77	16.45
3380	13.45	16.30		3380	13.47	16.10		3380	13.76	16.42
3390	13.43	16.27		3390	13.48	16.10		3390	13.74	16.40
3400	13.42	16.24		3400	13.46	16.06		3400	13.75	16.38
3410	13.41	16.22		3410	13.45	16.04		3410	13.73	16.35
3420	13.40	16.20		3420	13.43	16.01		3420	13.71	16.32
3430	13.40	16.17		3430	13.42	15.99		3430	13.71	16.30

3440	13.38	16.14		3440	13.41	15.96		3440	13.69	16.27
3450	13.36	16.12		3450	13.41	15.94		3450	13.69	16.25
3460	13.35	16.10		3460	13.41	15.92		3460	13.68	16.22
3470	13.36	16.09		3470	13.39	15.89		3470	13.68	16.20
3480	13.35	16.04		3480	13.39	15.87		3480	13.65	16.17
3490	13.34	16.03		3490	13.38	15.85		3490	13.64	16.14
3500	13.33	15.99		3500	13.37	15.81		3500	13.64	16.13
3510	13.32	15.97		3510	13.36	15.79		3510	13.63	16.10
3520	13.31	15.93		3520	13.34	15.77		3520	13.62	16.08
3530	13.30	15.92		3530	13.35	15.74		3530	13.61	16.06
3540	13.29	15.90		3540	13.33	15.72		3540	13.61	16.03
3550	13.27	15.87		3550	13.31	15.68		3550	13.60	16.00
3560	13.27	15.85		3560	13.32	15.68		3560	13.60	15.99
3570	13.26	15.83		3570	13.30	15.64		3570	13.59	15.96
3580	13.24	15.81		3580	13.31	15.63		3580	13.55	15.93
3590	13.23	15.77		3590	13.29	15.59		3590	13.56	15.91
3600	13.23	15.75		3600	13.28	15.58		3600	13.54	15.89
3610	13.22	15.73		3610	13.27	15.55		3610	13.54	15.87
3620	13.21	15.71		3620	13.26	15.55		3620	13.53	15.84
3630	13.21	15.68		3630	13.25	15.50		3630	13.52	15.82
3640	13.19	15.67		3640	13.24	15.48		3640	13.51	15.80
3650	13.18	15.63		3650	13.22	15.46		3650	13.50	15.77
3660	13.17	15.60		3660	13.21	15.44		3660	13.50	15.75
3670	13.16	15.58		3670	13.22	15.41		3670	13.49	15.73
3680	13.17	15.55		3680	13.20	15.38		3680	13.47	15.71
3690	13.15	15.54		3690	13.20	15.36		3690	13.45	15.69
3700	13.14	15.51		3700	13.18	15.35		3700	13.45	15.66
3710	13.14	15.50		3710	13.17	15.34		3710	13.44	15.63
3720	13.13	15.48		3720	13.17	15.31		3720	13.44	15.61
3730	13.12	15.44		3730	13.15	15.28		3730	13.44	15.60
3740	13.11	15.43		3740	13.15	15.25		3740	13.42	15.57
3750	13.11	15.41		3750	13.15	15.25		3750	13.41	15.55
3760	13.09	15.38		3760	13.13	15.21		3760	13.40	15.52
3770	13.07	15.35		3770	13.13	15.19		3770	13.39	15.51
3780	13.08	15.35		3780	13.13	15.17		3780	13.39	15.48
3790	13.08	15.32		3790	13.11	15.15		3790	13.38	15.47
3800	13.05	15.31		3800	13.11	15.14		3800	13.37	15.44
3810	13.05	15.27		3810	13.09	15.12		3810	13.35	15.41
3820	13.03	15.25		3820	13.08	15.09		3820	13.35	15.40
3830	13.03	15.22		3830	13.07	15.07		3830	13.34	15.39
3840	13.02	15.20		3840	13.07	15.06		3840	13.33	15.36
3850	13.02	15.19		3850	13.06	15.04		3850	13.32	15.33
3860	13.02	15.16		3860	13.06	15.02		3860	13.31	15.32
3870	13.00	15.15						3870	13.30	15.30

3880	12.99	15.11					3880	13.30	15.27
3890	12.99	15.11					3890	13.28	15.26
3900	12.98	15.09					3900	13.29	15.24
3910	12.96	15.06					3910	13.27	15.20
3920	12.95	15.05					3920	13.26	15.20
3930	12.95	15.02					3930	13.27	15.17
							3940	13.23	15.15
							3950	13.24	15.12
							3960	13.23	15.12
							3970	13.22	15.09
							3980	13.21	15.08
							3990	13.20	15.07
							4000	13.19	15.04
							4010	13.18	15.01

## Melting Process

Inlet T 32 °C								
Melting	Run A		Melting	Run B		Melting	Run C	
Time (s)	Tfin (°C)	Tpcm (°C)	Time (s)	Tfin (°C)	Tpcm (°C)	Time (s)	Tfin (°C)	Tpcm (°C)
0	22.87	15.08	0	23.01	14.99	0	22.50	15.05
10	22.94	15.18	10	23.12	15.12	10	22.62	15.17
20	23.02	15.30	20	23.20	15.22	20	22.72	15.26
30	23.09	15.42	30	23.28	15.34	30	22.84	15.35
40	23.17	15.54	40	23.35	15.45	40	22.95	15.46
50	23.24	15.65	50	23.44	15.56	50	23.05	15.57
60	23.32	15.77	60	23.51	15.68	60	23.15	15.68
70	23.38	15.89	70	23.56	15.78	70	23.25	15.78
80	23.46	15.98	80	23.64	15.90	80	23.36	15.87
90	23.51	16.10	90	23.71	16.00	90	23.43	15.99
100	23.58	16.22	100	23.78	16.13	100	23.51	16.08
110	23.63	16.31	110	23.84	16.22	110	23.58	16.19
120	23.69	16.42	120	23.91	16.32	120	23.68	16.30
130	23.74	16.53	130	23.97	16.42	130	23.74	16.39
140	23.80	16.63	140	24.02	16.52	140	23.81	16.48
150	23.86	16.73	150	24.08	16.62	150	23.88	16.57
160	23.91	16.83	160	24.13	16.71	160	23.94	16.69
170	23.96	16.93	170	24.19	16.83	170	24.01	16.79
180	24.01	17.03	180	24.23	16.91	180	24.08	16.87
190	24.06	17.11	190	24.27	16.99	190	24.13	16.98
200	24.11	17.21	200	24.33	17.09	200	24.20	17.05
210	24.15	17.30	210	24.39	17.19	210	24.26	17.15
220	24.20	17.40	220	24.44	17.28	220	24.33	17.25
230	24.23	17.49	230	24.49	17.36	230	24.37	17.34
240	24.29	17.58	240	24.52	17.44	240	24.43	17.43
250	24.33	17.66	250	24.56	17.52	250	24.48	17.52
260	24.39	17.75	260	24.61	17.62	260	24.54	17.61
270	24.42	17.83	270	24.66	17.71	270	24.58	17.69
280	24.46	17.92	280	24.70	17.78	280	24.62	17.77
290	24.49	18.01	290	24.75	17.88	290	24.67	17.86
300	24.54	18.08	300	24.78	17.95	300	24.71	17.94
310	24.58	18.16	310	24.83	18.02	310	24.77	18.02
320	24.61	18.22	320	24.86	18.10	320	24.82	18.11
330	24.65	18.32	330	24.90	18.18	330	24.86	18.18
340	24.68	18.39	340	24.95	18.25	340	24.91	18.26
350	24.71	18.46	350	24.98	18.34	350	24.95	18.35
360	24.76	18.54	360	25.03	18.41	360	24.99	18.42
370	24.80	18.61	370	25.06	18.48	370	25.04	18.50

380	24.84	18.68		380	25.08	18.55		380	25.08	18.58
390	24.86	18.74		390	25.14	18.62		390	25.11	18.65
400	24.90	18.81		400	25.17	18.68		400	25.14	18.73
410	24.91	18.88		410	25.20	18.76		410	25.20	18.79
420	24.95	18.96		420	25.23	18.83		420	25.22	18.87
430	24.98	19.02		430	25.26	18.90		430	25.27	18.93
440	25.02	19.10		440	25.29	18.96		440	25.30	19.00
450	25.05	19.15		450	25.31	19.03		450	25.34	19.08
460	25.08	19.23		460	25.36	19.09		460	25.36	19.16
470	25.11	19.28		470	25.39	19.15		470	25.40	19.22
480	25.14	19.33		480	25.42	19.21		480	25.44	19.28
490	25.18	19.40		490	25.45	19.28		490	25.47	19.35
500	25.21	19.46		500	25.49	19.34		500	25.50	19.41
510	25.23	19.52		510	25.51	19.39		510	25.54	19.48
520	25.25	19.57		520	25.55	19.45		520	25.56	19.53
530	25.28	19.65		530	25.56	19.51		530	25.60	19.61
540	25.31	19.69		540	25.59	19.56		540	25.63	19.66
550	25.35	19.74		550	25.63	19.62		550	25.66	19.72
560	25.37	19.80		560	25.66	19.67		560	25.70	19.79
570	25.40	19.87		570	25.69	19.72		570	25.72	19.85
580	25.41	19.90		580	25.72	19.78		580	25.77	19.90
590	25.45	19.97		590	25.75	19.83		590	25.79	19.96
600	25.46	20.01		600	25.77	19.89		600	25.81	20.02
610	25.51	20.06		610	25.79	19.95		610	25.86	20.08
620	25.53	20.12		620	25.83	20.00		620	25.89	20.13
630	25.55	20.16		630	25.85	20.05		630	25.90	20.18
640	25.58	20.22		640	25.88	20.10		640	25.93	20.24
650	25.60	20.26		650	25.90	20.14		650	25.96	20.28
660	25.64	20.31		660	25.94	20.20		660	25.98	20.34
670	25.64	20.33		670	25.96	20.24		670	26.00	20.41
680	25.66	20.38		680	26.00	20.28		680	26.04	20.44
690	25.70	20.44		690	26.01	20.31		690	26.06	20.50
700	25.72	20.47		700	26.03	20.36		700	26.09	20.55
710	25.76	20.53		710	26.07	20.42		710	26.11	20.58
720	25.77	20.56		720	26.08	20.45		720	26.13	20.65
730	25.79	20.60		730	26.10	20.51		730	26.18	20.70
740	25.80	20.64		740	26.12	20.55		740	26.19	20.74
750	25.85	20.68		750	26.15	20.59		750	26.22	20.79
760	25.86	20.73		760	26.17	20.63		760	26.23	20.84
770	25.88	20.78		770	26.21	20.68		770	26.28	20.90
780	25.91	20.80		780	26.22	20.72		780	26.30	20.93
790	25.92	20.84		790	26.24	20.76		790	26.32	20.98
800	25.94	20.89		800	26.26	20.81		800	26.33	21.02
810	25.97	20.92		810	26.29	20.83		810	26.36	21.05

820	25.99	20.96		820	26.31	20.87		820	26.38	21.10
830	26.02	21.00		830	26.33	20.91		830	26.41	21.16
840	26.02	21.03		840	26.36	20.94		840	26.43	21.18
850	26.05	21.06		850	26.38	20.98		850	26.46	21.23
860	26.07	21.09		860	26.40	21.02		860	26.48	21.26
870	26.08	21.12		870	26.42	21.06		870	26.50	21.32
880	26.10	21.15		880	26.44	21.08		880	26.52	21.34
890	26.14	21.19		890	26.46	21.13		890	26.55	21.38
900	26.15	21.23		900	26.48	21.16		900	26.56	21.43
910	26.18	21.24		910	26.50	21.20		910	26.58	21.46
920	26.19	21.28		920	26.52	21.23		920	26.61	21.48
930	26.21	21.31		930	26.54	21.27		930	26.64	21.53
940	26.22	21.33		940	26.56	21.28		940	26.65	21.57
950	26.25	21.36		950	26.57	21.32		950	26.68	21.61
960	26.25	21.40		960	26.60	21.36		960	26.69	21.64
970	26.29	21.42		970	26.62	21.40		970	26.71	21.68
980	26.31	21.45		980	26.63	21.42		980	26.73	21.71
990	26.34	21.48		990	26.65	21.46		990	26.75	21.73
1000	26.35	21.50		1000	26.67	21.48		1000	26.77	21.77
1010	26.37	21.52		1010	26.70	21.50		1010	26.78	21.80
1020	26.38	21.54		1020	26.71	21.54		1020	26.81	21.84
1030	26.40	21.57		1030	26.73	21.57		1030	26.83	21.86
1040	26.42	21.60		1040	26.75	21.60		1040	26.84	21.90
1050	26.44	21.61		1050	26.76	21.62		1050	26.86	21.93
1060	26.45	21.64		1060	26.79	21.66		1060	26.89	21.98
1070	26.47	21.65		1070	26.80	21.67		1070	26.91	22.00
1080	26.49	21.67		1080	26.82	21.71		1080	26.93	22.02
1090	26.50	21.69		1090	26.83	21.73		1090	26.94	22.06
1100	26.53	21.72		1100	26.85	21.75		1100	26.97	22.09
1110	26.54	21.74		1110	26.89	21.80		1110	26.99	22.11
1120	26.55	21.75		1120	26.89	21.81		1120	26.99	22.14
1130	26.57	21.78		1130	26.92	21.84		1130	27.01	22.17
1140	26.58	21.80		1140	26.92	21.87		1140	27.02	22.19
1150	26.61	21.82		1150	26.95	21.88		1150	27.04	22.21
1160	26.63	21.83		1160	26.97	21.90		1160	27.07	22.24
1170	26.65	21.86		1170	26.98	21.92		1170	27.08	22.28
1180	26.66	21.87		1180	26.99	21.95		1180	27.10	22.30
1190	26.67	21.90		1190	27.01	21.99		1190	27.11	22.33
1200	26.69	21.90		1200	27.02	22.00		1200	27.13	22.34
1210	26.71	21.91		1210	27.05	22.03		1210	27.14	22.37
1220	26.74	21.95		1220	27.07	22.03		1220	27.16	22.41
1230	26.75	21.94		1230	27.08	22.06		1230	27.18	22.43
1240	26.75	21.96		1240	27.09	22.09		1240	27.19	22.44
1250	26.79	21.98		1250	27.11	22.10		1250	27.21	22.46

1260	26.80	22.01		1260	27.13	22.14		1260	27.22	22.49
1270	26.80	22.00		1270	27.14	22.16		1270	27.24	22.52
1280	26.83	22.03		1280	27.15	22.16		1280	27.26	22.54
1290	26.84	22.04		1290	27.17	22.19		1290	27.26	22.56
1300	26.86	22.06		1300	27.19	22.21		1300	27.30	22.59
1310	26.86	22.07		1310	27.20	22.23		1310	27.31	22.61
1320	26.89	22.09		1320	27.22	22.25		1320	27.33	22.64
1330	26.90	22.11		1330	27.24	22.27		1330	27.34	22.66
1340	26.92	22.12		1340	27.25	22.29		1340	27.35	22.68
1350	26.93	22.13		1350	27.27	22.31		1350	27.36	22.71
1360	26.94	22.16		1360	27.26	22.33		1360	27.37	22.74
1370	26.97	22.17		1370	27.30	22.35		1370	27.40	22.76
1380	26.98	22.18		1380	27.31	22.38		1380	27.41	22.78
1390	26.99	22.19		1390	27.32	22.39		1390	27.43	22.80
1400	27.00	22.20		1400	27.33	22.40		1400	27.45	22.83
1410	27.02	22.24		1410	27.36	22.43		1410	27.45	22.84
1420	27.03	22.24		1420	27.37	22.44		1420	27.46	22.86
1430	27.05	22.25		1430	27.38	22.46		1430	27.47	22.89
1440	27.06	22.27		1440	27.40	22.48		1440	27.50	22.91
1450	27.08	22.28		1450	27.41	22.51		1450	27.50	22.94
1460	27.09	22.30		1460	27.43	22.53		1460	27.53	22.96
1470	27.10	22.31		1470	27.44	22.54		1470	27.53	22.97
1480	27.12	22.32		1480	27.47	22.56		1480	27.56	22.99
1490	27.14	22.33		1490	27.47	22.57		1490	27.56	23.02
1500	27.14	22.36		1500	27.49	22.60		1500	27.57	23.04
1510	27.15	22.37		1510	27.49	22.61		1510	27.59	23.07
1520	27.17	22.38		1520	27.51	22.64		1520	27.60	23.08
1530	27.19	22.40		1530	27.52	22.66		1530	27.62	23.11
1540	27.20	22.41		1540	27.54	22.69		1540	27.63	23.14
1550	27.21	22.41		1550	27.55	22.70		1550	27.64	23.13
1560	27.23	22.45		1560	27.56	22.72		1560	27.66	23.17
1570	27.23	22.45		1570	27.58	22.72		1570	27.66	23.17
1580	27.27	22.46		1580	27.60	22.74		1580	27.68	23.19
1590	27.26	22.48		1590	27.61	22.77		1590	27.70	23.22
1600	27.28	22.50		1600	27.62	22.78		1600	27.71	23.24
1610	27.31	22.51		1610	27.63	22.80		1610	27.71	23.27
1620	27.34	22.53		1620	27.65	22.83		1620	27.73	23.27
1630	27.34	22.54		1630	27.66	22.85		1630	27.75	23.30
1640	27.35	22.56		1640	27.67	22.86		1640	27.77	23.33
1650	27.36	22.57		1650	27.68	22.88		1650	27.77	23.34
1660	27.38	22.59		1660	27.70	22.90		1660	27.79	23.36
1670	27.39	22.61		1670	27.72	22.93		1670	27.80	23.38
1680	27.39	22.60		1680	27.72	22.93		1680	27.80	23.40
1690	27.41	22.63		1690	27.75	22.97		1690	27.82	23.42

1700	27.44	22.66		1700	27.74	22.97		1700	27.84	23.45
1710	27.45	22.67		1710	27.76	22.99		1710	27.85	23.45
1720	27.46	22.68		1720	27.77	23.01		1720	27.86	23.47
1730	27.46	22.69		1730	27.78	23.03		1730	27.88	23.49
1740	27.47	22.71		1740	27.80	23.06		1740	27.88	23.51
1750	27.48	22.72		1750	27.81	23.07		1750	27.89	23.54
1760	27.50	22.74		1760	27.82	23.09		1760	27.90	23.55
1770	27.51	22.75		1770	27.83	23.11		1770	27.92	23.57
1780	27.52	22.79		1780	27.85	23.13		1780	27.94	23.59
1790	27.53	22.79		1790	27.85	23.14		1790	27.95	23.61
1800	27.55	22.80		1800	27.86	23.17		1800	27.95	23.63
1810	27.57	22.82		1810	27.89	23.20		1810	27.97	23.64
1820	27.57	22.83		1820	27.91	23.21		1820	27.98	23.66
1830	27.59	22.85		1830	27.91	23.22		1830	27.99	23.67
1840	27.59	22.86		1840	27.92	23.24		1840	28.01	23.68
1850	27.61	22.88		1850	27.93	23.26		1850	28.01	23.72
1860	27.61	22.89		1860	27.95	23.29		1860	28.03	23.74
1870	27.63	22.91		1870	27.95	23.30		1870	28.03	23.75
1880	27.65	22.93		1880	27.96	23.32		1880	28.04	23.77
1890	27.67	22.95		1890	27.98	23.34		1890	28.06	23.79
1900	27.66	22.96		1900	28.00	23.36		1900	28.07	23.79
1910	27.68	22.98		1910	28.00	23.38		1910	28.08	23.81
1920	27.70	23.00		1920	28.02	23.40		1920	28.11	23.84
1930	27.70	23.00		1930	28.03	23.40		1930	28.11	23.86
1940	27.72	23.03		1940	28.04	23.44		1940	28.13	23.88
1950	27.72	23.03		1950	28.05	23.44		1950	28.12	23.88
1960	27.73	23.05		1960	28.05	23.46		1960	28.14	23.91
1970	27.75	23.08		1970	28.07	23.48		1970	28.14	23.92
1980	27.75	23.09		1980	28.08	23.50		1980	28.16	23.94
1990	27.76	23.11		1990	28.09	23.52		1990	28.16	23.95
2000	27.78	23.13		2000	28.11	23.54		2000	28.18	23.99
2010	27.79	23.13		2010	28.11	23.55		2010	28.19	23.99
2020	27.80	23.16		2020	28.12	23.56		2020	28.21	24.01
2030	27.81	23.19		2030	28.13	23.60		2030	28.22	24.03
2040	27.82	23.19		2040	28.14	23.61		2040	28.22	24.05
2050	27.83	23.21		2050	28.16	23.62		2050	28.23	24.07
2060	27.84	23.22		2060	28.18	23.66		2060	28.24	24.08
2070	27.86	23.25		2070	28.18	23.66		2070	28.26	24.09
2080	27.86	23.25		2080	28.19	23.68		2080	28.26	24.10
2090	27.87	23.27		2090	28.21	23.70		2090	28.26	24.12
2100	27.88	23.30		2100	28.20	23.73		2100	28.29	24.15
2110	27.89	23.29		2110	28.22	23.74		2110	28.29	24.15
2120	27.90	23.33		2120	28.23	23.76		2120	28.31	24.18
2130	27.91	23.33		2130	28.24	23.77		2130	28.31	24.18

2140	27.93	23.34		2140	28.26	23.78		2140	28.32	24.21
2150	27.95	23.38		2150	28.26	23.79		2150	28.33	24.22
2160	27.95	23.38		2160	28.27	23.82		2160	28.34	24.23
2170	27.97	23.42		2170	28.28	23.83		2170	28.35	24.25
2180	27.96	23.41		2180	28.30	23.85		2180	28.36	24.26
2190	27.97	23.43		2190	28.31	23.87		2190	28.38	24.28
2200	27.98	23.45		2200	28.32	23.89		2200	28.38	24.31
2210	27.99	23.46		2210	28.34	23.91		2210	28.39	24.32
2220	28.00	23.48		2220	28.35	23.93		2220	28.40	24.34
2230	28.01	23.50		2230	28.35	23.94		2230	28.41	24.35
2240	28.03	23.53		2240	28.36	23.95		2240	28.42	24.37
2250	28.03	23.54		2250	28.38	23.98		2250	28.44	24.37
2260	28.05	23.54		2260	28.37	23.99		2260	28.45	24.40
2270	28.05	23.56		2270	28.40	24.01		2270	28.47	24.42
2280	28.07	23.59		2280	28.41	24.03		2280	28.47	24.43
2290	28.06	23.61		2290	28.41	24.03		2290	28.47	24.45
2300	28.09	23.62		2300	28.43	24.06		2300	28.49	24.47
2310	28.09	23.62		2310	28.44	24.08		2310	28.50	24.48
2320	28.11	23.66		2320	28.45	24.09		2320	28.50	24.48
2330	28.11	23.67		2330	28.47	24.11		2330	28.53	24.53
2340	28.11	23.67		2340	28.46	24.12		2340	28.52	24.52
2350	28.13	23.69		2350	28.47	24.14		2350	28.54	24.55
2360	28.13	23.71		2360	28.49	24.15		2360	28.54	24.55
2370	28.15	23.72		2370	28.49	24.17		2370	28.55	24.58
2380	28.17	23.75		2380	28.50	24.19		2380	28.56	24.59
2390	28.17	23.76		2390	28.52	24.20		2390	28.57	24.60
2400	28.17	23.78		2400	28.54	24.21		2400	28.58	24.63
2410	28.19	23.79		2410	28.55	24.24		2410	28.59	24.64
2420	28.20	23.81		2420	28.54	24.25		2420	28.60	24.65
2430	28.21	23.82		2430	28.55	24.26		2430	28.61	24.66
2440	28.22	23.84		2440	28.56	24.28		2440	28.63	24.69
2450	28.24	23.85		2450	28.58	24.30		2450	28.63	24.70
2460	28.23	23.87		2460	28.57	24.31		2460	28.64	24.72
2470	28.26	23.88		2470	28.60	24.33		2470	28.65	24.72
2480	28.26	23.89		2480	28.60	24.34		2480	28.67	24.75
2490	28.27	23.91		2490	28.60	24.36		2490	28.66	24.76
2500	28.28	23.94		2500	28.62	24.38		2500	28.66	24.78
2510	28.29	23.94		2510	28.63	24.38		2510	28.69	24.79
2520	28.30	23.97		2520	28.64	24.40		2520	28.71	24.81
2530	28.32	23.99		2530	28.65	24.42		2530	28.70	24.83
2540	28.33	24.01		2540	28.65	24.43		2540	28.71	24.85
2550	28.34	24.02		2550	28.67	24.46		2550	28.71	24.84
2560	28.34	24.04		2560	28.68	24.47		2560	28.72	24.88
2570	28.35	24.06		2570	28.68	24.48		2570	28.74	24.90

2580	28.34	24.07		2580	28.70	24.51		2580	28.76	24.91
2590	28.37	24.09		2590	28.70	24.52		2590	28.77	24.92
2600	28.36	24.09		2600	28.71	24.53		2600	28.78	24.94
2610	28.39	24.12		2610	28.73	24.56		2610	28.79	24.97
2620	28.41	24.13		2620	28.73	24.56		2620	28.79	24.98
2630	28.40	24.15		2630	28.75	24.59		2630	28.80	24.99
2640	28.41	24.17		2640	28.77	24.61		2640	28.81	25.01
2650	28.42	24.18		2650	28.76	24.61		2650	28.82	25.03
2660	28.44	24.21		2660	28.76	24.64		2660	28.83	25.03
2670	28.43	24.21		2670	28.79	24.65		2670	28.83	25.06
2680	28.45	24.23		2680	28.79	24.68		2680	28.85	25.07
2690	28.46	24.24		2690	28.81	24.67		2690	28.86	25.09
2700	28.46	24.26		2700	28.81	24.71		2700	28.87	25.11
2710	28.48	24.28		2710	28.82	24.72		2710	28.88	25.12
2720	28.49	24.29		2720	28.84	24.73		2720	28.89	25.14
2730	28.49	24.31		2730	28.84	24.76		2730	28.90	25.15
2740	28.50	24.32		2740	28.85	24.77		2740	28.91	25.17
2750	28.51	24.34		2750	28.86	24.78		2750	28.92	25.21
2760	28.52	24.35		2760	28.86	24.80		2760	28.94	25.22
2770	28.53	24.37		2770	28.87	24.81		2770	28.94	25.23
2780	28.54	24.38		2780	28.88	24.83		2780	28.94	25.24
2790	28.55	24.42		2790	28.89	24.85		2790	28.95	25.26
2800	28.55	24.41		2800	28.91	24.86		2800	28.97	25.29
2810	28.56	24.43		2810	28.91	24.88		2810	28.98	25.29
2820	28.57	24.45		2820	28.92	24.92		2820	28.98	25.33
2830	28.58	24.47		2830	28.94	24.92		2830	28.98	25.34
2840	28.58	24.47		2840	28.94	24.94		2840	29.00	25.36
2850	28.60	24.50		2850	28.94	24.95		2850	29.00	25.37
2860	28.61	24.52		2860	28.96	24.97		2860	29.01	25.39
2870	28.62	24.53		2870	28.96	24.98		2870	29.01	25.40
2880	28.64	24.56		2880	28.98	25.01		2880	29.03	25.43
2890	28.64	24.55		2890	28.97	25.04		2890	29.04	25.45
2900	28.64	24.58		2900	29.00	25.04		2900	29.05	25.46
2910	28.66	24.60		2910	29.00	25.07		2910	29.05	25.48
2920	28.66	24.62		2920	29.02	25.09		2920	29.07	25.50
2930	28.67	24.63		2930	29.02	25.11		2930	29.08	25.52
2940	28.68	24.65		2940	29.03	25.11		2940	29.09	25.54
2950	28.69	24.68		2950	29.04	25.12		2950	29.10	25.56
2960	28.70	24.67		2960	29.04	25.14		2960	29.10	25.58
2970	28.71	24.69		2970	29.07	25.17		2970	29.11	25.61
2980	28.71	24.71		2980	29.05	25.18		2980	29.12	25.60
2990	28.71	24.73		2990	29.06	25.20		2990	29.12	25.63
3000	28.74	24.75		3000	29.07	25.22		3000	29.12	25.66
3010	28.74	24.75		3010	29.08	25.23		3010	29.14	25.68

3020	28.75	24.78		3020	29.09	25.26		3020	29.15	25.70
3030	28.75	24.79		3030	29.10	25.26		3030	29.15	25.71
3040	28.79	24.80		3040	29.12	25.29		3040	29.18	25.74
3050	28.78	24.83		3050	29.13	25.31		3050	29.18	25.76
3060	28.80	24.85		3060	29.13	25.32		3060	29.19	25.76
3070	28.79	24.86		3070	29.13	25.33		3070	29.20	25.79
3080	28.80	24.87		3080	29.15	25.36		3080	29.21	25.81
3090	28.81	24.89		3090	29.15	25.37		3090	29.22	25.82
3100	28.83	24.91		3100	29.16	25.39		3100	29.22	25.86
3110	28.83	24.94		3110	29.16	25.41		3110	29.24	25.87
3120	28.84	24.96		3120	29.18	25.44		3120	29.24	25.90
3130	28.84	24.97		3130	29.18	25.46		3130	29.25	25.91
3140	28.85	24.98		3140	29.19	25.47		3140	29.25	25.94
3150	28.88	25.00		3150	29.20	25.49		3150	29.27	25.96
3160	28.87	25.01		3160	29.21	25.52		3160	29.28	25.98
3170	28.88	25.03		3170	29.23	25.53		3170	29.28	26.00
3180	28.89	25.05		3180	29.23	25.56		3180	29.30	26.03
3190	28.90	25.06		3190	29.24	25.57		3190	29.31	26.05
3200	28.91	25.09		3200	29.24	25.59		3200	29.32	26.06
3210	28.92	25.10		3210	29.25	25.61		3210	29.33	26.08
3220	28.93	25.11		3220	29.27	25.62		3220	29.32	26.12
3230	28.94	25.14		3230	29.27	25.64		3230	29.34	26.14
3240	28.95	25.15		3240	29.29	25.67		3240	29.34	26.15
3250	28.96	25.17		3250	29.29	25.68		3250	29.34	26.17
3260	28.97	25.18		3260	29.30	25.71		3260	29.36	26.19
3270	28.97	25.21		3270	29.29	25.73		3270	29.37	26.22
3280	28.98	25.23		3280	29.32	25.75		3280	29.38	26.25
3290	29.00	25.26		3290	29.31	25.78		3290	29.39	26.26
3300	29.00	25.26		3300	29.33	25.81		3300	29.40	26.29
3310	29.00	25.28		3310	29.34	25.82		3310	29.41	26.31
3320	29.01	25.31		3320	29.35	25.84		3320	29.40	26.33
3330	29.04	25.33		3330	29.35	25.87		3330	29.41	26.37
3340	29.04	25.34		3340	29.37	25.89		3340	29.43	26.39
3350	29.04	25.36		3350	29.38	25.91		3350	29.43	26.40
3360	29.05	25.38		3360	29.38	25.94		3360	29.43	26.43
3370	29.06	25.40		3370	29.39	25.95		3370	29.45	26.45
3380	29.06	25.42		3380	29.39	25.98		3380	29.46	26.48
3390	29.08	25.45		3390	29.42	26.01		3390	29.47	26.51
3400	29.08	25.45		3400	29.42	26.03		3400	29.48	26.53
3410	29.10	25.47		3410	29.42	26.05		3410	29.48	26.56
3420	29.09	25.50		3420	29.42	26.07		3420	29.50	26.59
3430	29.11	25.52		3430	29.43	26.09		3430	29.51	26.62
3440	29.10	25.53		3440	29.45	26.12		3440	29.53	26.65
3450	29.13	25.55		3450	29.45	26.14		3450	29.51	26.66

3460	29.14	25.58		3460	29.47	26.17		3460	29.52	26.69
3470	29.14	25.60		3470	29.47	26.21		3470	29.53	26.71
3480	29.15	25.62		3480	29.48	26.21		3480	29.55	26.75
3490	29.16	25.64		3490	29.49	26.25		3490	29.56	26.76
3500	29.17	25.67		3500	29.51	26.27		3500	29.55	26.79
3510	29.18	25.69		3510	29.52	26.30		3510	29.58	26.83
3520	29.18	25.71		3520	29.52	26.32		3520	29.58	26.86
3530	29.20	25.74		3530	29.53	26.35		3530	29.60	26.89
3540	29.20	25.76		3540	29.53	26.38		3540	29.60	26.89
3550	29.21	25.79		3550	29.54	26.40		3550	29.60	26.93
3560	29.22	25.80		3560	29.54	26.41		3560	29.62	26.97
3570	29.23	25.83		3570	29.57	26.45		3570	29.62	27.00
3580	29.22	25.85		3580	29.57	26.47		3580	29.63	27.03
3590	29.25	25.87		3590	29.58	26.50		3590	29.64	27.05
3600	29.24	25.88		3600	29.59	26.54		3600	29.64	27.07
3610	29.26	25.91		3610	29.60	26.56		3610	29.66	27.10
3620	29.27	25.93		3620	29.60	26.57		3620	29.67	27.13
3630	29.28	25.95		3630	29.62	26.61		3630	29.69	27.16
3640	29.28	25.98		3640	29.62	26.64		3640	29.69	27.19
3650	29.30	26.02		3650	29.62	26.66		3650	29.70	27.23
3660	29.30	26.02		3660	29.64	26.69		3660	29.70	27.25
3670	29.32	26.06		3670	29.65	26.72		3670	29.72	27.28
3680	29.33	26.08		3680	29.65	26.74		3680	29.72	27.31
3690	29.33	26.11		3690	29.67	26.77		3690	29.73	27.34
3700	29.34	26.13		3700	29.67	26.80		3700	29.73	27.37
3710	29.35	26.15		3710	29.67	26.82		3710	29.75	27.40
3720	29.36	26.18		3720	29.69	26.85		3720	29.76	27.44
3730	29.37	26.21		3730	29.70	26.89		3730	29.76	27.46
3740	29.37	26.23		3740	29.70	26.91		3740	29.78	27.49
3750	29.38	26.27		3750	29.71	26.93		3750	29.78	27.50
3760	29.39	26.28		3760	29.71	26.96		3760	29.80	27.54
3770	29.40	26.32		3770	29.73	27.00		3770	29.79	27.58
3780	29.40	26.32		3780	29.73	27.02		3780	29.81	27.60
3790	29.41	26.36		3790	29.74	27.06		3790	29.84	27.64
3800	29.41	26.38		3800	29.75	27.08		3800	29.82	27.66
3810	29.43	26.40		3810	29.75	27.10		3810	29.84	27.70
3820	29.44	26.43		3820	29.76	27.13		3820	29.85	27.71
3830	29.46	26.47		3830	29.77	27.17		3830	29.86	27.75
3840	29.45	26.49		3840	29.80	27.21		3840	29.86	27.79
3850	29.48	26.52		3850	29.79	27.23		3850	29.88	27.82
3860	29.48	26.54		3860	29.80	27.25		3860	29.88	27.86
3870	29.48	26.56		3870	29.82	27.29		3870	29.90	27.87
3880	29.50	26.60		3880	29.83	27.31		3880	29.90	27.90
3890	29.51	26.63		3890	29.83	27.35		3890	29.92	27.95

3900	29.51	26.64		3900	29.84	27.37		3900	29.92	27.96
3910	29.53	26.68		3910	29.86	27.41		3910	29.93	27.99
3920	29.54	26.72		3920	29.86	27.43		3920	29.93	28.03
3930	29.53	26.74		3930	29.87	27.47		3930	29.95	28.06
3940	29.55	26.77		3940	29.88	27.49		3940	29.97	28.08
3950	29.55	26.80		3950	29.88	27.53		3950	29.97	28.11
3960	29.56	26.83		3960	29.90	27.56		3960	29.99	28.16
3970	29.58	26.85		3970	29.90	27.59		3970	29.99	28.17
3980	29.59	26.88		3980	29.91	27.62		3980	30.01	28.20
3990	29.60	26.90		3990	29.92	27.66		3990	30.02	28.23
4000	29.61	26.94		4000	29.93	27.69		4000	30.02	28.26
4010	29.61	26.97		4010	29.95	27.72		4010	30.03	28.29
4020	29.62	27.00		4020	29.95	27.74		4020	30.05	28.32
4030	29.63	27.04		4030	29.96	27.78		4030	30.04	28.34
4040	29.63	27.06		4040	29.96	27.81		4040	30.06	28.38
4050	29.65	27.09		4050	29.98	27.83		4050	30.07	28.41
4060	29.65	27.12		4060	29.99	27.85		4060	30.07	28.42
4070	29.67	27.15		4070	29.99	27.88		4070	30.09	28.45
4080	29.67	27.18		4080	30.00	27.92		4080	30.09	28.47
4090	29.69	27.21		4090	30.02	27.97		4090	30.11	28.51
4100	29.70	27.24		4100	30.01	27.99		4100	30.12	28.54
4110	29.71	27.28		4110	30.02	27.99		4110	30.13	28.57
4120	29.71	27.30		4120	30.03	28.04		4120	30.15	28.60
4130	29.71	27.32		4130	30.05	28.07		4130	30.14	28.62
4140	29.72	27.37		4140	30.06	28.10		4140	30.15	28.65
4150	29.74	27.39		4150	30.06	28.13		4150	30.17	28.68
4160	29.75	27.42		4160	30.07	28.16		4160	30.17	28.70
4170	29.76	27.45		4170	30.08	28.19		4170	30.18	28.73
4180	29.77	27.47		4180	30.08	28.21		4180	30.18	28.75
4190	29.77	27.51		4190	30.09	28.24		4190	30.19	28.78
4200	29.79	27.53		4200	30.11	28.27		4200	30.20	28.81
4210	29.79	27.58		4210	30.12	28.31		4210	30.21	28.82
4220	29.81	27.60		4220	30.11	28.32		4220	30.22	28.85
4230	29.81	27.63		4230	30.13	28.37		4230	30.22	28.87
4240	29.83	27.65		4240	30.14	28.39		4240	30.23	28.90
4250	29.83	27.69		4250	30.14	28.42		4250	30.24	28.92
4260	29.85	27.72		4260	30.16	28.46		4260	30.26	28.94
4270	29.85	27.75		4270	30.17	28.49		4270	30.25	28.97
4280	29.87	27.79		4280	30.18	28.52		4280	30.27	28.99
4290	29.88	27.82		4290	30.18	28.55		4290	30.29	29.03
4300	29.87	27.83		4300	30.20	28.57		4300	30.30	29.04
4310	29.88	27.85		4310	30.20	28.60		4310	30.32	29.09
4320	29.90	27.90		4320	30.21	28.62		4320	30.31	29.09
4330	29.92	27.92		4330	30.22	28.65		4330	30.31	29.11

4340	29.92	27.94		4340	30.23	28.67		4340	30.32	29.15
4350	29.93	27.98		4350	30.25	28.71		4350	30.35	29.16
4360	29.95	28.02		4360	30.26	28.72		4360	30.35	29.18
4370	29.94	28.04		4370	30.26	28.76		4370	30.36	29.21
4380	29.95	28.07		4380	30.27	28.78		4380	30.37	29.23
4390	29.98	28.09		4390	30.27	28.81		4390	30.37	29.24
4400	29.99	28.12		4400	30.29	28.84		4400	30.38	29.27
4410	30.00	28.16		4410	30.30	28.86		4410	30.40	29.31
4420	30.01	28.18		4420	30.31	28.89		4420	30.40	29.32
4430	30.00	28.22		4430	30.31	28.92		4430	30.41	29.35
4440	30.02	28.24		4440	30.32	28.93				
4450	30.03	28.26		4450	30.32	28.95				
4460	30.04	28.31		4460	30.33	28.99				
4470	30.05	28.32		4470	30.35	29.00				
4480	30.06	28.35								
4490	30.07	28.37								
4500	30.07	28.40								
4510	30.09	28.45								
4520	30.10	28.46								
4530	30.12	28.49								
4540	30.12	28.51								
4550	30.13	28.53								
4560	30.13	28.57								
4570	30.15	28.60								
4580	30.16	28.62								
4590	30.16	28.65								
4600	30.17	28.69								
4610	30.18	28.70								
4620	30.21	28.73								
4630	30.20	28.77								
4640	30.21	28.77								
4650	30.24	28.82								
4660	30.24	28.84								
4670	30.24	28.87								
4680	30.27	28.89								
4690	30.26	28.91								
4700	30.27	28.93								
4710	30.28	28.96								
4720	30.30	28.99								
4730	30.29	29.01								